UNIVERSITÀ
DI TRENTO
Department of
Physics

PhD in Physics

# Methods for Investigating Magnetoreception in Honeybees: Toward Testing the Radical Pair Mechanism

Alan Sven Oesterle

Supervised by Albrecht Haase

January 2026

**University of Trento**
*Department of Physics*
Via Sommarive 14
38123 Povo (TN)

# Acknowledgements

I am grateful to my supervisor, Albrecht Haase, for his guidance and for helping me navigate the many challenges of this project. I would also like to thank my colleagues, whose patience and expertise were invaluable in helping me master the procedures and equipment essential to this study. My heartfelt appreciation goes to my family for their constant encouragement, strength, and unwavering support throughout this journey. Finally, I extend my gratitude to the honeybees whose cooperation made this research possible, their remarkable resilience and contribution are sincerely appreciated.

# Abstract

Honey bees (*Apis mellifera*) serve as a compelling model for studying magnetoreception, as they are able to navigate over distances of up to 10 km, and prior behavioral studies indicate they possess magnetic sensitivity [1, 2, 3, 4]. However, the underlying neural and biochemical mechanisms of magnetoreception remain largely unresolved. This study investigates the intersection of quantum biology and neuroscience by exploring the radical pair mechanism (RPM) as a potential basis for magnetic sensitivity in bees. Since the RPM predicts that magnetic sensing is coupled to the visual system, we combined behavioral conditioning with *in vivo* brain imaging using both visual and magnetic stimuli [5, 6]. Classical conditioning was done by the proboscis extension response (PER), pairing visual or magnetic cues with sucrose rewards. Concurrently, two-photon calcium imaging targeted the anterior optic tubercle (AOTu), a brain region implicated in chromatic processing and potentially in navigation, to assess neural responses to visual and magnetic stimuli [7]. PER conditioning achieved $\sim$50$\%$ learning success with visual stimulus, whereas magnetic stimulus alone elicited no behavioral response. Imaging in four responsive bees revealed a $\sim$0.2$\%$ fluorescence decrease in the visually stimulated AOTu during magnetic stimulation. These results provide initial evidence that RPM-linked magnetic signals can be detected in higher-order bee brain regions through neural amplification, providing support to the hypothesis of visual magnetic integration. This work offers a novel avenue for future experiments to directly test RPM predictions, including light dependence, polarity independence, and disruption by radiofrequency fields [5, 6, 8, 9].

# Contents

# 1 Introduction

The aptitude of various animals to navigate has fascinated scientists for centuries. Among other suggestions was the theory of Russian zoologist Aleksandr von Middendorf, who proposed, in the 1850s idea that animals might detect the Earth's magnetic field and use it for navigation [10]. However, it was not until the 1960s that magnetoreception in birds became widely accepted as a mechanism underlying their migratory behavior. Since then, numerous behavioral studies have demonstrated that this sensory ability extends beyond birds, occurring in species such as sea turtles [11], rodents [6], and various invertebrates such as butterflies [12], cockroaches [13], and lobsters [14]. In addition to providing directional information, the Earth's magnetic field can also offer positional information through the inclination angle and field strength. Some animals are even capable of detecting subtle variations in these parameters, enabling them not only to use the magnetic field as a compass for orientation, but also to interpret the magnetic topography of their environment to construct a form of magnetic map. Despite these advances, our understanding of magnetoreception remains incomplete, with key questions persisting about the biophysical and neurological mechanisms that underpin this remarkable sense.

Two main hypotheses have been proposed to explain the mechanisms underlying magnetoreception: a mechanical model and a chemical model [5, 15, 16]. The mechanical hypothesis suggests that ferromagnetic nanoparticles, known as magnetite, exist within specialized cells and behave similarly to a compass needle, exerting mechanical forces as they align with the Earth's magnetic field [15, 17, 18]. In contrast, the chemical hypothesis, known as the radical pair mechanism (RPM), proposes that magnetoreception arises from photochemical reactions that generate long-lived, spin-correlated radical pairs [5, 19]. Magnetic fields can affect these radical pairs, leading to changes in the yields of their reaction products. Numerous studies indicate that in most animals, magnetic sensing is light-dependent and sensitive to the inclination rather than the polarity of the magnetic field, providing strong support for the RPM as the more dominant mechanism [8, 16, 19]. However, it is also possible that both mechanisms operate simultaneously, each fulfilling a distinct physiological or behavioral role in the overall process of magnetic sensing [4].

In Steiner and Ulrich [20], numerous radical reactions, including many organic reactions, are listed that have been shown to be affected by magnetic fields. As magnetoreception is shown to be light-sensitive, the most promising location for these magnetically sensitive radical pairs is believed to be within the protein cryptochrome (Cry), a blue-light photoreceptor that plays a crucial role in regulating circadian rhythms [8, 16, 19, 21]. Because Cry is found in the eyes, it is often suggested that magnetoreception may function in conjunction with vision. In the current simplified RPM model, blue light is absorbed by Cry, initiating a sequence of electron transfer reactions that generate a radical pair. The spin dynamics of this pair can be modulated by an external magnetic field, potentially leading to downstream changes in neural activity. However, besides the light-sensitive variants of Cry, other variants of Cry exist that are light-insensitive [12, 22]. Interestingly, species possessing only light-insensitive Cry, such as the *P. americana* cockroach, have also demonstrated the ability to sense magnetic fields [13]. This raises the possibility that alternative radical pairs could be involved in magnetoreception, ones generated not by light activation but through chemical reduction by a reducing agent [22, 23]. It is also conceivable that cryptochrome itself may not serve as the primary magnetoreceptor, but instead acts as a downstream component within a broader signaling cascade [22, 24].

The question of whether some animals can truly detect magnetic fields remains actively debated, as highlighted by a recent large-scale replication study by Bassetto et al. [25], which failed to find robust magnetic field effects on Drosophila behavior under experimental conditions and called earlier positive reports into question. Consequently, selecting an appropriate species as a model for magnetic sensing or cryptochrome-based magnetoreception requires considerable caution. The honeybee (*Apis mellifera*) is an attractive model organism for studying magnetoreception due to its remarkable navigational abilities. Honeybees were among the first invertebrates for which multiple laboratories, using various behavioral experiments, reported evidence of magnetoreception [26]. Bees can travel more than 10 km from their hives while foraging, relying on multiple strategies to navigate their environment, including landmark navigation, analyzing the sky's polarization patterns, and magnetoreception [1, 2, 3]. The polarized light from the sky forms a pattern linked to the sun's position, known as the sky compass, which enables bees to estimate the sun's location even when it is hidden by clouds or other obstacles. Both the sky compass and magnetoreception are believed to be perceived through modulated patterns of light intensity, suggesting that these sensory systems may provide complementary information to support the bee's precise orientation and navigation [2, 27]. Furthermore, the fact that honeybees

possess only a light-insensitive Cry offers valuable insights into the role of Cry in the magnetoreception reaction mechanism [22, 28].

Beyond behavioral studies, most research on the RPM of magnetoreception has focused on either Cry, single-neuron responses, or activity within the retina [24, 29]. No studies were found that examined downstream neural signaling beyond the level of photoreceptors. Neural circuits are traditionally examined using immediate early gene expression or electrophysiology [30]. More recently, *in vivo* two-photon calcium fluorescent imaging has enabled optophysiological recordings of neuronal circuit activity with high temporal and spatial resolution [3, 30]. In honeybees, whose brains are approximately 1 $mm^3$ in size, this technique allows for the investigation of neural activity across the entire brain. The infrared light employed in this technique can penetrate roughly 1 mm into highly scattering tissues, such as the brain, enabling imaging of higher-order central brain regions, provided that the region of interest can be stained with a calcium-sensitive fluorescent dye [3, 31, 32]. The anterior optic tubercle (AOTu) was chosen as the primary region of interest, as it is a higher-order structure involved in processing the chromatic properties of visual stimuli and is believed to play a role in navigation [7, 33]. This opens a new avenue for research in magnetoreception, enabling exploration further down the signaling cascade and leveraging neural amplification as a natural means to enhance the weak primary signals originating from cryptochrome or the retina. This is particularly relevant because *in vivo* experiments investigating quantum phenomena in neural systems are sparse, as these effects are expected to be weak and easily disrupted in the warm, noisy conditions of biological tissue [10, 34].

Motivated by this opportunity to better understand magnetoreception, this thesis integrates behavioral experiments in honeybees with *in vivo* two-photon calcium fluorescence imaging. The results from the behavioral studies serve to determine the optimal magnetic stimulation parameters for application in *in vivo* imaging. Among the various behavioral paradigms available for bees, classical conditioning based on the proboscis extension response (PER) was chosen due to its simplicity and compatibility with diverse types of stimuli [35, 36]. In this paradigm, bees learn to associate a conditioned stimulus (CS) with an unconditioned stimulus (US), typically a sucrose reward. PER experiments have been performed using various CS types, including olfactory, visual, and mechanosensory stimuli. Bees have also been shown to associate with a magnetic stimulus, as demonstrated by Liang et al. [37]. However, the magnetic field used in their experiments was approximately five times stronger than the Earth's natural field, and the bees' eyes were painted over during testing. Although visual

stimuli are more challenging to use with harnessed bees than free-flying ones, the harnessed setup allows for more precise control over the stimulus [38, 39, 40].

To conduct the PER experiments, a new setup was constructed, based on an existing design that automated execution of the entire experimental sequence, while recording behavioral responses [41]. The design was modified to enable bees to be positioned within as well as be removed from the center of a magnetic coil system. The setup was continuously refined until it produced responses consistent with those reported in literature under visual stimulus conditions, before proceeding to test magnetic stimuli. As for the two-photon imaging experiments, a coil system was developed to generate a homogeneous magnetic stimulus across the bee's body while maintaining optical access for imaging. The imaging setup and preparation were further modified to minimize interference from visual stimuli and to provide adequate optical filtering, ensuring that background light did not saturate the photomultiplier tubes used for fluorescence detection. Experiments were first conducted using visual stimuli to confirm that the AOTu exhibited responses consistent with those reported in the literature, thereby verifying that the preparation did not damage this structure, before proceeding with magnetic stimulation experiments. The magnetic coil system was designed to enable the systematic exploration of responses to a variety of magnetic stimuli. This included stimuli applied in different spatial orientations and with varied temporal profiles, such as slow linear ramps or sinusoidal fields. The magnetic setup was also designed with the intent to test several key predictions of the RPM, including polarity independence and the potential disruption of magnetic responses by radio frequency fields [5, 42].

In this thesis, the theoretical foundations of magnetoreception and honeybee vision are first introduced, providing the necessary biological and biophysical context. This is followed by a detailed description of the experimental approaches, including the magnetic coil setup, the classical conditioning paradigms, and the two-photon calcium imaging techniques. The subsequent chapters present and analyze the behavioral and imaging results, which are then integrated and discussed in light of current models of magnetoreception. Finally, the thesis concludes with an integration of the main findings and an outlook discussing how they may advance our understanding of magnetoreception in honeybees, as well as directions for future research.

# Theoretical Background

# 2

## 2.1 Magnetoreception

Magnetoreception is the ability that allows organisms to detect and orient themselves using the Earth's magnetic fields. Although there is an abundance of behavioral data to show that a variety of different animals are capable of magnetoreception, the understanding of the principal mechanism underlying this sense and how it is translated into a neural signal remains unresolved [4, 15]. Two possible mechanisms for how terrestrial animals sense magnetic fields have been shown: ferromagnetic base detection and radical pair mechanism (RPM).

The first possible mechanism, ferromagnetic base detection, relies on crystalline magnetic iron nanoparticles called magnetite, which are able to react to magnetic fields as weak as the Earch's field ($\sim 50\ \mu T$) [5, 15, 17]. Magnetites can be found in a variety of sizes, they can be larger crystals ($\sim 50\ nm$) with a permanent magnetic moment that can rotate into alignment with a magnetic field, or smaller crystals ($\sim 20\ nm$) that are superparamagnetic and can attract or repel other crystals close to them. No matter the type of crystal, their movements can be detected by either mechanoreceptors or by the opening and closing ion channels. For example, in honeybees, magnetites have been found in their abdomen and antenna [43, 44]. Furthermore, it was observed that severing the ventral nerve cord between the abdomen and the thorax can disrupt the bee's response to magnetic stimuli [37].

In contrast, the RPM model is based on a chemical reaction that is modulated by the Earth's magnetic field. The energy of the Earth's magnetic field that interacts with molecules present in an organism is more than a million times smaller than the thermal energy ($k_B T$) of these molecules in physiological conditions and would thus be overwhelmed by random motion [5, 45]. To influence such a system while it is in a state of equilibrium, the energy required to alter its state must be on the same order of magnitude as the system's thermal energy. However, if a system is in a non-equilibrium state, then a tiny amount of energy could have a significant impact on the outcome of

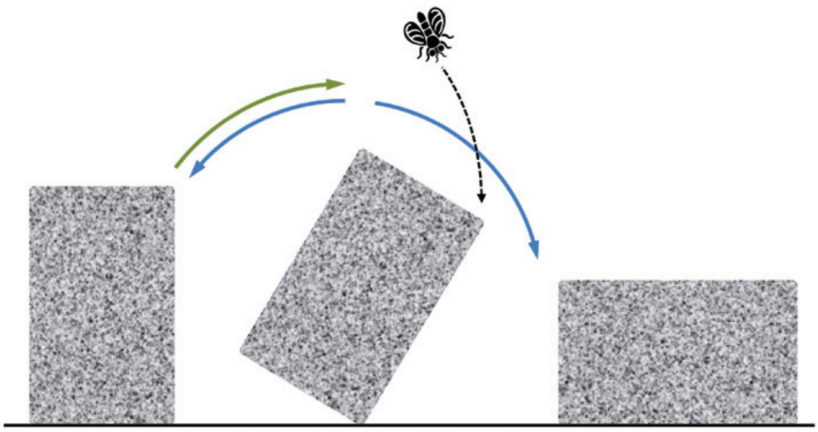

**Figure 2.1.:** A depiction of the radical pair analogy of how a fly could influence the which direction a brick would fall if the brick was prepared in a non-equilibrium state. From [45].

the state. The analogy of a fly attempting to tip over a heavy stone block is commonly used to explain this phenomenon, which asks if a fly would be able to tip over a stone block by bumping into it (Figure 2.1). Obviously, a fly bumping into a stone block would have very little effect on the block. However, if the block would be put in a state of non-equilibrium, by balancing it on its edge, then if the fly were to land on one side of the block while it is teetering in that direction, the block would be more likely to fall in that direction, even though the energy supplied by the fly is tiny.

In the RPM model, the chemical reactions involve radical pairs whose dynamics can be modulated by magnetic fields. As these radical pairs exist in a non-equilibrium state, even weak magnetic fields can modify their spin states, that will then impact the yield of the chemical reaction [5, 42]. Steiner and Ulrich [20] list numerous radical reactions, including organic reactions, that have been shown to be affected by magnetic fields. In addition, there is strong evidence that magnetoreception is light dependent, as observed in these studies [8, 12, 21], therefore the most likely location of the radical pairs involved in magnetoreception is in the cryptochrome, a type of flavoprotein that is found in the retina [16, 46, 47].

### 2.1.1 Radical Pairs

A radical is a molecule that contains unpaired electron in its outermost shell (unpaired valence electrons) and when two radicals are created simultaneously, they form a radical pair. The two unpaired electrons of a radical pair are either found in the

singlet or triplet state, unlike all other paired electrons of the molecule that can only be in the singlet state [5, 42, 48, 49]. Radical pairs can be formed through various processes, such as photochemical or redox reactions, and the radical pair's initial spin state may be either singlet or triplet. In the case of cryptochrome, the radical pair is formed by a photo-induced electron transfer, in which an electron is excited by the absorption of a photon. As a consequence of spin conservation, the total spin angular momentum remains unchanged, the radical pair initially forms in the singlet state, since the electrons were paired in a singlet configuration before excitation. A general reaction scheme depicting a radical pair reaction formed by photo-induced electron transfer is depicted in Figure 2.2. In brief, two molecules, A and B, form a radical pair when an electron in one molecule gets excited by absorbing a photon and then moves to the other molecule. The radical pair will originally be in the singlet state, but will then oscillate coherently between the singlet and triplet state. Then, it can either recombine and relax back to the ground state with a rate constant $k_s$ or continue the reaction to form a product with a rate constant $k_f$. The back reaction to relax to the ground state can only be done when the radical pair is in the singlet state due to spin conservation, while the forward reaction to make the product can be done in either of the spin states. The reaction yield depends not only on the two rate constants but also on the proportion of the radical pair occupying each spin state. The coherent interconversion between the spin states is sensitive to the external magnetic field due to the Zeeman effect, which shifts the energy levels associated with different magnetic moments within the radical pair. Therefore, if the magnetic field were to increase the proportion of the radical pair in the triplet state, then more products would be created at the end of the chemical reaction as a result of an inhibition of the back reaction. The influence of an external magnetic field on a radical pair can be described by the spin density operators, together with an effective spin Hamiltonian.

The effective spin Hamiltonian that is often used to characterize the time evolution of the spin states in radical pairs is shown in equation 2.1 [20, 50, 51].

$$\hat{H} = \sum_{i=1,2} g_e \mu_B \boldsymbol{B} \cdot \hat{S}_i + \sum_{i=1,2} \sum_{k=1}^{N_i} \hat{S}_i \cdot A_{ik} \cdot \hat{I}_{ik} - J(\frac{1}{2} + 2\hat{S}_1 \cdot \hat{S}_2) + \hat{S}_1 \cdot \boldsymbol{D} \cdot \hat{S}_2 \qquad (2.1)$$

The first term of this equation is from the Zeeman interaction of the external magnetic field $\boldsymbol{B}$ with the electron spin $\hat{S}_i$, and $g_e$ and $\mu_B$ are the g-value of the electron and the Bohr magneton respectively. The second term is for the hyperfine interactions of the electron with the nuclear spins $\hat{I}_{ik}$ in each radical and $A_{ik}$ are the hyperfine coupling tensors. The third and fourth terms are for the exchange and dipolar interaction of

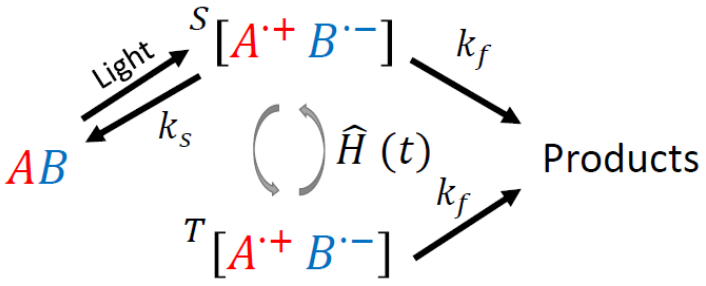


**Figure 2.2.:** Schematic representation of a simple radical-pair reaction. Reactant molecules (AB) are converted into products through the formation of a radical pair ($[A^{\cdot+}B^{\cdot-}]$). $k_s$ and $k_f$ denote the rate constants for the spin-selective back reaction and non-spin-selective forward reaction, respectively. Curved arrows indicate coherent interconversion between the singlet (S) and triplet (T) states, governed by the effective spin Hamiltonian $\hat{H}(t)$.

the two electron spins with $J$ and $D$ as the coupling constant and the dipolar coupling tensor, respectively.

Magnetic field effects on radical pair reactions are usually modeled through the spin density operators of the radical pair, shown in equation 2.2 [51, 52]

$$\frac{d}{dt}\hat{\rho}(t) = -\frac{i}{\hbar}\left[\hat{H}, \hat{\rho}(t)\right] - \left\{\frac{k_s}{2}\hat{P}_s + \frac{k_t}{2}\hat{P}_t, \hat{\rho}(t)\right\} \tag{2.2}$$

In this equation, $k_s$ and $k_t$ are the recombination rate constants for the singlet and triplet pairs, respectively, and $\hat{P}_s$ and $\hat{P}_t$ are the projection operators onto singlet and triplet electronic states, respectively. This equation can be used to calculate the yield of the chemical reaction using semiclassical methods, as described by Fay et al. [51]. Figure 2.3 depicts the spin state dynamics at different magnetic field strengths and orientations for a simple model of a radical pair containing two nitrogen nuclei in one radical with anisotropic hyperfine interactions and no nuclei on the other radical [5]. The singlet-triplet interconversion without an external magnetic field is shown in Figure 2.3a, and it is caused by the hyperfine interaction between the electron and the nearby nuclei. Figure 2.3b depicts that with the inclusion of a $50\ \mu T$ magnetic field, there is still this fast oscillation from the hyperfine, but it is now superimposed with a slower modulation that is added by the Zeeman interaction. If the magnetic field is rotated $90°$, as shown in Figure 2.3c, there is still the fast and slow oscillation from the hyperfine and Zeeman interactions, but the radical pair behaves differently. This is due to the hyperfine interaction being anisotropic because the unpaired electron of the radical is delocalized and interacts with several nuclei simultaneously and the

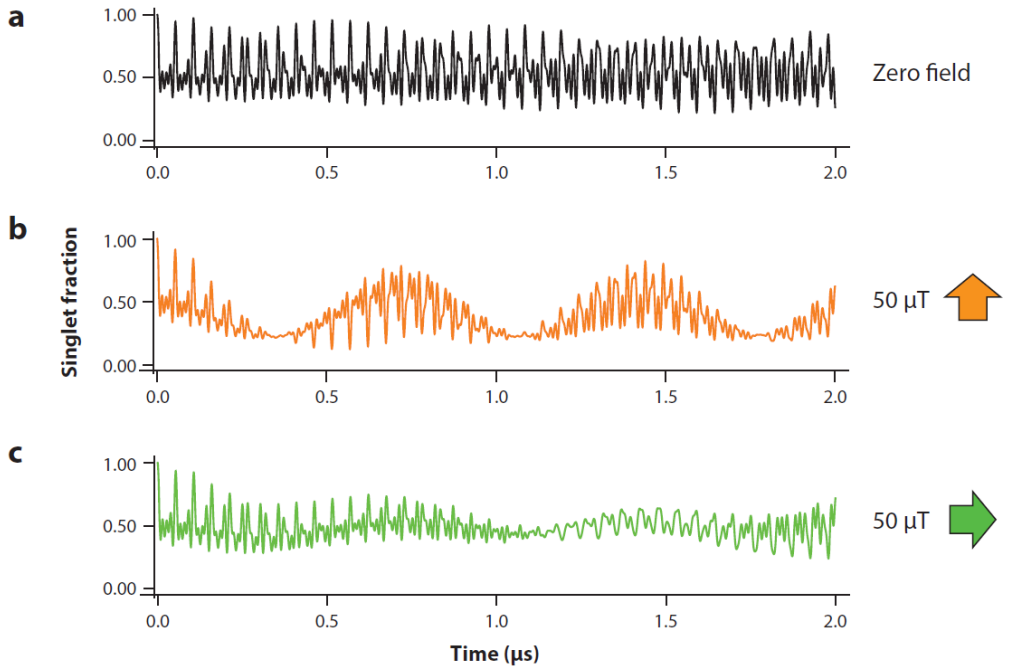


**Figure 2.3.:** Interconversion between singlet and triplet states in a simple radical pair model containing two nitrogen nuclei in one radical with anisotropic hyperfine interactions. The fraction of radical pairs in the singlet state is plotted over time, assuming an initial population entirely in the singlet state. (a) No external magnetic field; (b) with a $50\mu T$ magnetic field; (c) with a $50\mu T$ magnetic field rotated by $90°$. From [5].

symmetry in the molecular orbital of the unpaired electron is low. Therefore, as the anisotropy incorporates the directional component of the magnetic field into the radical pair reaction, the system is able to function as a magnetic direction sensor.

### 2.1.2 Cryptochrome

Cryptochromes (Cry) are a family of photo-receptor proteins that are found in various organisms and are known for their use in a diverse set of functions. Other than their implication in magnetoreception, Crys are well known for their role in the circadian rhythm and in regulating plant growth [54, 55, 56]. Crys are classified as a type of flavoproteins, meaning they are enzymes that have a flavin adenine dinucleotide (FAD) cofactor that is noncovalently bound to the protein at a FAD binding site [5, 24, 57]. The commonly upheld reaction scheme for magnetoreception through Cry involves FAD in a fully oxidized state. The FAD absorbs blue light and then gets reduced, which triggers a series of electron transfers from a chain of tryptophan (Trp) residues to the FAD. This forms a radical pair between the photoreduced FAD ($FAD^{\circ-}$) and the

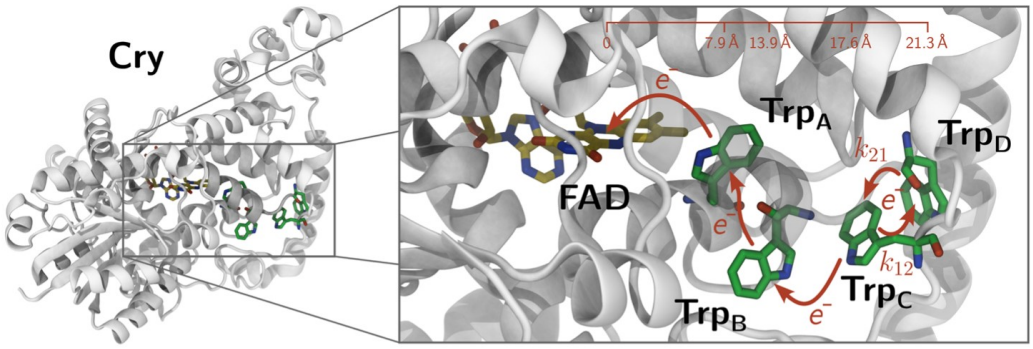


**Figure 2.4.:** Illustration of the cryptochrome protein structure depicting electron transfer to the FAD cofactor along the tryptophan chain. From [53].

oxidized Trp ($TrpH^{\circ+}$). Several alternatively proposed reaction schemes exist, which suggest that either a different radical pair is used or a different activation mechanism such as a light-independent activation by a reducing agent [22, 23, 58].

In insects, there are two types of Crys that can be found, the drosophila-like Cry1 that is light sensitive, and the mammal-like Cry2 that is light insensitive [12, 56]. For example, drosophilae only have Cry1 present, monarch butterflies have both Cry1 and Cry2, while honeybees have been found to only have Cry2 present [28]. Whether and how Cry2 can be involved in magnetoreception still requires further research because Cry2 has a low FAD-binding affinity, whereas the currently accepted radical pair reaction scheme in the RPM model is thought to rely on high-affinity FAD binding [56]. Studies by Gegear et al. [59] and Foley et al. [60] show that Cry1-deficient transgenic drosophilas did not respond to a magnetic stimuli, however, transgenic drosophilas lacking Cry1 but expressing Cry2 can recover their light-dependent magnetosensitivity, suggesting that Cry2 may still sustain the necessary reactions for magnetoreception. Another study by Bradlaught et al. [24] observed that a Cry1 modified to have the FAD binding site and the Trp chain removed still retains its light-dependent magnetosensitivity. The study also showed that a free FAD by itself without the protein can still induce a magnetic response through the formation of a radical pair, suggesting that the cryptochrome protein might be used to direct the radical pair closer to certain cellular effectors.

In both drosophilae and monarch butterflies, Cry1 is expressed in both the antenna and the eyes [12, 61, 62]. This was discovered through experiments in which the antennae or eyes of monarch butterflies were covered with black paint to reduce light exposure, resulting in a significant reduction in magnetoreceptive responses [12].

Similar results were found by Bazalova et al. [13] when the eyes of *P. americana* cockroaches, which only have Cry2 present, were treated the same way. Through the use of immunohistochemical staining, Cry2 was found to be located in the hemispherical layer of laminal glia cells underneath the retina of these cockroaches. While there is a lack of experimental data to show where Cry2 is found in honeybees, it is safe to assume that it would be found in their eyes and antenna, similar to other insects.

### 2.1.3 The Magnetosensitive Eye

Unlike other senses, magnetic receptors could in principle be found anywhere in the body of an organism as magnetic fields can penetrate all tissue types. However, as the RPM is a light dependent reaction and it was found that cryptochrome is expressed in the eyes of insects as observed by Wan et. al. [12] and Bazalova et. al. [13], that painting over the eyes of monarch butterflies and cockroaches disrupts magnetosensitivity, magnetoreception is most likely embedded in the visual system [5, 12, 13, 63]. The structure of the eye makes it the most optimal candidate location for RPM as it possesses dense sensory nerve endings that are responsive to light. Besides, the retina has a hemispherical structure that allows for immediate detection of the direction of the light [4]. The magnetic field would thus behave as a secondary stimulus, by modulating the primary light detection mechanism. However, to utilize this information, the organism must be able to discriminate between visual changes arising from light intensity and those induced by magnetic influences [5]. Therefore, magnetoreception is thought to be perceived as a pattern of light and dark generated by magnetic fields that is superimposed onto the normal vision of the animal [19].

To orient itself with magnetoreception, an animal can be imagined at the center of a pattern projected onto a surrounding sphere, allowing it to remain aligned with the magnetic field as it moves through its environment (Figure 2.5). For such a pattern to emerge, the radical pairs involved in magnetoreception must be somewhat oriented with each other, as complete rotational disorder would cause the directional information from the hyperfine interaction to be averaged out [5, 64]. Therefore, it was initially suggested that the cryptochrome within the cells of the retina, must not be randomly oriented. A study by Solov'Yov et al. [63] demonstrated that cryptochrome only needs one rotational degree to be fixed for there to be no significant negative impact on magnetoreception and that it would only need it to be embedded in the membrane. However, as cryptochromes are small water soluble proteins, they are not expected to be able to align themselves inside the cell membranes. Interestingly, a

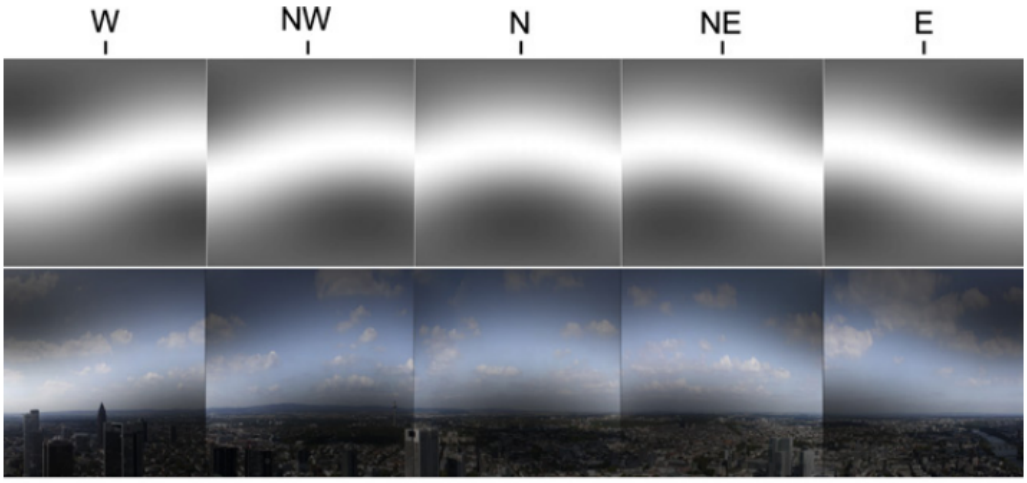


**Figure 2.5.:** An illustration showing a possible bright and dark pattern produced by magnetoreception, with the top row displaying the pattern alone and the bottom row showing it superimposed on normal vision for various directions. From [63].

study by Lau et al. [47] found that totally random oriented cryptochromes can still operate as a direction sensor utilizing the photoselection effect. The probability of light being absorbed by a molecule is proportional to $\cos^2 \Omega$, where $\Omega$ is the angle between the dipole of the electronic transition vector ($\boldsymbol{\mu}$), and the electric vector of the incident light ($\boldsymbol{e}$). As $\boldsymbol{\mu}$ is determined by the electronic structure of the molecule and its direction is fixed within the molecule, and because the electric vector is perpendicular to the propagation direction of light, the absorption of light is anisotropic. Therefore, the cryptochromes that get photoexcited would on average be in alignment with one another and the radical pairs created would have some amount of rotational order. Moreover, the light does not need to be polarized, as the anisotropic absorption is due to the fact that $\boldsymbol{e}$ is plane perpendicular to the direction of the light propagation. If the light were to be polarized, as sunlight is naturally polarized, the photoselection effect would then be more pronounced.

### 2.1.4 Decoherence

Environmental interactions lead to the decay of spin coherence between the two electrons, converting the radical pair from a quantum superposition to a classical mixture and thereby limiting the time it can respond to a magnetic field. However, the decoherence emerging from the nuclear environment of the molecule is essential for the spin dynamics of the radical pair, as it initiates the interconversion between the singlet and triplet states, allowing the external magnetic field to have an effect [48]. For a weak magnetic field ($\sim 50\ \mu T$) to modulate the spin dynamics of a radical pair,

both the lifetime of the radical pair and the spin coherence must last at least as long as the Larmor period of the electrons [5, 50, 51]. The Larmor frequency of an electron in a magnetic field with strength $B$ is determined by equation 2.3.

$$v_L = \frac{g_e \mu_B B}{h} \tag{2.3}$$

In this equation, $h$, $g_e$ and $\mu_B$ are Planck's constant, the g-value of the electron and the Bohr magneton, respectively. Thus, a magnetic field at the strength of the Earth's magnetic field ($\sim 50\ \mu T$), would have a Larmor frequency of $\sim 1.4$ MHz with a period of $\sim 700$ ns. Thus, the radical pair in cryptochrome is assumed to have a lifetime of approximately 1 $\mu$s [5, 50].

One of the key factors determining the lifetime of a radical pair in cryptochromes is the electron transfer rate. This rate depends on parameters such as the distance between the radicals and the redox potentials of the cryptochrome, which may be evolutionarily tuned to achieve an optimal lifetime [5, 65]. As for the spin coherence, spin relaxation is caused by the fluctuation of local magnetic fields from the stochastic modulations of the molecular thermal motions that the electron experiences. How spin relaxation can be sufficiently slow to allow generation of radical pairs within a protein at physiological temperatures ($\sim 40°C$) is uncertain, as little is known about spin relaxation in cryptochromes at weak magnetic fields ($\sim 50\ \mu T$). Some studies, such as by Luo et al. [50] and Kattnig et al. [66], propose that quick spin relaxation would not diminish directional sensitivity but could instead enhance it. Moreover, Luo et al. [50] propose that the fast spin relaxation brings about an extra population relaxation that can last for several milliseconds. The emergence of this slow population relaxation relies on the direction of the external weak magnetic field, which would then enhance the directional sensitivity of the radical pair.

### 2.1.5 Radio Frequency Magnetic Noise

Magnetic fields that oscillate at the same frequency as the singlet-triplet oscillation can modulate the rate of the singlet-triplet interconversion in the radical pair system and consequently modify the reaction yield [5, 42]. For radical pairs with one radical that lacks hyperfine interactions, this will cause a strong resonance to arise at the Larmor frequency. For a radical pair with a large number of hyperfine couplings, the singlet-triplet interconversion frequencies are distributed over a broader range, thereby enhancing the pair's susceptibility to magnetic fields of frequencies near the Larmor

frequency. Weak broadband electromagnetic noise with frequencies ranging between .1-10 MHz and intensities as low as 15 nT has been shown in many studies to disrupt magnetoreception in numerous species [6, 9, 67, 68, 69]. However, how a radio frequency field, that is significantly lower than the Earth's magnetic field (around 50 $\mu$T), influences an animal's magnetoreception is unknown in the current model of the RPM, as such an influence would require the radical pair to maintain a very long spin coherence lifetime [70].

## 2.2 Honeybee Vision

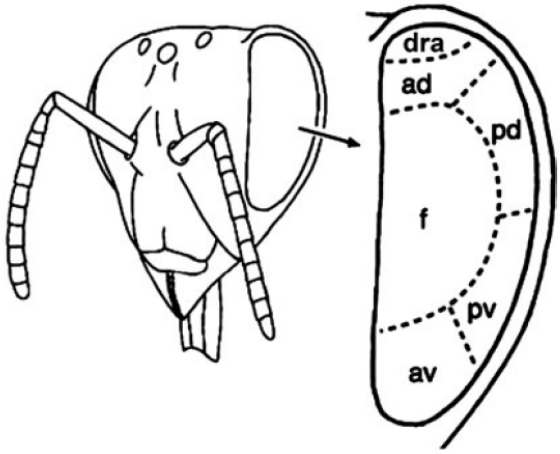


**Figure 2.6.:** Diagram of the honeybee head and compound eye showing labeled regions: dorsal rim area (dra), anterior dorsal (ad), posterior dorsal (pd), frontal (f), anterior ventral (av), posterior ventral (pv). From [3, 71].

The compound eyes of the honeybee (Figure 2.6) are made up of ommatidia, each having nine photoreceptor cells [3]. Moreover, in the photoreceptor cells, there are three possible types of photoreceptors present, each peaking in either the ultraviolet, blue, or green regions of the light spectrum (Figure 2.7). Thus, the ommatidia can be separated into three different types based on the composition of the types of photoreceptor present. Each ommatidium has six green photoreceptors, type I has one ultraviolet and one blue photoreceptor, type II has two ultraviolet photoreceptors, and type III has two blue photoreceptors. The function of the ninth photoreceptor is uncertain, but it is presumed to be UV sensitive [71]. Different ommatidial types are randomly distributed across the compound eye. However, there are two regions in the eyes where the three types of ommatidia are not spread randomly, the dorsal rim area (DRA), which contains more ultraviolet photoreceptors (type II), and the anterior ventral (AV) region, which contains more blue photoreceptors (type III) [3]. The DRA

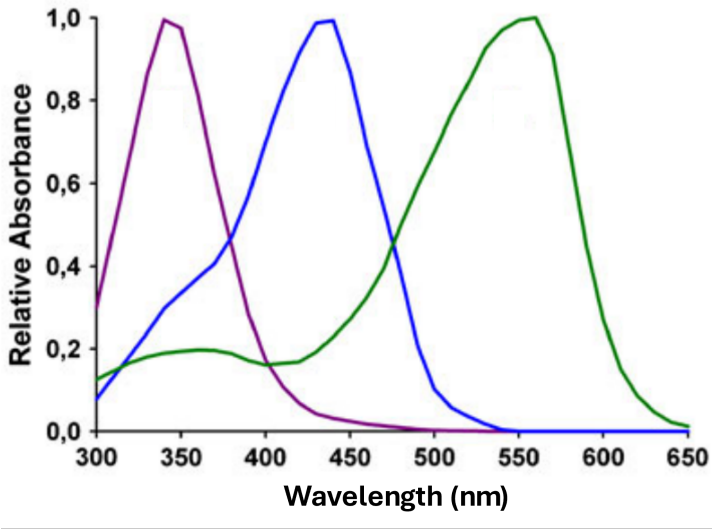


**Figure 2.7.:** Absorption spectra of honeybee photoreceptors sensitive to UV, blue, and green wavelengths. From [3].

is made up of orthogonally arranged polarization-sensitive ultraviolet photoreceptors that are suitable for the analysis of the sky polarization pattern for the sky compass [2, 72].

Visual information from the retina is conveyed to the central brain region through the optical lobe, which is composed of three visual neuropils: the lamina, the medulla, and the lobula [3, 33]. In the lamina, axons from the green photoreceptors connect to lamina monopolar cells, which serve as first-order processing interneurons responsible for receiving and relaying visual information from the photoreceptors [73]. The axons originating from lamina monopolar cells, together with those from blue and ultraviolet photoreceptors, project into the medulla, which houses color and spatial opponent neurons. These neurons compare inputs with opposing polarities, such as excitation by one wavelength and inhibition by another, thereby enhancing chromatic and spatial contrast in visual processing [74, 75, 76, 77]. The lobula contains as well many color and spatial opponent neurons that preserve and amplify the chromatic properties of the medulla neurons. Signals from the medulla and lobula travel through different tracks to the central brain and mushroom bodies, higher-order centers responsible for complex information processing [78].

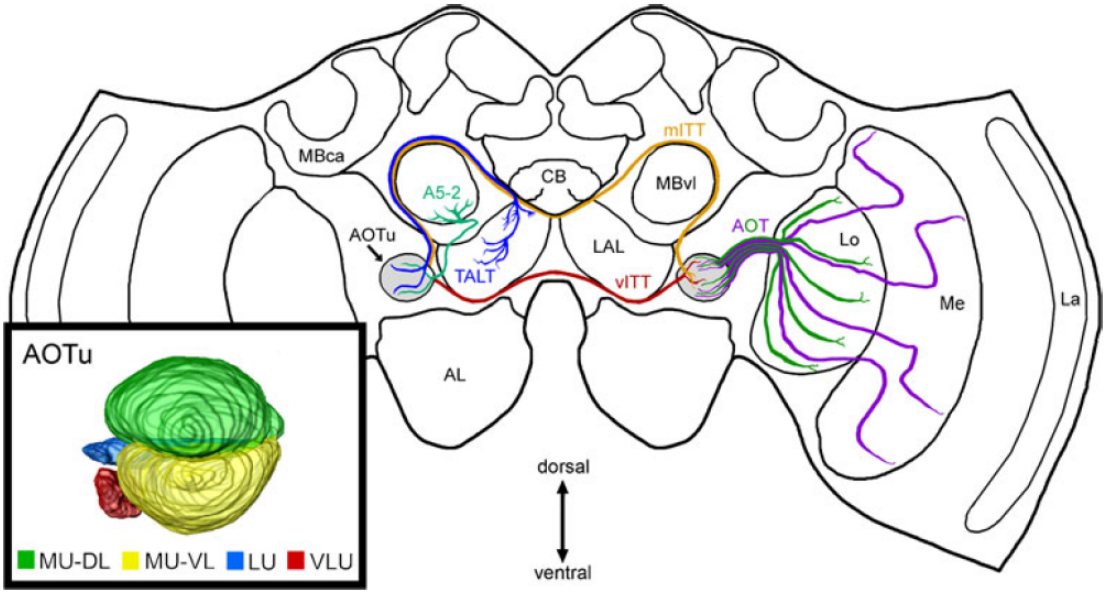


**Figure 2.8.:** Diagram depicting the neural connections between the AOTu and associated brain neuropils. Abbreviations: La, lamina; Me, medulla; Lo, lobula; AL, antennal lobe; MBvl, mushroom body vertical lobe; MBca, mushroom body calyx; CB, central body; LAL, lateral accessory lobe; AOT, anterior optic tract; vITT, ventral inter-tubercle tract; mITT, medial inter-tubercle tract; TALT, tubercle–accessory lobe tract. (left inset) Three-dimensional reconstruction showing the different compartments of the AOTu: major unit dorsal lobe (MU-DL, green), major unit ventral lobe (MU-VL, yellow), ventrolateral unit (VLU, red), and lateral unit (LU, blue). From [3, 33]

### 2.2.1 The Anterior Optic Tubercle

The visual input from the medulla and lobula travels via the anterior optic tract (AOT) to the anterior optic tubercle (AOTu), a higher-order visual structure [33, 79]. The structure and neural connectivity of the AOTu is depicted in Figure 2.8, where it can be seen that it is divided into four subunits, the major unit dorsal lobe (MU-DL), the major unit ventral lobe (MU-VL), the ventrolateral unit (VLU), and the lateral unit (LU). The output of the AOTu is sent to the lateral accessory lobe (LAL) by the tubercle accessory lobe tract. The AOTu of each brain hemisphere is interconnected by the ventral inter tubercle tract (vITT) and the medial inter tubercle tract (mITT). There is also a specific neuron described as the A5-2 neuron that links the AOTu with the vertical lobe of the mushroom bodies [80]. Both spatial and chromatic information are processed in different regions of the AOTu. Visual information from the dorsal and ventral parts of the eye are primarily processed in the MU-VL and MU-DL, respectively [33]. Similarly, ultraviolet and blue light produce stronger responses in the MU-VL and MU-DL, respectively; while green light produces a strong response in both the VL and

DL of the MU [7]. Visual input from the DAR of the eye travels through the dorsal medulla to the VLU before being sent further into the central brain, and is part of the sky compass neural pathway [81, 82]. The temporal dynamics of the AOTu differs with the type of light used, ultraviolet and blue light have an additional off response, while green light has a slow decrease in activity when the stimulus is turned off [7]. Different bright and dim combinations of blue and green light have different signal amplitudes, spatial patterns, and temporal dynamics than the monochromatic response, typically in a suppressive and nonlinear way. Such spatial and temporal chromatic processing in the AOTu supports the role of this structure in navigation and orientation.

# 3 Experimental Methods

## 3.1 Magnetic Coils Setup

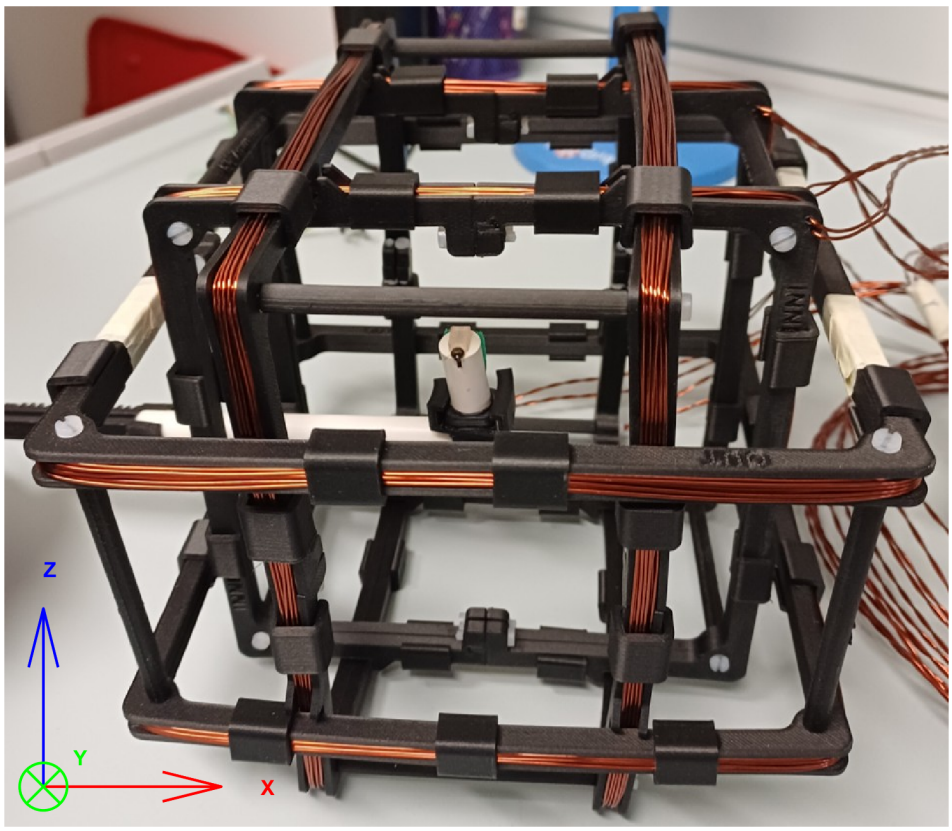


**Figure 3.1.:** Picture of the coil system without the shielding and with a bee mounted for a behavioral experiment in the center

The magnetic fields were generated using a three-axis coil system consisting of three square Helmholtz coils nested within one another, as depicted in Figure 3.1. A square Helmholtz coil is a pair of square coils that are separated from each other by the half of the length of the side of the square. When the current is passed through the two coils in the same direction, a uniform magnetic field is formed in the center. The separation distance of the largest coil pair was set to 90 mm as this would allow for the bee to be moved in and out of the coils during the behavioral experiments. Moreover the head of the bee would be in the center, as the height of the arm with the bee holder is approximately 45 mm. To allow the coils to nest within one another,

the nominal widths of each coil were 153.7 mm, 167.7 mm, and 181.7 mm, with corresponding gaps of 74.7 mm, 82.4 mm, and 90.0 mm for the inner, middle, and outer coil pairs, respectively. The magnetic field produced by each coil pair was simulated to verify that the field distribution was sufficiently homogeneous (Figure 3.2 and 3.3). The coils were composed by winding 1 mm diameter copper wire over 26 windings and distributed over 5 layers. Following the configuration outlined by Ahlers et al. [83], the individual coils were double-wrapped, meaning that two wires were independently wound around each coil in parallel to one another. When the windings of the individual coil are connected in series, the magnetic fields generated by both wires combine constructively, while in an anti-series configuration, the opposing fields effectively cancel out. Double-wrapped coils allow artifacts arising from electronic activation to be identified and distinguished from genuine magnetic field effects. A coil control unit was constructed to enable switching between series and anti-series configurations for each coil pair and to reverse the polarity of the magnetic field produced by each pair.

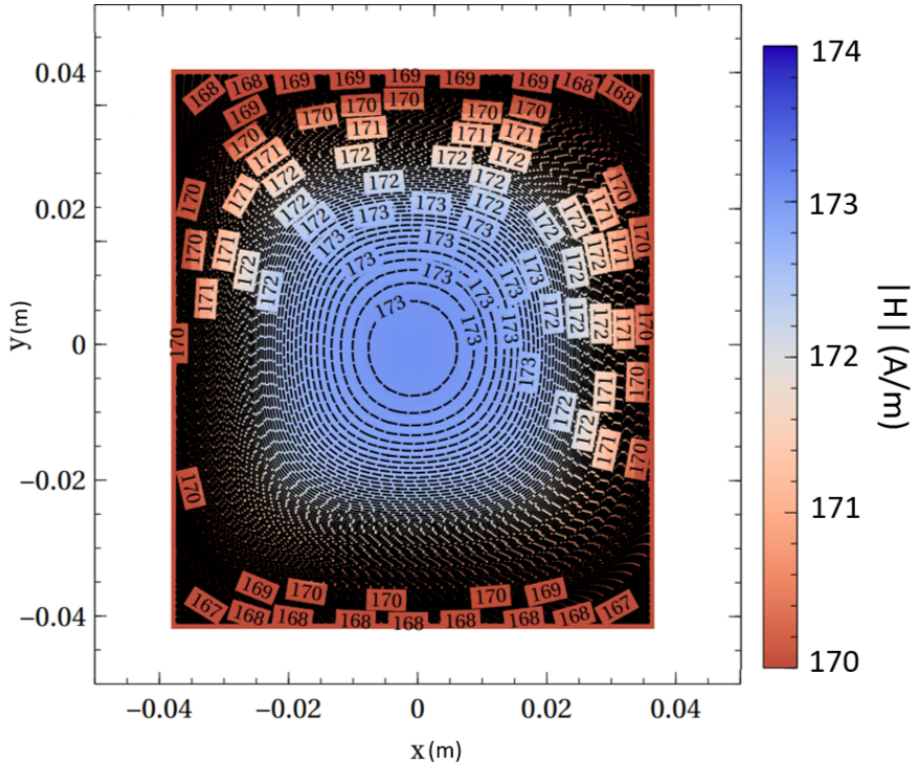


**Figure 3.2.:** Simulation of the magnetic field distribution in the central plane generated by the outer Helmholtz coil.

A power supply (Rohde & Schwarz; NGE100) was used to provide the current for the coils. This power supply can be controlled remotely and includes an EasyRamp feature that allows the output voltage and current to gradually ramp up over a defined time interval. To minimize electromagnetic interference, the coils were housed within a

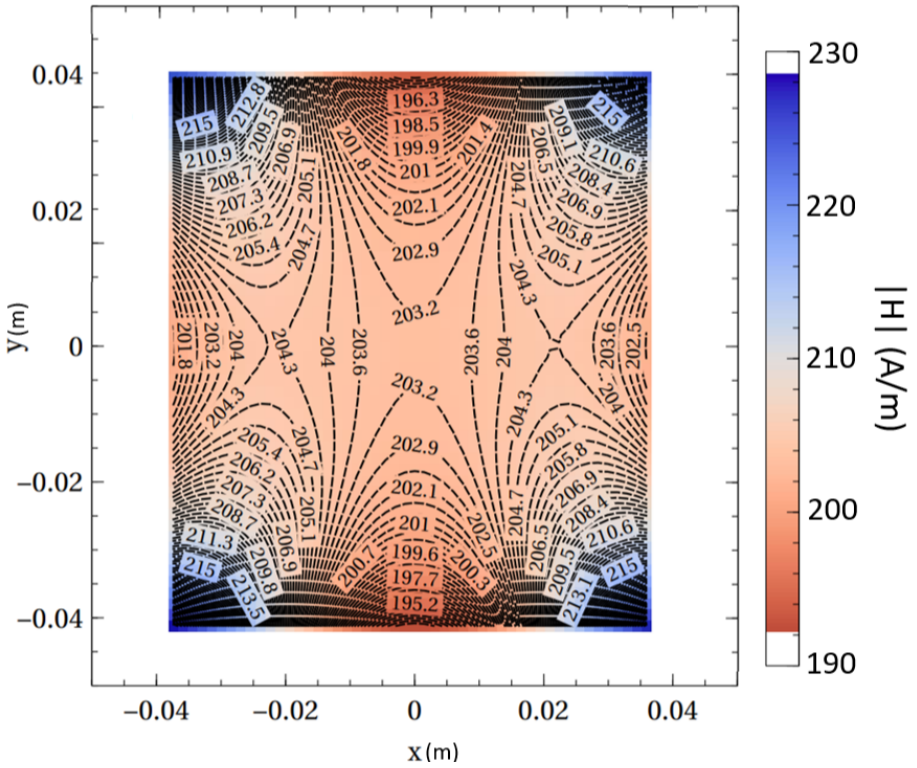


**Figure 3.3.:** Simulation of the magnetic field distribution 1 cm above the central plane generated by the inner Helmholtz coil.

1 cm thick aluminum enclosure to shield them from external radio-frequency magnetic fields. In addition, 0.5 mm thick mu-metal sheets (Holland Shielding) were placed on the exterior surface to remove static magnetic fields. Due to its high magnetic permeability, mu-metal channels magnetic flux, thereby diverting stray magnetic fields around the shielded enclosure, denying them to penetrate [84]. Since openings in the shielding are required, a small residual ambient magnetic field remains, which is compensated by using the coils.

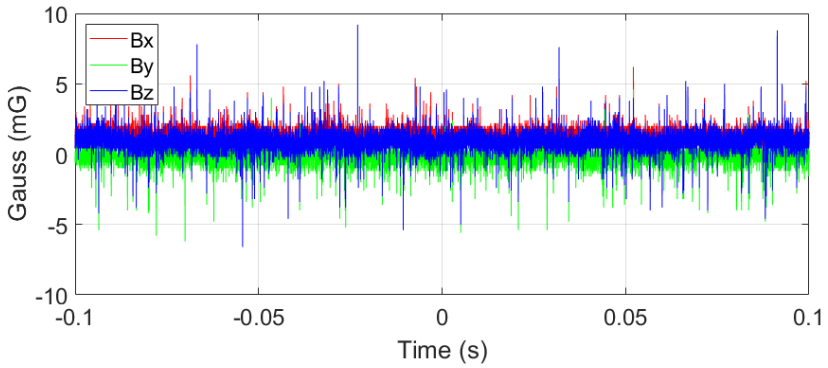


**Figure 3.4.:** Measurement of the zero magnetic field condition at the geometric center of the Helmholtz coils.

The resulting zero field condition produced a mean magnetic field of 1.3 mG, 0.2 mG, and 0.9 mG in the *X*, *Y*, and *Z* directions, respectively, with corresponding standard deviations of 0.7 mG, 0.6 mG, and 0.7 mG (Figure 3.4). The magnetic stimulus was generated by producing a 0.5 Gauss magnetic field in the *X* direction from an initially zero-field condition. To minimize high-frequency noise induced by sharp pulses, a current ramp was used and set to a 0.5-second ramp time to smooth the pulse shape (Figure 3.5a). For stimuli involving a gradual rise in the magnetic field, the current ramp was configured with a 5-second ramp interval (Figure 3.5b). For consistency and ease of interchange between the behavioral and two-photon experiments, an identical coil system and field parameters was employed in both configurations.

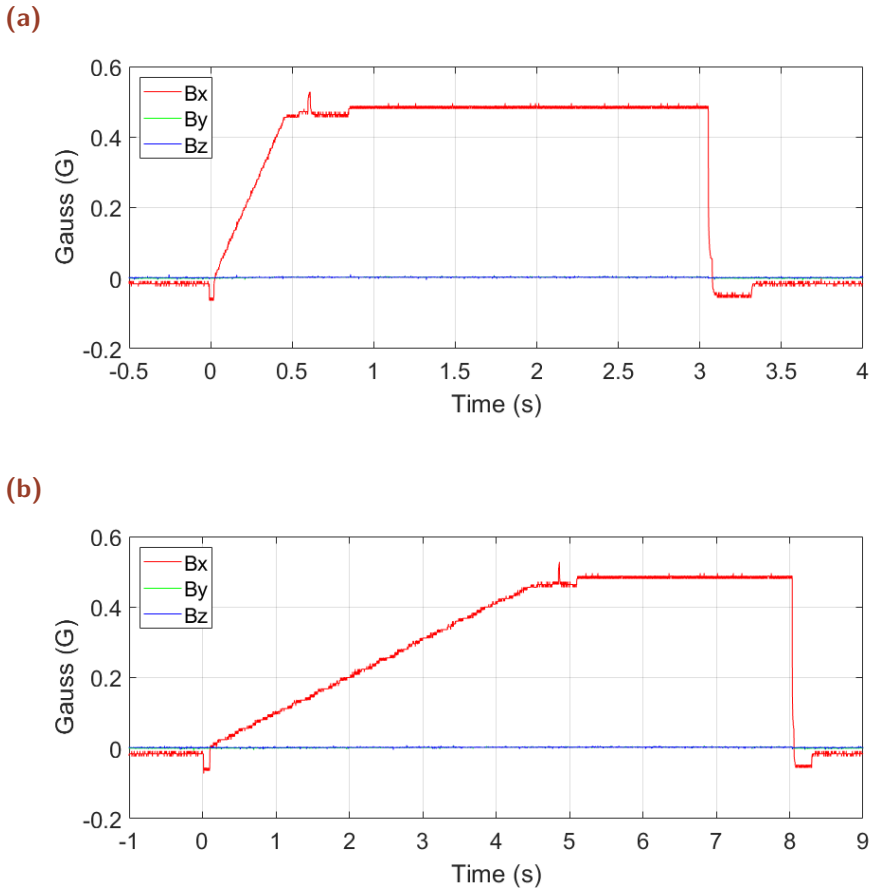


**Figure 3.5.:** Measurements of the 0.5 G magnetic field stimulus along the *X*-axis with (a) 0.5-second ramp time and (b) 5-second ramp time.

## 3.2 Classical Conditioning

Bees can be reliably trained to associate a variety of different stimuli, such as olfactory, visual, and mechanical stimuli, with a sucrose reward through classical (Pavlovian) conditioning [35, 39, 41]. Classical conditioning is a procedure where an association is formed by pairing a condition stimulus (CS), which does not trigger a behavioral response, with a biologically significant stimulus, the unconditioned stimulus (US) [35, 36]. With successful association, the unconditioned response can be triggered by the onset of the condition stimulus. For bees, a sucrose solution serves as the unconditioned stimulus (US), triggering the proboscis extension reflex (PER). When sucrose is applied to their antennae, they extend their proboscis, which constitutes the unconditioned response. The typical protocol for olfactory conditioning of harnessed bees is that an odor is delivered to the antenna, then after a few seconds the PER is triggered and the bees are fed some sucrose solution, producing a brief overlap of the CS and US. After a few trials, the bees will extend their proboscis with the onset of odors alone with a high success rate, between 80-90%.

Training harnessed bees with visual stimuli has been shown to be more difficult, it takes longer to learn, and has a much lower success rate ($\sim$50%), than with olfactory stimuli [38, 39, 40]. Consequently, there is no standard protocol when using visual stimulus and most studies have their own distinct set of parameters [38]. Compared to olfactory experiments, visual experiments require more trials and a longer duration of the stimuli. The stimuli also need to be on throughout the duration of the US (Figure 3.6), as turning off lights can cause an afterimage, as shown by Hori et al. [39] where bees were trained to react to red light but when testing with blue light, they only extended their proboscis when blue light was turned off, as the resulting afterimage appeared red.

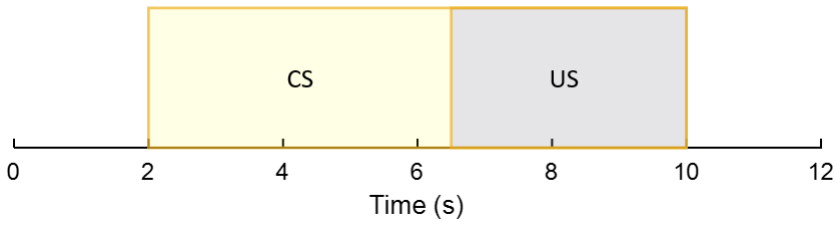


**Figure 3.6.:** Pulse sequence for PER training with a visual stimulus, where the yellow rectangle represents the conditioned stimulus (CS) and the blue rectangle represents the unconditioned stimulus (US). The CS persists for the entire duration of the US.

### 3.2.1 Bee Behavioral Preparation

**Figure 3.7.:** Picture of bee in the bee holder, showing the head holder at the top and the sponge at the back

Honeybees were collected from outdoor colonies kept at the University of Trento facilities in Rovereto, TN, Italy. The preparation of the honeybees was based on the procedures previously described in literature ([35, 36, 40, 41]). In brief, foragers were individually collected in front of the hives during the afternoon and were immobilized by placing them in ice until they stopped moving. They were then mounted in a holder by sliding their neck into the gap of the bee mount and their head was fixed by the head holder that was pushed into the slot of the bee mount until the back of the head holder was aligned with the back of the mount (Figure 3.7). A sponge was also placed at the back of the bee to restrict some of the motion of the bee's body and make it more comfortable. After all the bees were harnessed, they were all fed 4 droplets. Each droplet was approximately 4 $\mu$L of a 35% (w/w) sucrose solution. The bees were then placed in a dark box with a wet paper towel and kept overnight to starve them. One hour before the start of the experiment the PER of the bees were tested by touching their antenna with the sucrose solution. Only bees demonstrating a robust response were included, which generally accounted for about 90% of the tested individuals. They were then placed back in the box to keep them in a dark environment prior to the experiment.

### 3.2.2 PER Setup

(a)

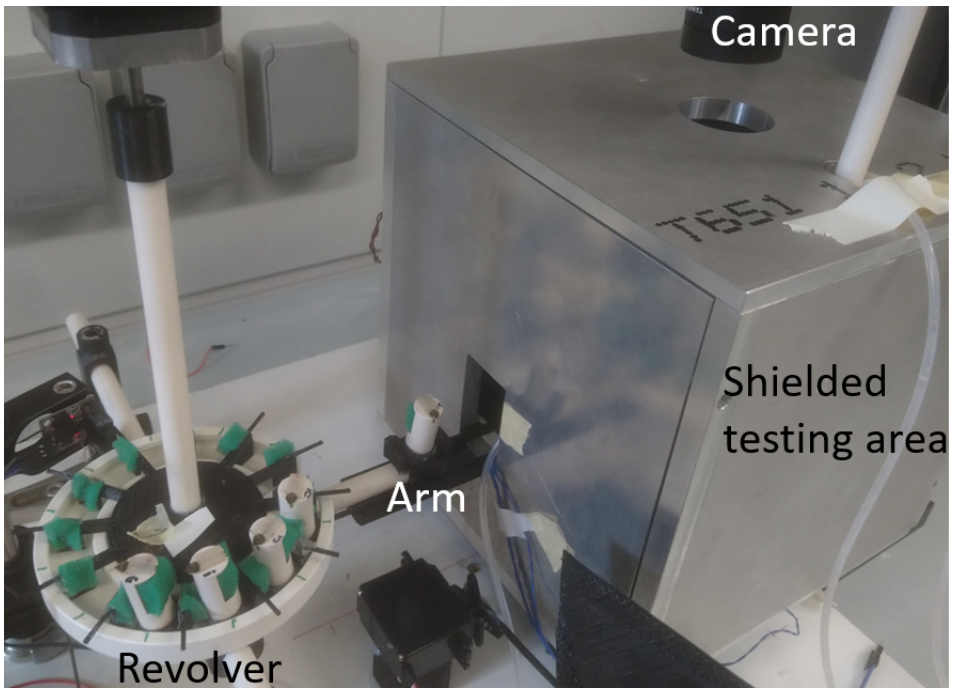


(b)

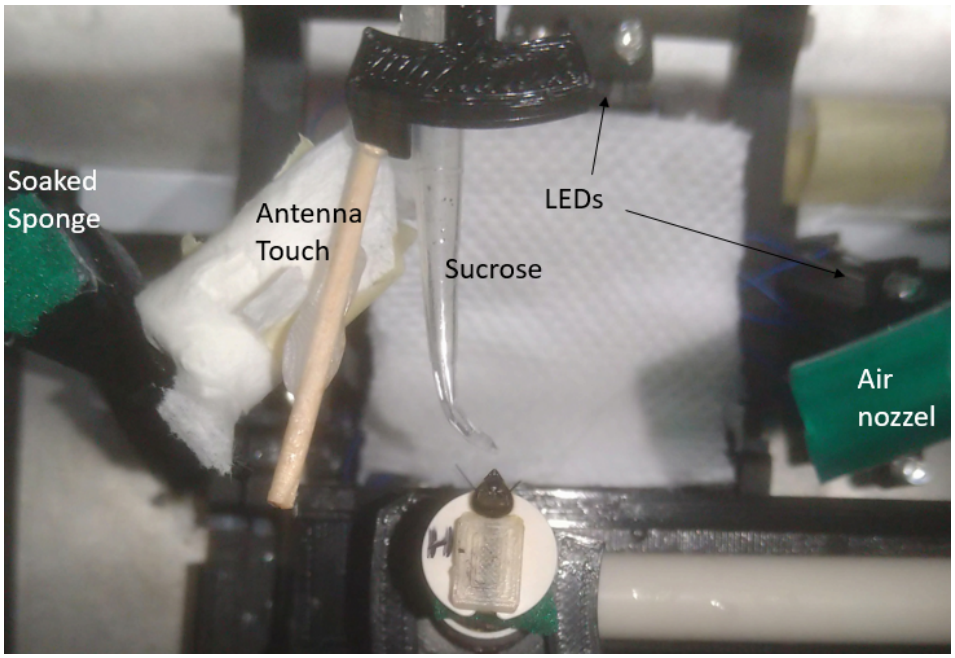


**Figure 3.8.:** The full setup for the behavioral experiment. (a), The automated setup for the behavioral experiment showing the bee revolver, the mechanical arm and the shielded testing area. (b) Inside the testing area showing the components needed to condition the bees.

The experimental setup and protocol used for the PER experiments was based on the work from Strelevitz et al. [41]. The setup was modified so that bees could be transferred in and out of the center of the magnetic coil set, with the testing area located away from the waiting site to reduce potential effects of stray magnetic fields between trials. Our setup (Figure 3.8 and 3.9) consisted primarily of a revolver, an arm, a feeder, a stimulus generator, and a camera. The revolver had a plastic ring where 12 bees could be placed, and a rotator that moved the bees around the ring, as depicted in Figure 3.8a. The rotator used a stepper motor with a micro-stepper driver to allow for 1/16 micro-steps for a smoother rotation. A rotary encoder was used to determine the correct position of the next bee on the arm. The bees were moved from the revolver to the center of the testing area (Figure 3.8b) with the arm that is attached to a gear rack, driven by a gear attached to a DC motor. Arm positioning was regulated using two position encoders, and to ensure consistent alignment, the arm was guided along a bridge with a groove. The feeder was composed of a bent 100 $\mu$L pipette tip and a sucrose-soaked toothpick attached to a servo motor. A syringe attached to a microinjector was connected to the pipette tip of the feeder to make a droplet of sucrose solution that was between 2-3 $\mu$L at the end of the pipette tip. A set of 6 blue LEDs were positioned in, under and around the bee to use as visual stimuli, while the magnetic stimuli were created using the setup as described in 3.1. A camera was placed above the bee to record the response of the bee during the trial. In addition a rectangular piece of plastic, attached to a servo motor, blocked any light coming out of the entrance of the testing area and a tube inside the testing area aimed at the head of the bee continuously blew low pressure air, as it increases responsiveness of the bees. The hardware was governed by Arduino boards programmed to control the activation and motion of the motors, sensors, and LEDs (Figure 3.10). These boards operated in response to a predefined set of serial commands sent from the computer.

Experiments using visual or magnetic stimuli were performed in a dark room. The bee was given 25 s of familiarization after it was moved to the center of the testing area. The CS was then applied for a total of 8 s with the last 3.5 s having both the CS and US applied. The bee then had 7 s of rest before being moved out of the testing area and the next bee was moved in. To condition the PER with the feeder, the toothpick that had been soaked in a sucrose solution was rotated above the head of the bee, touching the antenna, while a small droplet of sucrose solution was fed to the bee. Initially touching the antenna was necessary as it helped the bee notice the droplet for feeding. The toothpick with the sucrose solution was kept on a wet sponge to prevent the drying out of the solution during the experiment. Before the start of the experiment, the position of the feeder was adjusted such that both the tip of the toothpick, which was

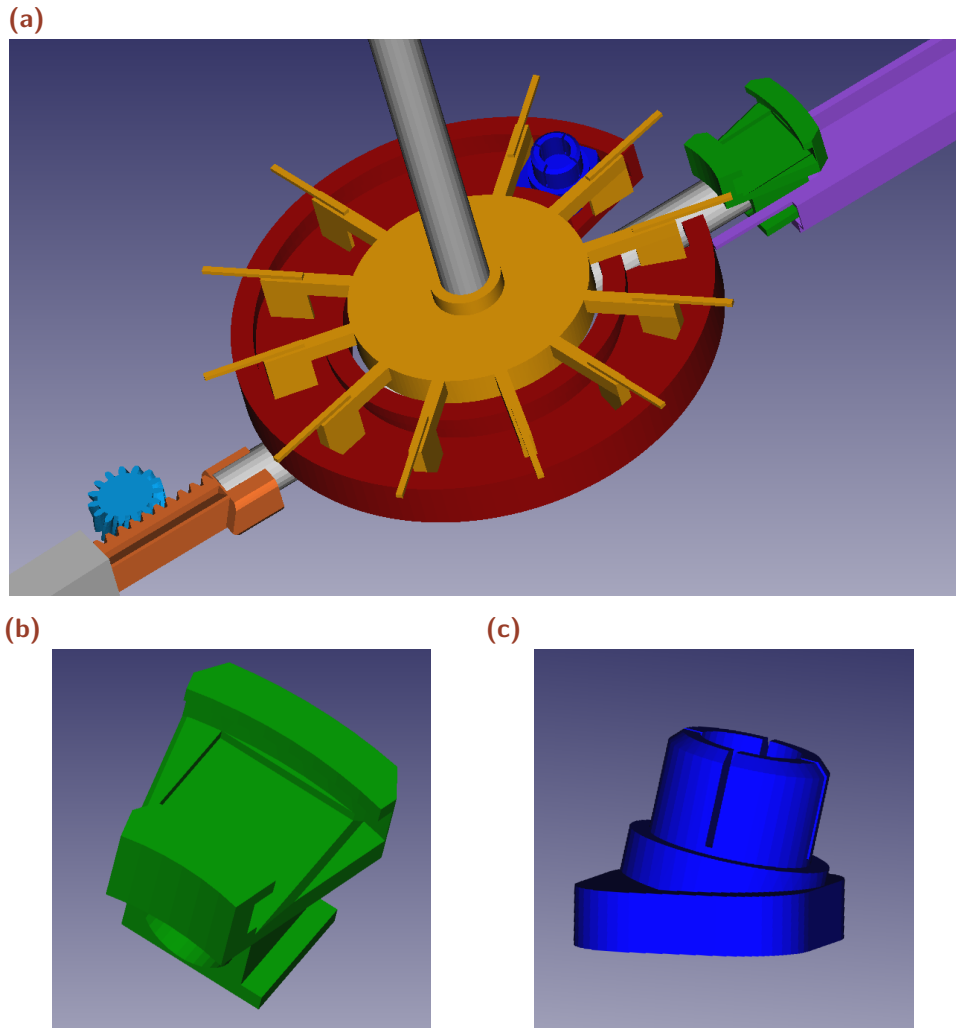


**Figure 3.9.:** 3D schematic of the mechanical assembly: red indicates the plastic ring, yellow the rotator, blue the base of the bee mount, green the base of the arm, orange the arm's gear rack with the light blue gear, and purple the bridge. (b) Close-up of the arm base. (c) Close-up of the bee mount base.

able to make contact with the antenna without colliding with the head, and the pipette tip with the droplet was within reach of the proboscis for all of the bees.

The experiment was automated and run through a Matlab code that contained the parameters for all of the sequencing and time, commanded the Arduino boards, and controlled the video recording of the camera. The first two trials were with unpaired stimuli in order to get the bees familiarized with the movement of the setup. The next two trials were paired, and the subsequent trials were alternated between paired and unpaired, yielding a total of 20 trials, 10 of each. In the trials with the unpaired stimulus, the feeder still rotated slightly to keep the variations between the paired and unpaired trials low. The duration of the trial with the time it took to move to the next

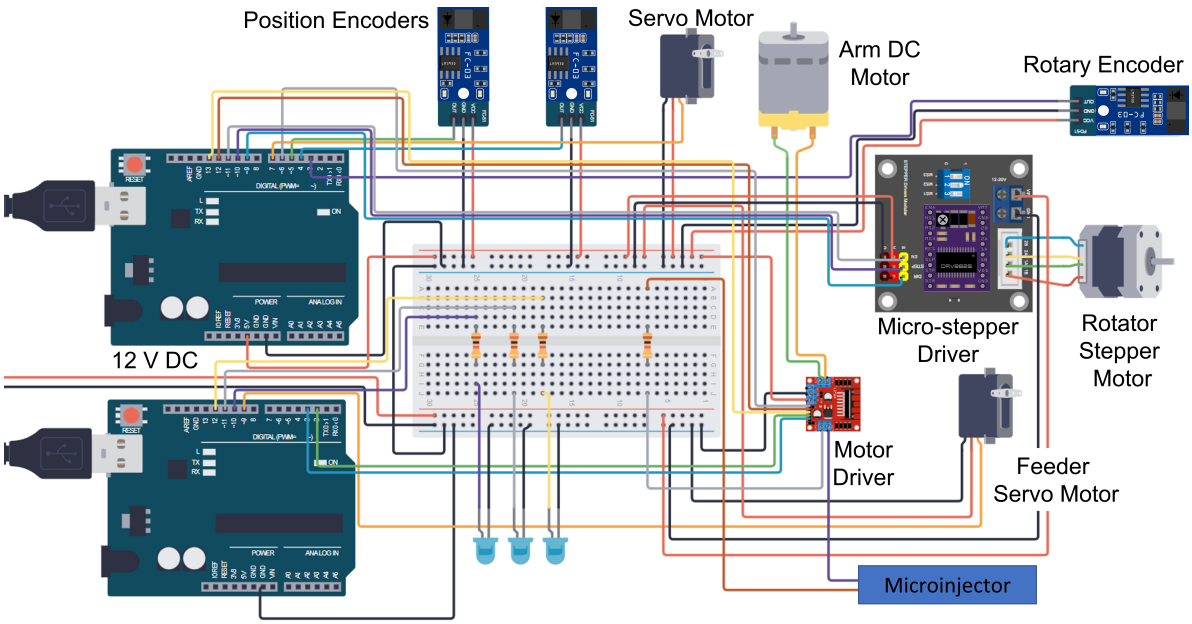


**Figure 3.10.:** Schematic diagram of the electrical circuit used for PER training.

bee led to an inter-trial time of 18 minutes. Each of the frames of the recording was classified using the convolutional neural network (CNN) model from Strelevitz et al. [41] (Figure 3.11). The frames were classified as licking if the proboscis was extended beyond the mandibles' of the bee and as rest otherwise. This provided the temporal dynamics of the bee's decision to extend its proboscis along with the conventional binary response. At the end of the experiment, the bees were marked on the thorax with a colored dot and then released.

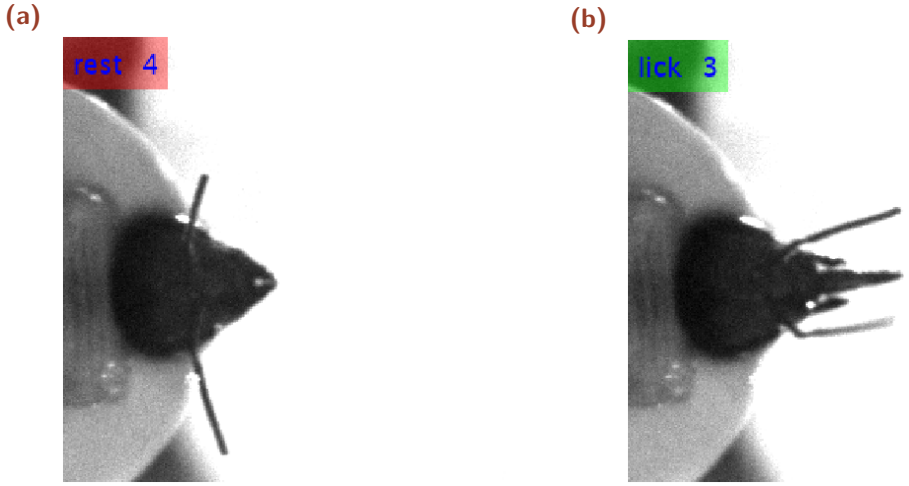


**Figure 3.11.:** Illustration of labeled frames from camera recordings showing (a) the resting state and (b) the licking state.

## 3.3 Two-Photon Calcium Imaging

One of the methods of recording neuronal activity is by measuring the change in calcium levels through the use of calcium-binding fluorescent molecules with fluorescence microscopy [85]. Briefly, when a neuron fires an action potential, it increases the level of intracellular calcium $Ca^{2+}$. Therefore, the amount of intracellular calcium is related to the activity of neurons. In addition, there are multiple types of chemical and genetically coded calcium indicators, each with different binding characteristics, and one of the most commonly used is Fura-2 due to minimal leakage from cells, which ensures high spatial contrast [86]. Fura-2 is a ratiometric calcium indicator whose absorption peak shifts from 340 nm to 380 nm as $Ca^{2+}$ transitions between the bound and free states, with an emission peak around 510 nm for both states. When Fura-2 is excited at wavelengths corresponding to its $Ca^{2+}$ bound state, the observed fluorescence decreases proportionally with increasing neuronal activity. Among the various types of fluorescent microscopes used to monitor brain activity, two-photon fluorescence imaging is particularly well suited for *in vivo* calcium imaging in the brain.

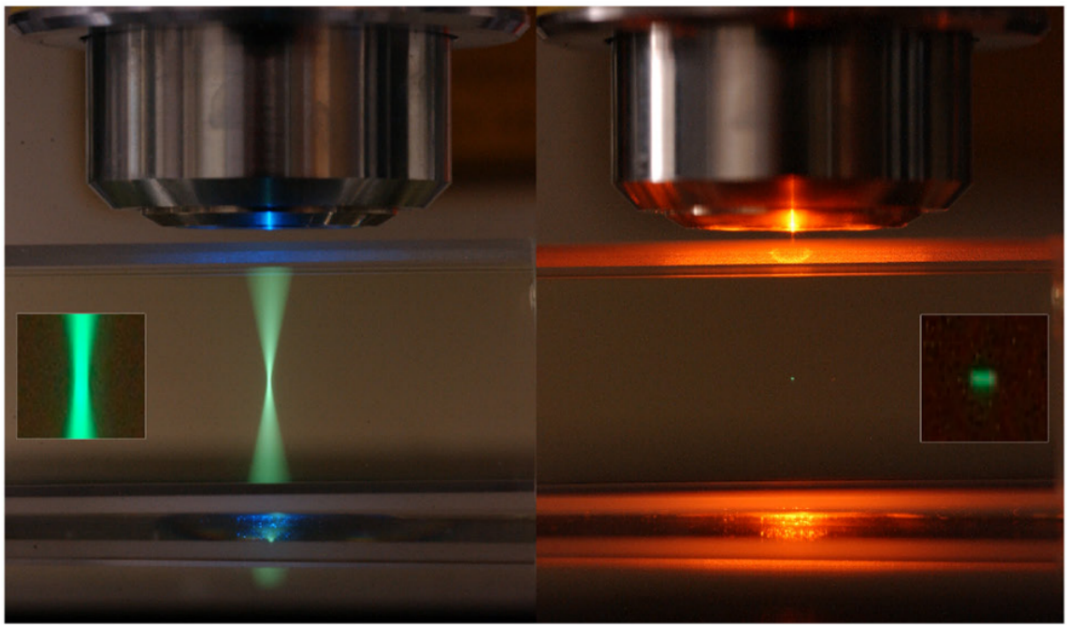

**Figure 3.12.:** Image illustrating the difference in excitation volume of fluorescence obtained with single-photon microscopy (left) versus two-photon microscopy (right). Image by Steve Ruzin and Holly Aaron at UC Berkeley

In two-photon fluorescent imaging, two lower-energy photons arrive at the fluorescent molecule simultaneously (within ~0.5 fs) and their energy is combined to excite a molecule [31, 87, 88]. The excitement is a non linear process as it uses higher-order

light-matter interactions and the probability that two photons will be absorbed is proportional to the light intensity squared. The intensity of a focused beam is highest at the focal point and decreases quadratically before and after the focal plane. As a result, in two-photon microscopy, absorption is localized to a tiny region near the focal point. This differs from single-photon microscopy, where absorption can occur anywhere within the light cone (Figure 3.12). To generate an image, the focused beam is scanned across the sample and as excitation is constrained to be almost entirely in the focal plane, high three-dimensional resolution is achieved. Moreover, to achieve a sufficiently strong signal, very short pulses with high intensity are needed, as it will increase the probability that two photons interact with a molecule while maintaining the overall power low [87, 88]. Other benefits of using two-photon microcopy, is that the imaging depth is deeper and has low photobleaching and phototoxicity. The imaging depth of 1 mm in tissue with two-photon microcopy is possible since it commonly uses near infrared light that has a higher penetration depth in tissues than visible light, and it is less affected by light scattering as all acquired fluorescence photons are assumed to have originated from the focal volume[31, 32]. Similarly, photobleaching and phototoxicity are limited to the focal plane due to the absence of out-of-focus excitation and low one-photon absorption of infrared light in tissue[31, 87]. Photobleaching is caused when an excited fluorophore can transfer energy to oxygen molecules present and create reactive oxygen species, which can damage the fluorophores making them unable to fluoresce [85, 87, 89]. Phototoxicity is the damage of the tissue when it is exposed to the laser, which is typically the result of the laser heating the tissue or the reactive oxygen species interacting with the tissue.

### 3.3.1 Two-Photon Setup

The optical setup for calcium imaging (Figure 3.13) was composed of a two-photon microscope (Ultima IV; Bruker) integrated with an ultra-short pulsed laser (Mai Tai Deep See HP, Spectra-Physics) tuned to 780 nm for Fura-2 excitation. The configuration of the microscope was epi-fluorescence with a 20x water-immersion objective (NA 1.0; Olympus; XLUMPLFLN20XW). The fluorescence was passed through a 525 $\pm$35 nm filter (Chroma) and captured by a photomultiplier tube (PMT) (Hamamatsu; PN H11706-40). The laser power was between 4 and 5 mW and allowed for an optimal signal-to-noise ratio with minimal photo-damage after prolonged exposure. Given that the width of the AOTu is approximately 120 $\mu$m, images were acquired at a resolution of 128 $\times$ 128 pixels with a pixel size of 2 $\times$ 2 $\mu$m allowing for a sufficiently fast acquisition rate of approximately 6 Hz.

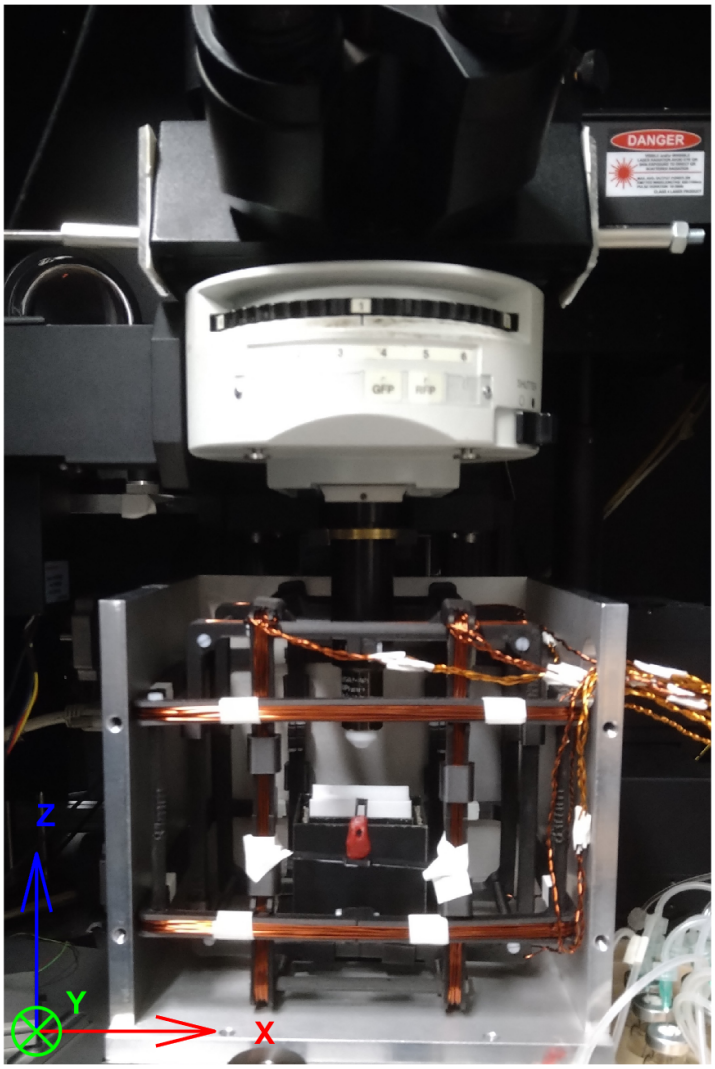


**Figure 3.13.:** Image of the two-photon imaging apparatus showing the coil assembly and shielding.

### 3.3.2 Data Analysis

Two-photon calcium imaging data were processed and analyzed using custom MATLAB scripts, treating each bee and recording separately. Each recording generated multi-frame TIFF files representing consecutive two-photon scans over time, which were assembled into three-dimensional datasets, with each element reflecting fluorescence intensity at a specific spatial location and time point.

For visualization and selection of the region of interest (ROI), the images were averaged into a single image. Within each ROI, mean fluorescence was calculated across all spatial pixels, resulting in a time series trace that captured the temporal

dynamics of calcium-dependent activity. Since increased neural activity raises extracellular calcium and subsequently decreases Fura-2 fluorescence, the traces were inverted according to standard practice so that neural activation appears as a positive signal change. To improve signal quality, the extraction process included optional detrending to remove slow baseline drifts, deconvolution to compensate for the calcium indicator decay constant, and high-pass filtering to reduce low-frequency noise.

Each recording comprised multiple stimulation trials, which were segmented using stimulus timing information. Responses were characterized over defined pre-stimulus (5 s) and post-stimulus (5 s) intervals. For every ROI and stimulus condition, individual trials responses were aligned to stimulus onset and normalized to their pre-stimulus baseline, expressing changes as percentage variations in fluorescence ($-\Delta F/F$). Trials were averaged to derive the mean response and its standard deviation. ROIs demonstrating fluorescence changes greater than 1.96 times the pre-stimulus standard deviation were designated as significantly active and the standard deviation region of the curve was highlighted from blue to red, corresponding to a 95% confidence threshold. To statistically assess changes in activity, paired t-tests were performed for each ROI and stimulus, comparing pre- vs. stimulus, post- vs. stimulus, and pre- vs. post-stimulus periods across trial. Results appeared as bar plots illustrating mean fluorescence changes; statistically significant differences were indicated by red bars.

Time–frequency analysis was performed using Fourier transform and continuous wavelet transforms implemented in MATLAB. The Fourier transform was employed to identify any spikes within the frequency spectrum, while complex Morlet wavelets were used to decompose the signal into its frequency components, allowing for the examination of temporal changes in power across specific frequency bands.

### 3.3.3 Bee Imaging Preparation

The honeybees were prepared using methods adapted from previously published procedures [33, 90]. In brief, returning foragers honeybees were collected in front of their hives between 10 and 12 in the morning using a small plastic container. They were immobilized by chilling on ice until they ceased to move and were then placed in a custom-made Plexiglass mount, depicted in Figure 3.14a. A wedge-shaped piece of soft dental wax was slid between the bee's head and the top of the mount to immobilize the head. A sponge was placed behind the bee's body to support it and to limit movement. The bee was then fed a droplet of 5-6 $\mu$L of a 50% (w/w) sucrose

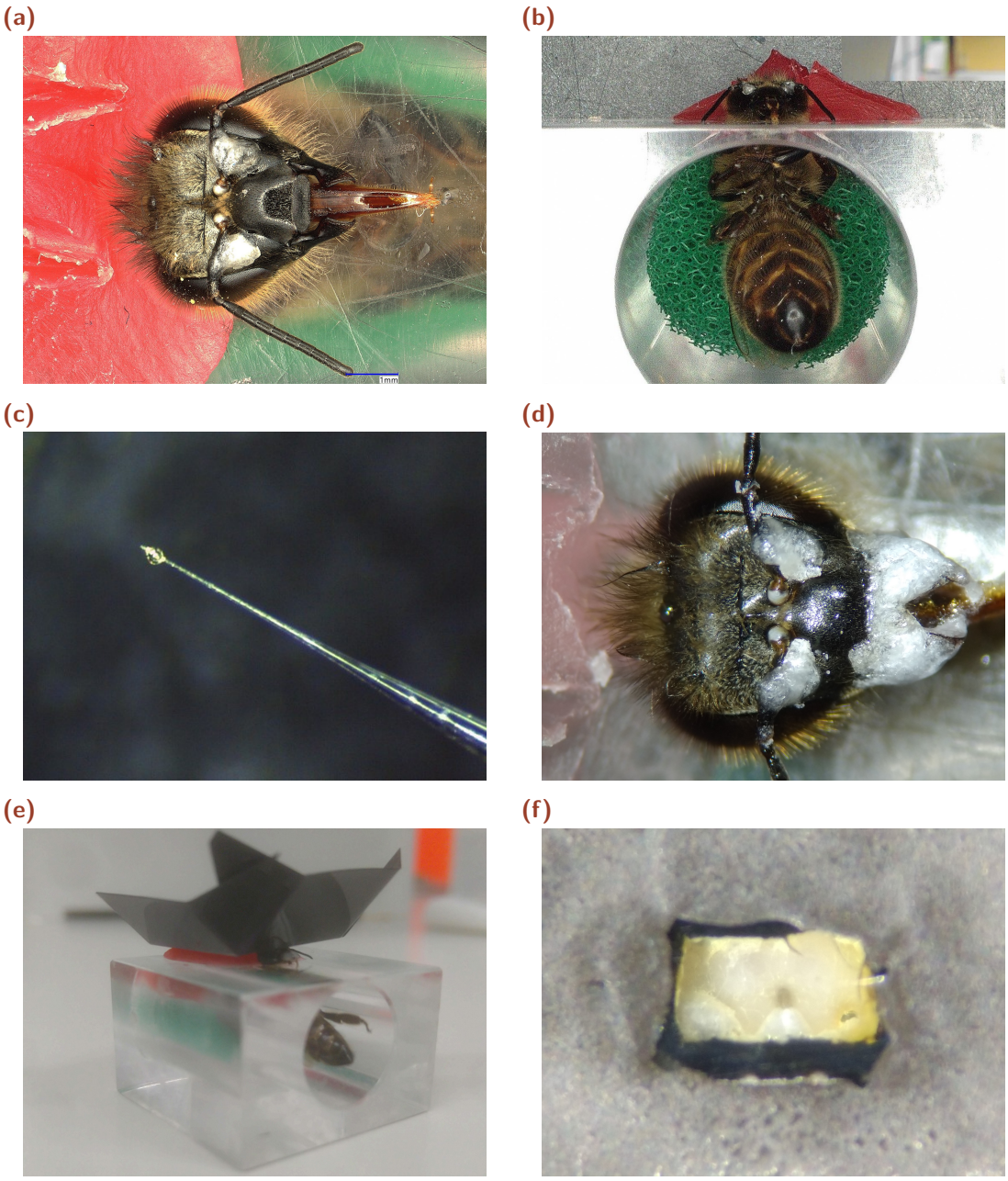


**Figure 3.14.:** Images illustrating the steps of bee preparation: (a) head fixed with wax, (b) bee mounted with a sponge at the back, (c) injection needle prepared with crystallized Fura-2 at the tip, (d) bee head with antennae and mandibles immobilized using n-eicosane, (e) prepared bee with plastic shield, (f) brain window visible at the top of the shield.

solution, to ensure that it would survive the preparation procedure. The movement of the antenna were restricted by using a thin bent copper wire and were fixed with a droplet of n-eicosane was placed at the base of each antenna (Figure 3.14b). The copper wire was then removed and a rectangular window was cut into the head cuticle and removed. The salivary glands on the left side of the brain were pushed aside or

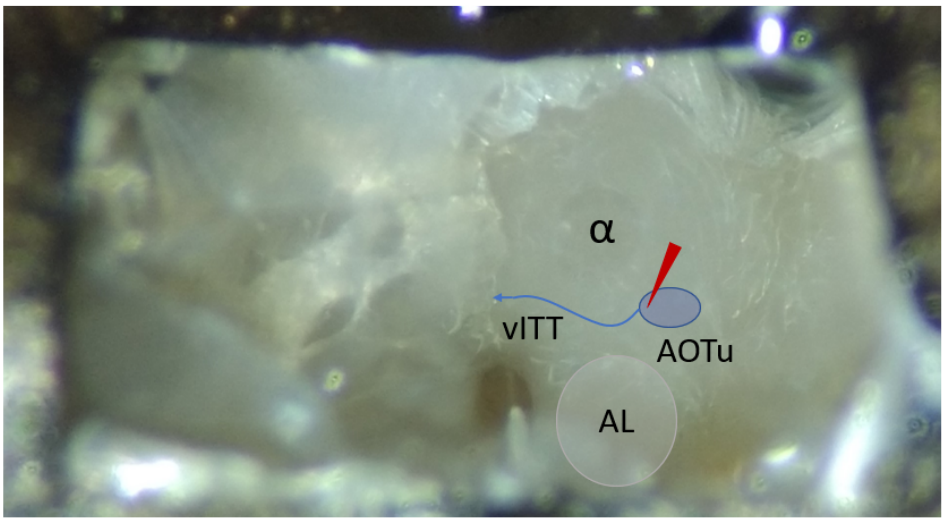


**Figure 3.15.:** Image of the bee brain with tracheae cleared on the right side; the injection site is indicated by a red triangle. The bee's antennae are oriented downward.

removed and part of the tracheae near the left AOTu was also carefully removed to expose the injection site. Three borosilicate glass needles each with a small amount of crystallized Fura-2-dextran (ThermoFisher Scientific) at the tip (Figure 3.14c) were injected into the left AOTu (Figure 3.15). The original piece of the cuticle was used to close the head capsule and the bee was fed a droplet of 3 $\mu$L of the 50% (w/w) sucrose solution. The bees were kept overnight in a dark and moist container allowing for the dye to travel to the right AOTu through the vITT. The next morning the bee's mandibles were immobilized with n-eicosane to reduce the bees' movement (Figure 3.14d), the head capsule was opened again, and the salivary glands and tracheae on top of the right AOTu were delicately removed. Most of the hemolymph atop of the brain was removed with a piece of paper towel and a droplet of transparent two-component silicone (Kwik-Sil; WPI) was used to seal the head. Before the silicone cured, a thin plastic sheet was placed on top of the bee's head in contact with the silicone (Figure 3.14e). The front and the sides of the plastic sheet were bent upwards and the entire sheet was painted with black acrylic paint, except for a small window to view the brain (Figure 3.14f). The brain activity in each bee can subsequently be recorded for 3–4 hours, until responses become undetectable.

### 3.3.4 Visual Stimulation

A visual stimulus was created using a single-mode diode laser (TOPTICA) that was coupled to an optical cable, which had a wavelength of 473 nm and a maximum output power of 50 mW after the optical cable (Figure 3.16). The laser beam traveled

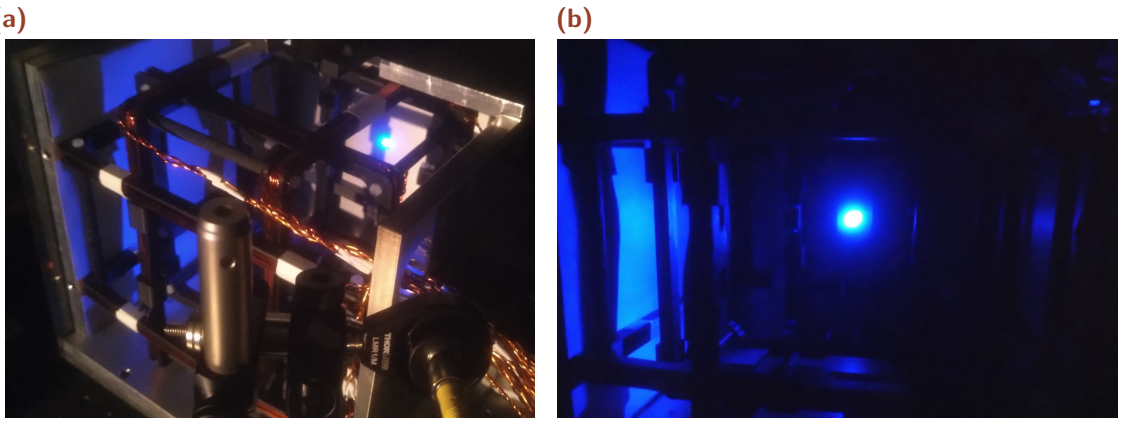


**Figure 3.16.:** Images depicting the visual stimulus: (a) side view showing the laser path through the hole in the shield before striking the back and scattering to the sides, (b) front view illustrating the laser hitting the back and scattering along the sides of the shield.

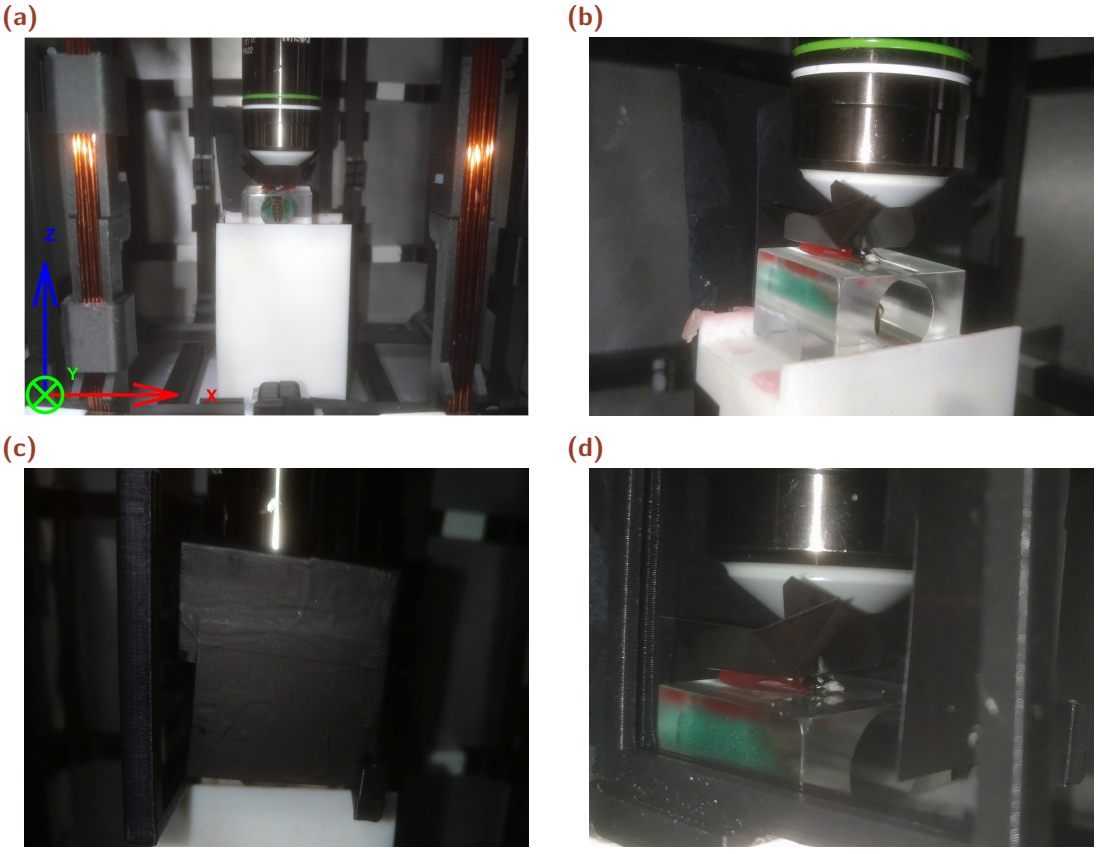


**Figure 3.17.:** Images of the bee positioned under the imaging objective for visual or magnetic stimulation: (c) front view, fully shielded from stray light, (d) side view with linear polarizer in place.

from a hole in the upper corner to the back wall of the aluminum shield. Due to the frosted aluminum surface, the light scattered uniformly onto the side wall, forming a homogeneous pattern covering the entire area of the wall. The resulting photon

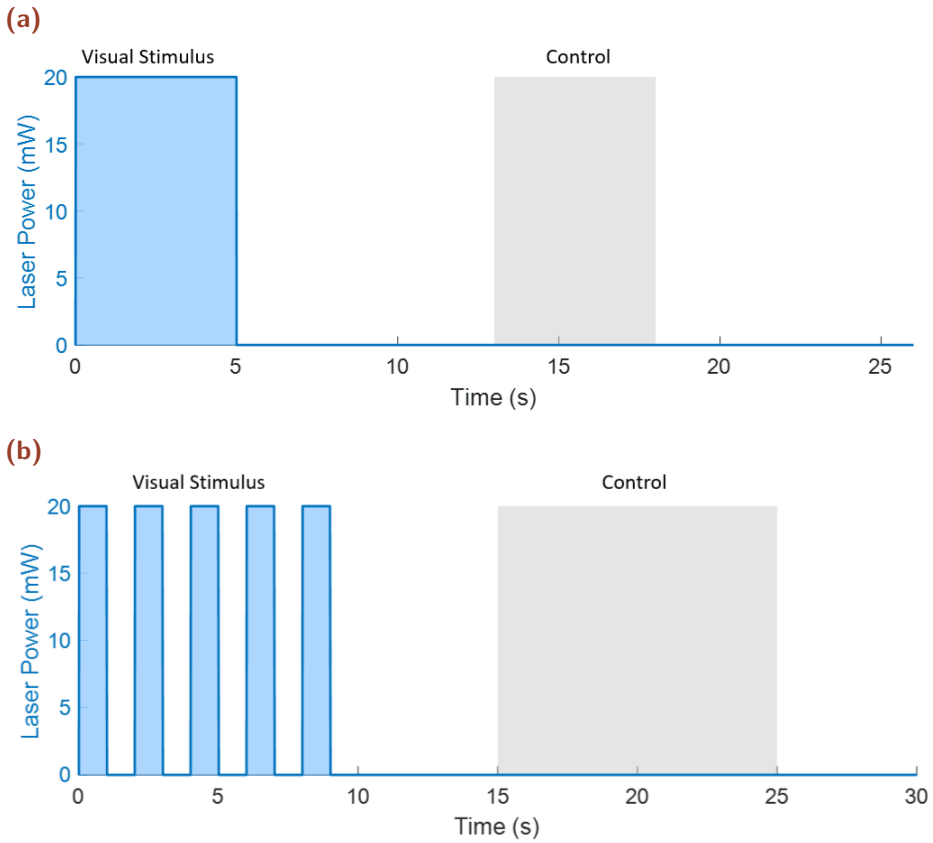


**Figure 3.18.:** (a) Pulse sequence for the visual stimulus, with the stimulus indicated in blue and the control interval in gray. (b) Pulse sequence for the light-pulse stimulus, with the control interval shown in gray.

flux reflected on the bee's eye was measured with an amplified photodiode and was approximately $4 \times 10^{17}\ photons \cdot m^{-2} \cdot s^{-1}$, which corresponds to roughly one hundredth of the blue-light photon flux under natural daylight conditions ($4 \times 10^{19}\ photons \cdot m^{-2} \cdot s^{-1}$). To prevent any of the stimulus light from interfering with the imaging, a piece of black plastic was used to cover the top, back, front and left side of the bee (Figure 3.17). In addition two 473-488 nm notch filters (Chroma) with an optical density greater than 6.5 were placed in front of the PMT. To increase the brightness of the light reflected from the side wall, a piece of white paper was placed on the surface and the output power of the laser during the experiments was 20 mW. For experiments done with polarized light, a linear film polarizer (Thorlabs) was placed on the right side of the bee (Figure 3.17d) and the output power of the stimulus laser was doubled to 40 mW. For each visual stimulation recording, 15 trials were done with either 3 or 5 seconds of stimulus and a trial period of 26 seconds (Figure 3.18a). The brain activity in the middle of the inter-stimulus interval was used to serve as the baseline control for unstimulated brain activity. Additionally, to investigate the response of the tubercle to dynamic visual stimulation, a sequence of light pulses was presented. In this protocol,

the visual stimulus was turned on for 1 s and off for 1 s over five consecutive cycles, followed by an inter-stimulus interval of 20 s before the next sequence began (Figure 3.18b).

### 3.3.5 Magnetic Stimulation

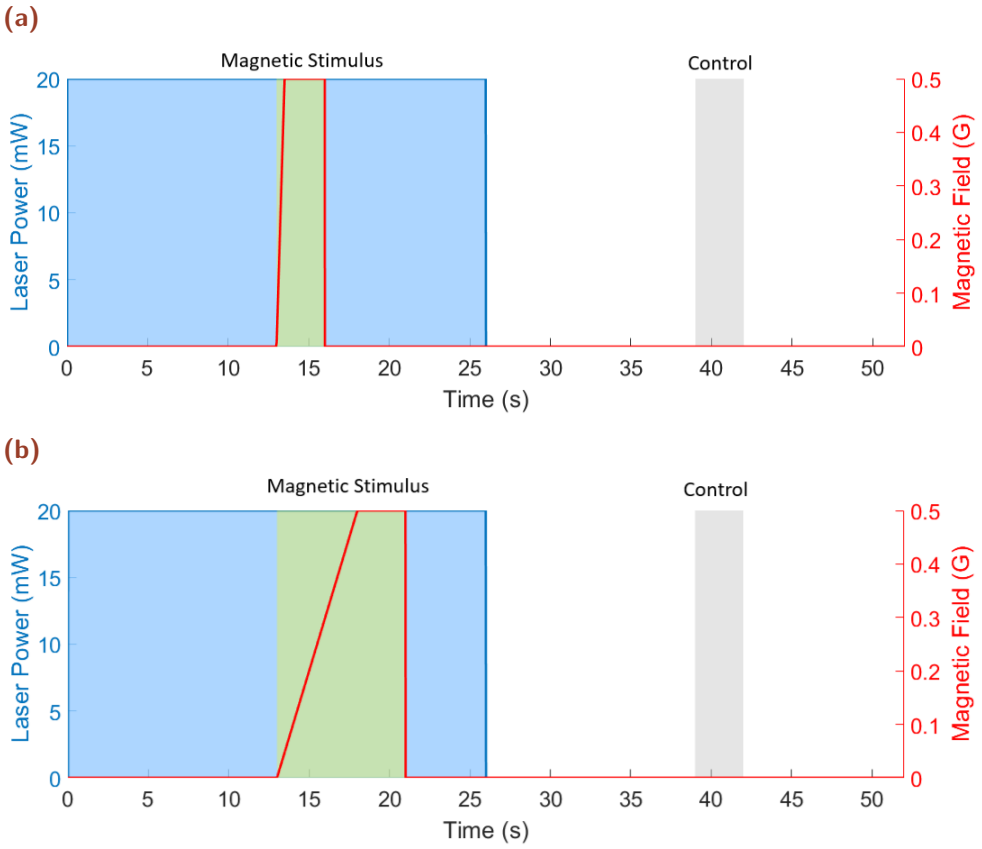


**Figure 3.19.:** Pulse sequences for magnetic stimuli, with the visual stimulus interval indicated in blue, the magnetic stimulus interval in yellow and the control interval in gray: (a) rapid magnetic field stimulus, (b) gradual magnetic field stimulus.

Magnetic stimulus was created using the setup described above in 3.1. The pulse sequence of each trial with the magnetic stimulus consisted of first the light turned on for 13 seconds, then the magnetic stimulus was on for 3 seconds and finally the light was turned off 10 seconds later (Figure 3.19a). The pulse sequence was designed in this way to confirm that the AOTu remained responsive in each trial. The trial periods were 52 seconds long and 10 trials were done for each stimulation recording. For experiments where the magnetic field slowly ramps up, the pulse sequence was the same except that the magnetic field was on for 8 seconds, increasing during the first 5 seconds whereas the light was turned off after 5 seconds (Figure 3.19b). As for the

visual stimulus, the brain activity in the middle of the inter-stimulus interval was used to serve as the baseline control for unstimulated brain activity.

# 4 Results and Discussion

## 4.1 Behavioral Experiments

### 4.1.1 Behavioral Results

The results for a single bee at different stages of its association between PER and the visual stimulus are illustrated in Figure 4.1. The frames of the video recording were labeled as licking when the classifier assigned at least an 80% probability of proboscis extension. Initially, the bee shows no response to the stimulus (Figure 4.1a). After several trials, it begins to exhibit guessing behavior by briefly extending its proboscis (Figure 4.1b). Over time, the bee becomes more confident, maintaining the proboscis extension until it receives the reward (Figures 4.1c and 4.1d). Concurrently, the decision time from the onset of the stimulus to the proboscis extension gradually decreases.

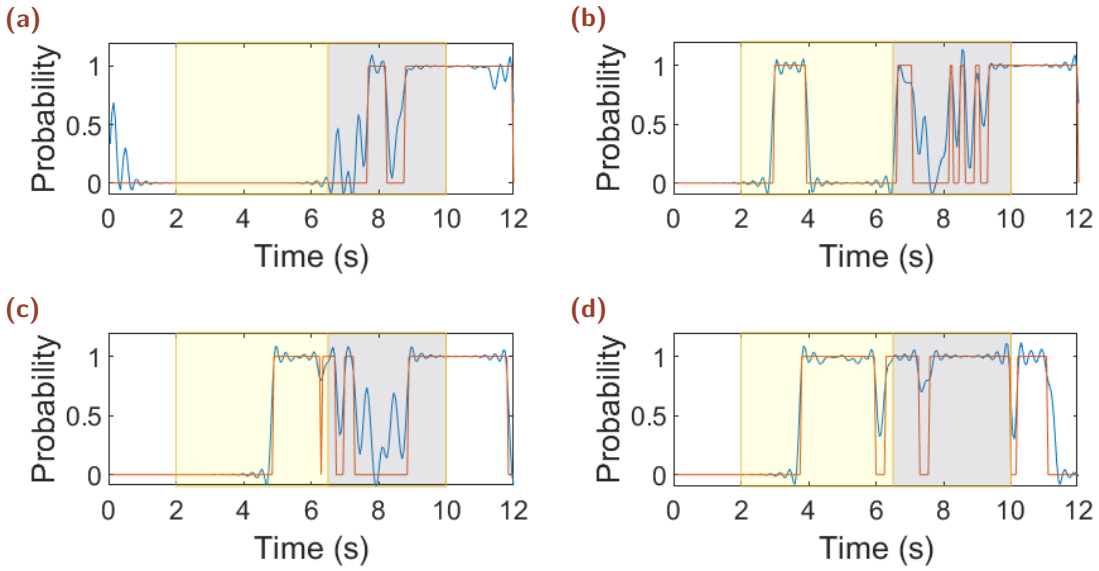


**Figure 4.1.:** Label classifier output for each frame of the recording of the same bee during the first (a), third (b), sixth (c), and seventh (d) training trials. The blue curve shows the probability of proboscis extension, while the red curve indicates the frame-by-frame labeling result. The yellow bar denotes the conditioned stimulus (CS), and the blue bar denotes the unconditioned stimulus (US).

(a)

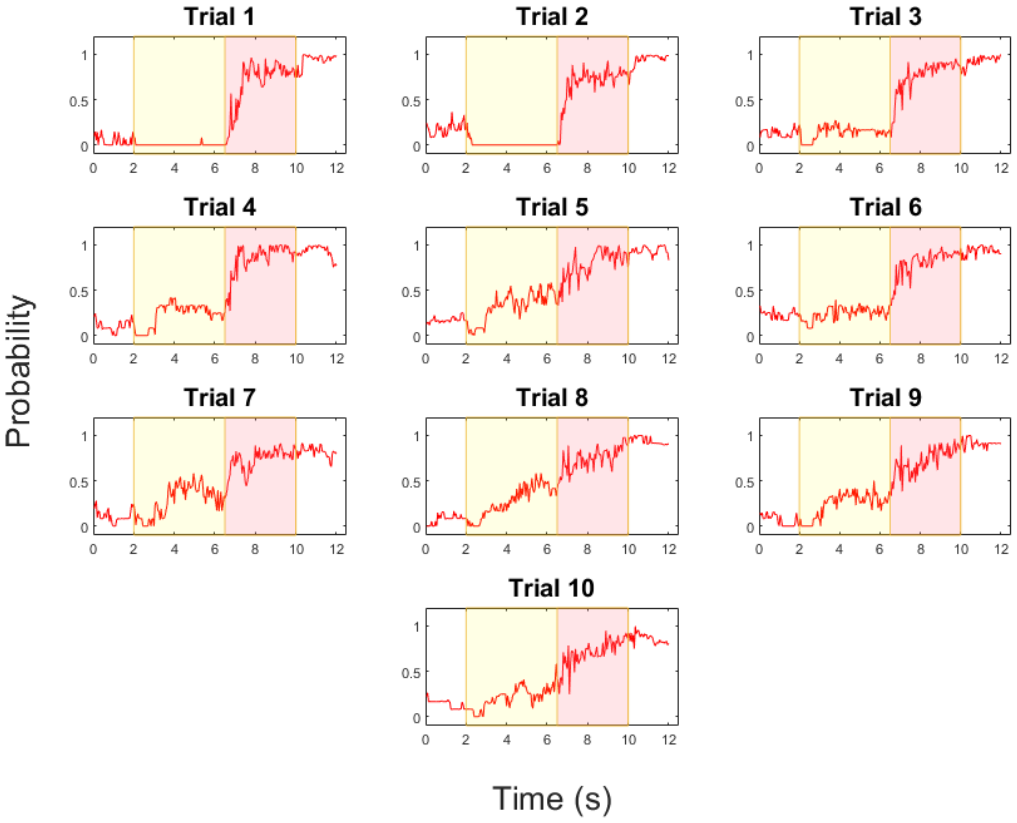


(b)

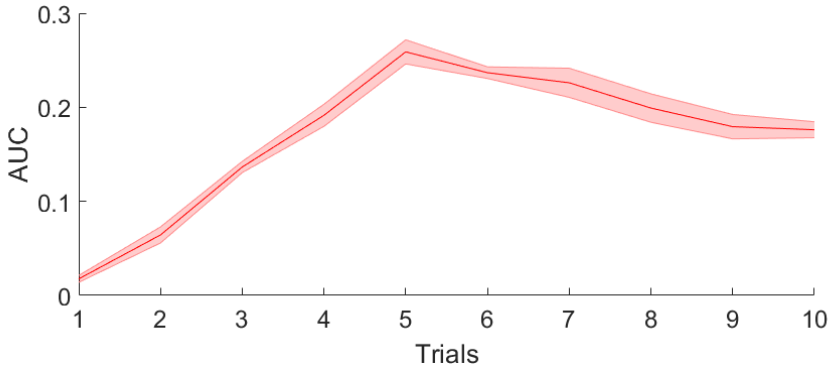


**Figure 4.2.:** Average response of the 12 bees trained to associate a visual stimulus with a reward. (a) Probability of proboscis extension over time across all trials, with the yellow bar indicating the conditioned stimulus (CS) and the red bar indicating the unconditioned stimulus (US). (b) Mean area under the probability curve for each trial.

Figure 4.2a illustrates the average response of all 12 bees across all trials. If all bees that responded to the stimulus were trained as effectively as the individual shown

in Figure 4.1, the area under the curve between the onset of the stimulus and the delivery of the reward would be expected to increase consistently over time. While this trend is observed during the first half of the trials, it does not persist in the later stages as seen in Figure 4.2b. This suggests that, although some bees demonstrated a strong learning response, a substantial proportion of those responding to the stimulus were not confident in their association between the stimulus and the reward. Moreover, the reduced response observed in the final trials indicates that the bees may have become overfed and consequently less motivated to extend their proboscis.

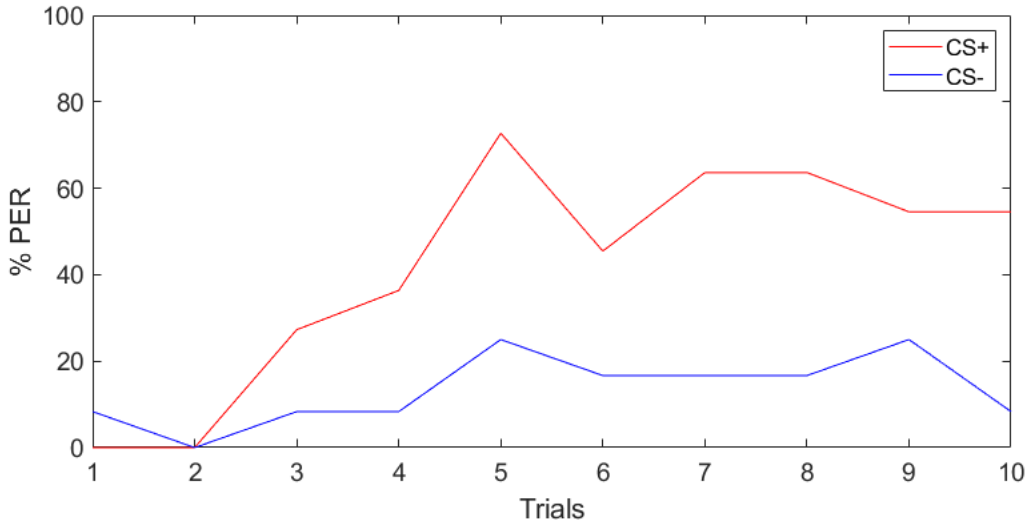


**Figure 4.3.:** A classical PER response curve of the honeybees with the percentage of the bees exhibiting a PER response for each trial to the visual stimulus with the paired stimulus in red (CS+) and the unpaired stimulus in blue (CS-)

The classic PER response across trials of the 12 bees is presented in Figure 4.3, which shows that approximately 50% of the bees responded to the visual stimulus. Although this represents a significantly lower learning rate compared to odor stimuli, where 80–90% of bees typically exhibit a conditioned response, a 50% response rate is consistent with results reported in the literature for visual stimulus conditioning [38].

Figure 4.4 illustrates the classic PER response across 8 trials from 12 bees exposed to a magnetic stimulus. Responses in the paired and unpaired trials were low and highly similar, showing that the bees did not learn to associate the magnetic stimulus and responded by random guessing.

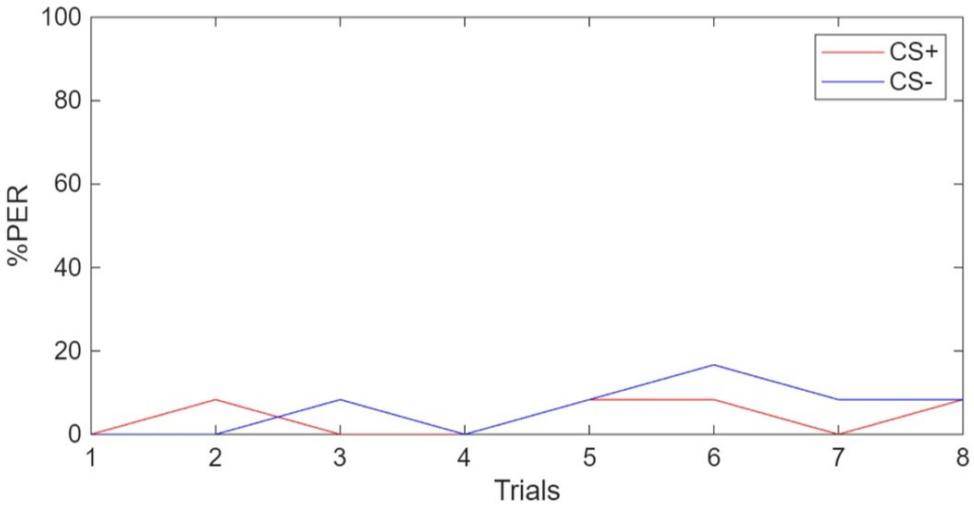


**Figure 4.4.:** A classical PER response curve of the honeybees with the percentage of the bees exhibiting a PER response for each trial to the magnetic stimulus with the paired stimulus in red (CS+) and the unpaired stimulus in blue (CS-)

### 4.1.2 Behavioral Discussion

Training bees in harnessed conditions with visual stimuli is inherently challenging, and numerous studies have independently refined their experimental protocols to optimize learning outcomes [38, 39, 91]. Factors such as stimulus duration, inter-trial interval, and the number of trials have been carefully adjusted, and some studies have even employed innovative approaches, such as incorporating motion cues or allowing limited head movement [38, 40, 92]. Nevertheless, even under optimized conditions, most studies achieve successful training in only approximately 50% of the bees, reflecting the inherent difficulty of visual conditioning in harnessed individuals.

For the bees to elicit learning responses to visual stimuli, it was essential to maintain their motivation throughout the experiment. Providing a small droplet of sucrose solution proved necessary, as it prevented satiation during the initial trials and sustained motivation until the final ones. This posed a challenge, as the sucrose droplet had to be positioned directly in front of the bees at a precise distance for them to locate it. To address this, the setup was modified, and careful attention was given during preparation to ensure that each bee was consistently placed in the exact same position within the testing area. Including a piece of paper towel to remove any remaining sucrose droplet at the end of the feeder before the next bee was fed significantly reduced the likelihood of bees becoming satiated too quickly and failing to learn. In experiments where this step was not included, bees that followed others which had

been unable to locate the droplet showed no evidence of learning in response to the stimulus, as they ended up being fed roughly twice the intended amount. Low-intensity air blown onto the bees' heads significantly increased their activity, resulting in greater responsiveness and willingness to engage in the task. However, this also caused the bees to extend their proboscis more often during unpaired trials or while waiting in the testing area before the stimulus began. A similar effect was reported by Strelevitz et al. [41], where low air flux elicited a strong PER response even without reward. The reason for the increases of the bees' engagement is unclear, one possibility being that the airflow simulates the sensation of flight making the bees more responsive to visual cues.

Experiments were also conducted using either magnetic stimuli alone or a combination of visual and magnetic stimuli (with the magnetic field varying from 0 to 0.5 Gauss along the $X$-axis). For magnetic stimuli only, the blue light remained on throughout the bee's time in the testing area. For the combined visual and magnetic stimulus experiment, bees were initially trained with the magnetic field oriented along the X-axis. Following the training, a memory test was conducted to assess whether they could distinguish this trained orientation from a magnetic field presented along the $Y$-axis. To date, no bees have shown a measurable response to the magnetic stimulus alone (Figure 4.4). While the combined stimuli were anticipated to enhance learning, the outcomes were inconclusive and showed no ability to discriminate between the two magnetic field directions in the memory test. One possible reason for the lack of observed learning in response to the magnetic stimulus is that while waiting between trials, the bees may still have been exposed to residual magnetic fields, either from the coils themselves or from other electronic components in the setup. During this waiting period, the bees were kept at a distance of 40–50 cm from the center of the coils. It was assumed that this distance, combined with the relatively weak magnetic stimulus, was sufficient to prevent the bees from sensing the magnetic field. Additionally, the bees were kept in the dark while waiting, based on the understanding that magnetoreception is light-dependent, and therefore no magnetic shielding was considered necessary in the waiting area. However, bees may still be capable of perceiving magnetic fields in the dark, either through light-independent activation of Cry, potentially facilitated by a reducing agent, or via magnetite particles located in their abdomen [22, 43]. This means they could detect the ambient magnetic field or residual magnetic fields from the stimuli. To address this possibility, one experiment was conducted where the magnetic stimulus switched from the ambient field to a zero field. Despite this adjustment, the bees still did not exhibit any response. It is also possible that training the bees with a visual stimulus alone presents a sufficiently challenging task, and that,

even if the bees are capable of detecting the magnetic field, adding a magnetic stimulus becomes too complex for them to learn effectively.

## 4.2 Two-Photon Imaging

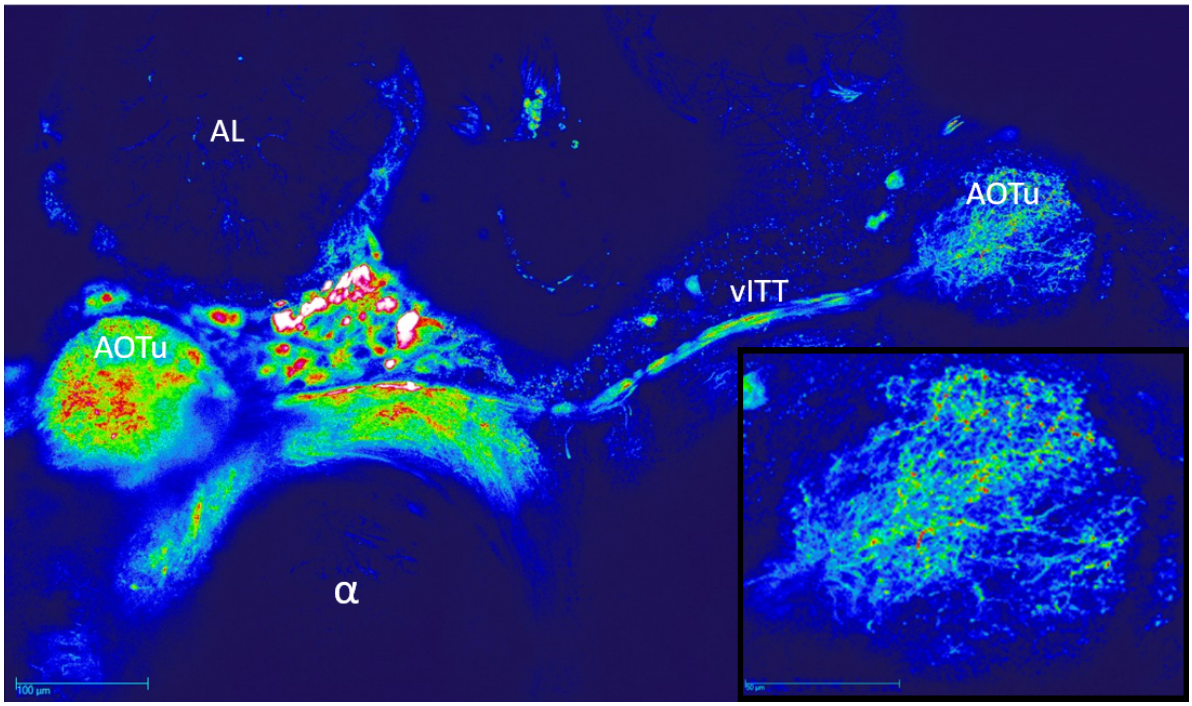


**Figure 4.5.:** Image of the bee brain showing staining, with the bottom-right inset providing a zoomed view of the AOTu. The injection site is located in the left AOTu, with dye diffusing to the right AOTu via the vITT. Abbreviations: AL, antennal lobe; $\alpha$, $\alpha$ lobe; vITT, ventral inter-tubercle tract.

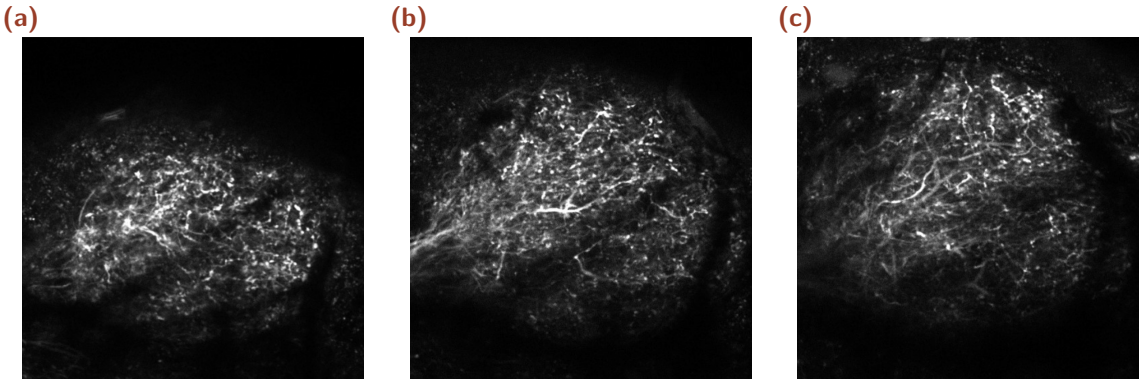


**Figure 4.6.:** Stained AOTu imaged at multiple planes: (a) $+20\ \mu m$ below the central plane, (b) central plane, (c) $+20\ \mu m$ above the central plane.

Figure 4.5 shows the spread of the dye from the injection site along the vITT, clearly staining the left AOTu. Complementarily, Figure 4.6 presents multiple optical

sections of the AOTu, confirming that the dye penetrates throughout the structure and results in uniform staining of the entire tubercle. Among the prepared bees, 40–50% had the AOTu fully stained and were still partially responsive to visual stimuli.

### 4.2.1 Visual Stimuli

The response of the AOTu to the visual stimulus in a single bee is shown in Figure 4.7a and exhibits temporal dynamics consistent with those reported in Mota et al. [7], as well as with the electrophysiological results presented in Mota et al. [79]. The calcium signal displays two peaks, an "on" and an "off" response, arising from the respective onset and offset of the light stimulus, as well as a tonic response during illumination. After the stimulus ends, the signal in the AOTu gradually returns to baseline over a period of about 10 seconds, likely due to a motion-related drift. The percentage change in fluorescence signal for the "on" and "off" responses reached peaks of only 0.8% and 1.1%, respectively, with a tonic response of around 0.5%. These values are substantially lower than those previously reported, where the on and off responses exhibited peaks of approximately 4% and 5%, respectively, and the tonic response of around 4%. The lower signal may result from imaging a thinner imaging plane, as the focal volume of a two-photon microscope is considerably smaller than that of a wide-field microscopy. The increase in background fluorescence caused by the visual stimulus (Figure 4.7b) was quantified by measuring changes in fluorescence intensity in a region located posterior to the AOTu (Figure 4.8). Although the bee and the objective were shielded from stray light as much as possible and two blue-light filters were used, a background change of approximately 0.3% was still detected. This indicates that the visual stimulus likely reduced the measured signal amplitude from the AOTu, although the exact extent of this effect remains uncertain. This established the upper limit for the visual stimulus laser intensity, because any background intensity change larger than 0.3% would alter the measured activity signal. Since motion correction was not applied in the analysis, it was crucial that the bee remained completely still during imaging. This was confirmed by examining control recordings (Figure 4.7c) for a flat, low-noise baseline.

Several parameters were found to be critical for obtaining reliable responses from the AOTu, such as the two-photon excitation power, the stimulus laser intensity, and the imaging plane. Increasing the power of the two-photon excitation laser strengthens the fluorescence signal and reduces interference from the stimulus light, though it also amplifies noise and may not necessarily improve the signal-to-noise ratio. An

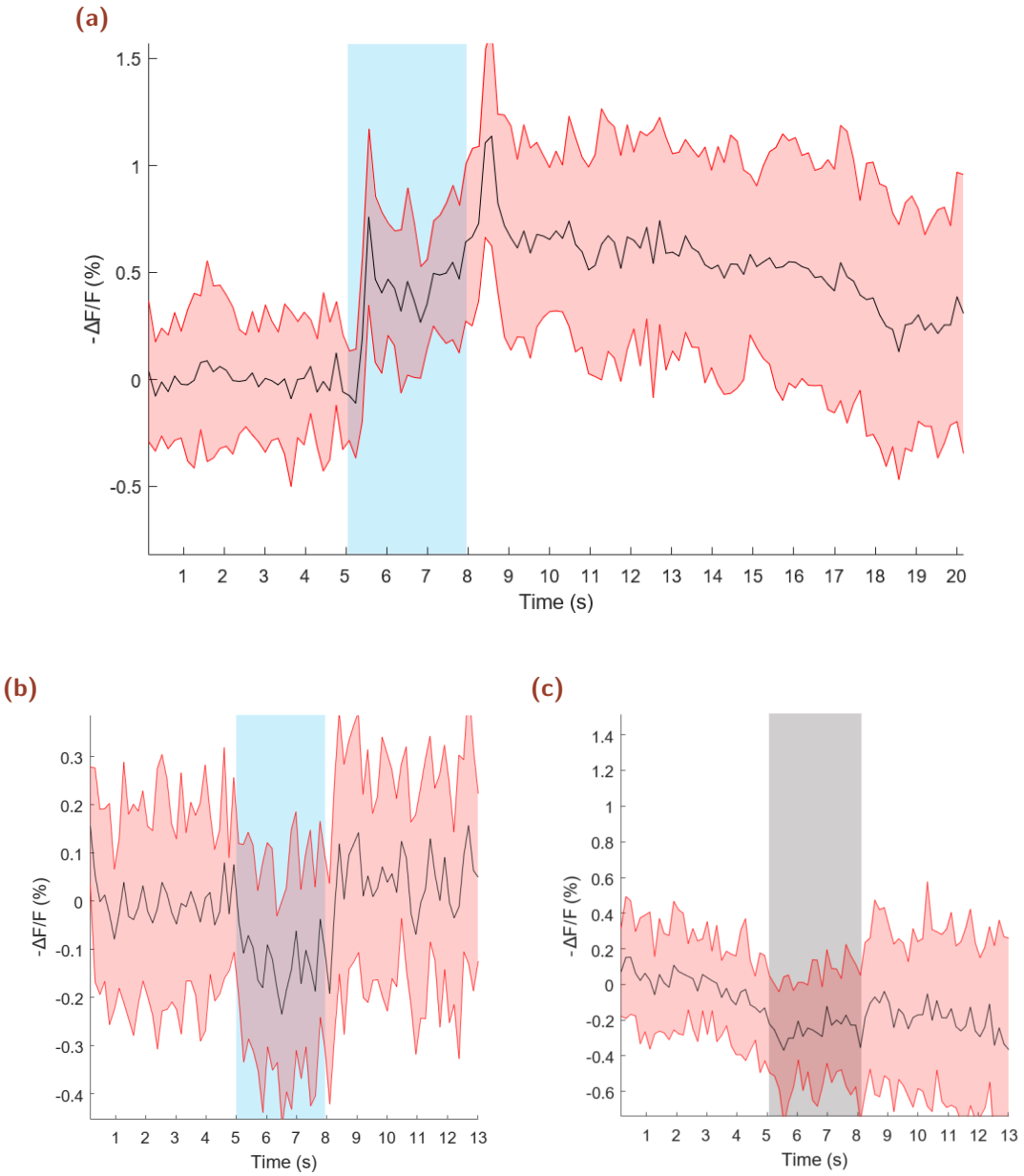


**Figure 4.7.:** Time-series of Fura-2 fluorescence changes during the visual stimulus sequence, showing the percentage change in fluorescence averaged over 15 trials. (a) Fluorescence response of the AOTu to the stimulus. (b) Fluorescence changes in the background region under the same stimulus. (c) The unstimulated brain activity recording of the AOTu during the control interval. Note that Fura-2 fluorescence decreases in response to elevated neural activity, fluorescence values are inverted for visualization. Red curves indicate responses that are significantly active, exceeding the 95% confidence threshold from the pre-stimulus standard deviation.

increase of approximately 0.2 mW can result in only small “on” and “off” responses being discernible (Figure 4.9). If the excitation power is too high, the signal becomes completely obscured by noise, whereas if it is too low, the effect of the stimulus

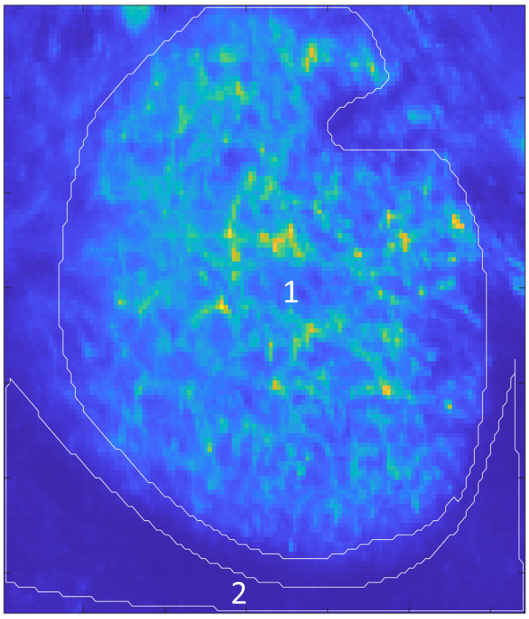


**Figure 4.8.:** Average fluorescence intensity calculated across all frames in the recording. Region 1 indicates the selected area corresponding to the AOTu, where signal values were measured. Region 2 represents a background reference area used to determine background fluorescence change.

laser becomes visible in the AOTu response. Increasing the power of the stimulus laser leads to stronger AOTu activation (Figure 4.10), but only up to a certain point, the peak amplitude of the on-response did not exceed 1.2%. Besides that, higher stimulus intensities also produced greater noise levels during stimulus presentation. The imaging plane was found to influence the results obtained from the AOTu. The most reliable responses were recorded at a plane approximately 10 $\mu$m above the center of the tubercle. At this depth, the imaged area was sufficiently large, and imaging deeper did not noticeably change the visible area of the tubercle but instead introduced additional noise (Figure 4.11). The rise in noise at greater depths is likely due to the higher two-photon excitation power required to maintain comparable fluorescence intensity, as laser power must be increased with imaging depth. While identifying parameters that elicit strong “on” and “off” responses is relatively straightforward, obtaining a response with a clear tonic response during stimulation is considerably more challenging. This difficulty is likely influenced by the overall quality of the preparation.

The response characteristics of the AOTu are highly sensitive to both the amount of dye introduced and any tissue damage incurred during preparation. Since the AOTu lies close to the brain surface, it is particularly susceptible to damage during the removal of tracheal, and even minor damage often results in the loss of the tonic response.

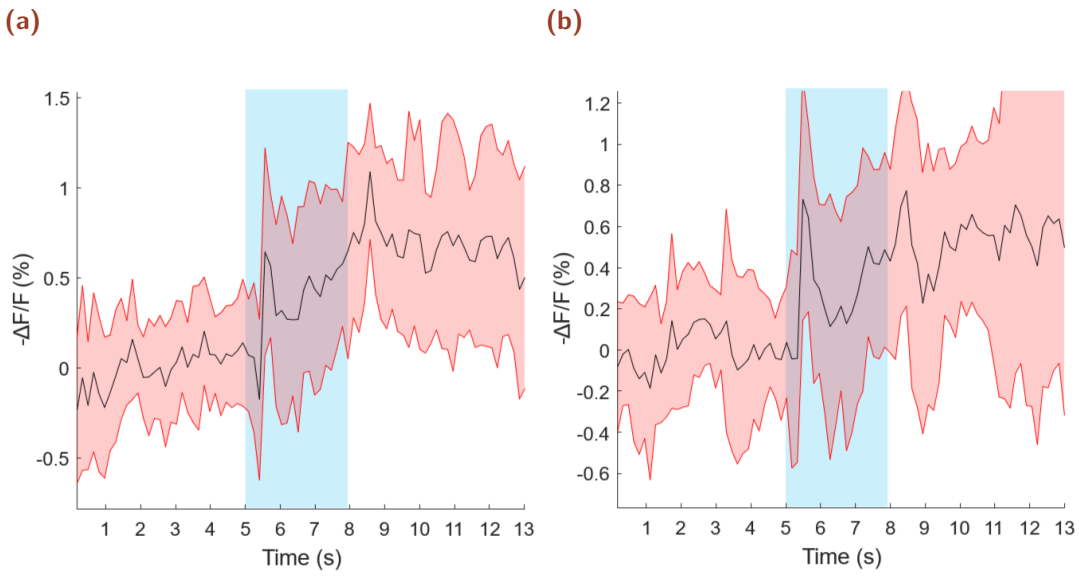


**Figure 4.9.:** Time-series recordings of fluorescence activity in the AOTu during visual stimulation with increased two-photon excitation power, showing the percentage change in fluorescence averaged over 15 trials. Responses are shown for a laser power increase of 0.2 mW (a) and 0.4 mW (b), compared to the recording presented in Figure 4.7a. Red curves indicate responses that are significantly active, exceeding the 95% confidence threshold from the pre-stimulus standard deviation.

Quantifying the extent of such damage is difficult as tubercles that appear well-stained can sometimes show only an “on” or “off” response, or no activity at all. Regarding dye concentration in the tubercle, too little dye resulted in high noise levels due to increased background fluorescence, while excessive staining caused the loss of activity entirely. In highly stained tubercles, even when the two-photon excitation power was reduced to compensate for high fluorescence levels, no response, or at most a very sharp “on” response was observed. The reason why high dye concentrations led to a loss of response in the tubercle remains unclear. One possible explanation is that the amount of extracellular calcium released is insufficient for a substantial fraction of the dye to bind, resulting in minimal detectable fluorescence changes. When injecting dye into the bee brain, it was found advantageous to use three borosilicate glass needles containing small amounts of dye rather than a single needle with the combined volume. A single injection tended to create a large injection site, allowing dye to leak into the mushroom bodies and increase background fluorescence. In contrast, performing three smaller injections at the same location reduced background fluorescence while still delivering sufficient dye to the tubercle.

Experiments were also conducted using horizontally and vertically polarized light as visual stimuli, with the stimulus laser power doubled to compensate for the intensity

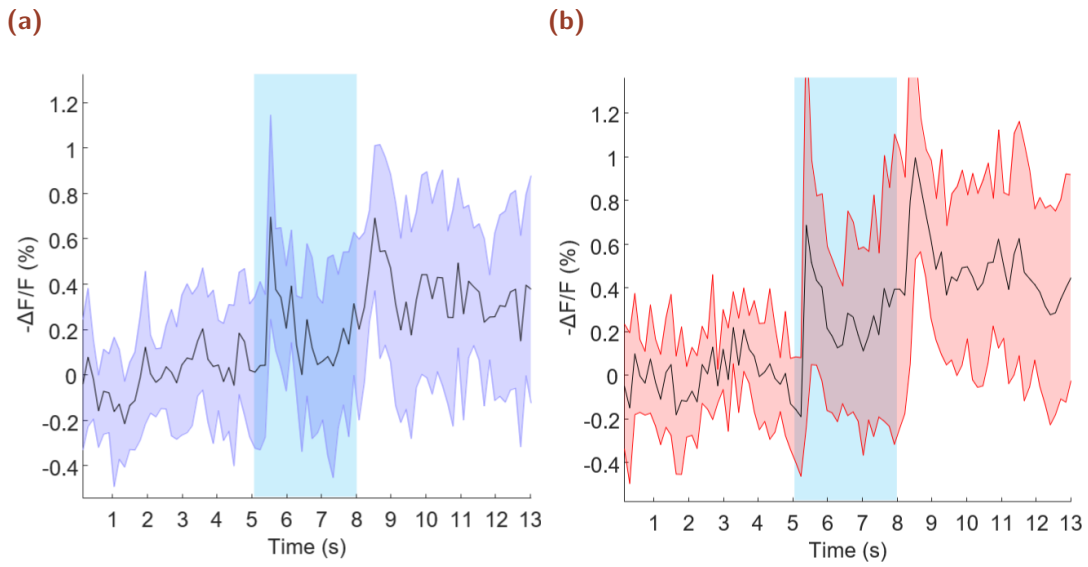


**Figure 4.10.:** Time-series recordings of fluorescence activity in the AOTu during visual stimulation with visual stimulus laser power at 10 mW (a) and 30 mW (b), showing the percentage change in fluorescence averaged over 15 trials. Red curves indicate responses that are significantly active, exceeding the 95% confidence threshold from the pre-stimulus standard deviation.

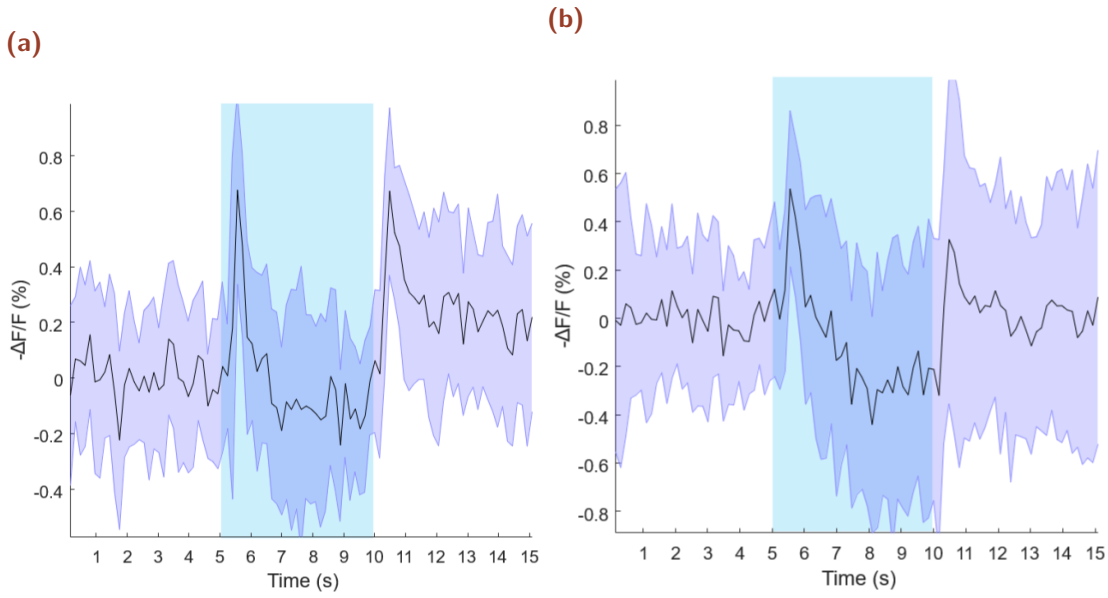


**Figure 4.11.:** Time-series recordings of fluorescence activity in the AOTu during visual stimulation, showing the percentage change in fluorescence averaged over 15 trials, taken at imaging depths of 10 $\mu m$ above (a) and 10 $\mu m$ below (b) the central plane. Curves in red indicate responses that are significantly active, exceeding the 95% confidence threshold from the pre-stimulus standard deviation.

loss caused by the linear polarizer (Figure 4.12). The responses of the AOTu to both polarization conditions showed no differences compared to those elicited by unpolarized light.

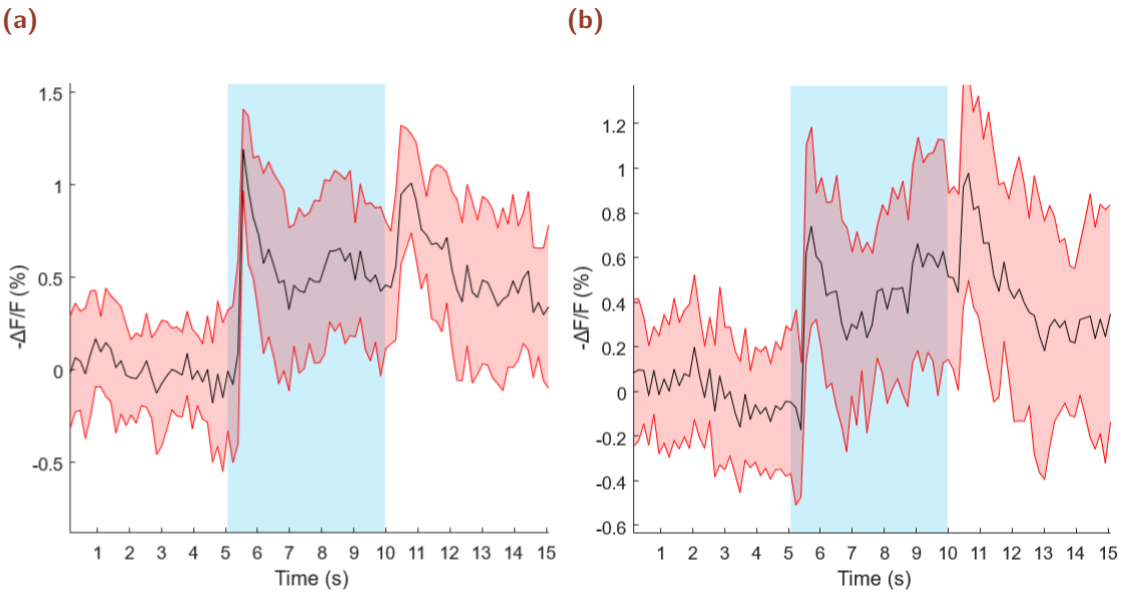


**Figure 4.12.:** Time-series recordings of fluorescence activity in the AOTu during visual stimulation with horizontal (a) and vertical (b) light polarization, showing the percentage change in fluorescence averaged over 15 trials. Red curves indicate responses that are significantly active, exceeding the 95% confidence threshold from the pre-stimulus standard deviation.

Figure 4.13 shows the results obtained when a series of short light pulses at a frequency of 0.5 Hz was used as the visual stimulus. In the temporal response of the AOTu, clear changes in fluorescence can be observed, however, the typical features of the visual response, such as distinct on and off phases are less apparent. Wavelet analysis of the signal revealed two dominant frequency components at 0.5 Hz and 1 Hz. The strong and sustained 1 Hz component observed throughout the stimulus period likely arises because the tubercle responds with both an on and an off peak to each light pulse, effectively doubling the frequency of the response relative to the stimulus frequency.

The response of the AOTu to this dynamic visual stimulus was investigated because it was initially unclear how the tubercle would respond to magnetic stimulation. It was hypothesized that the magnetic stimulus might not produce a clear change in fluorescence but could instead modulate ongoing neural activity within the tubercle. However, once it became evident that the magnetic stimulus did not modulate brain

activity and instead produced measurable changes in fluorescence, further experiments with the dynamic visual stimulus were no longer done.

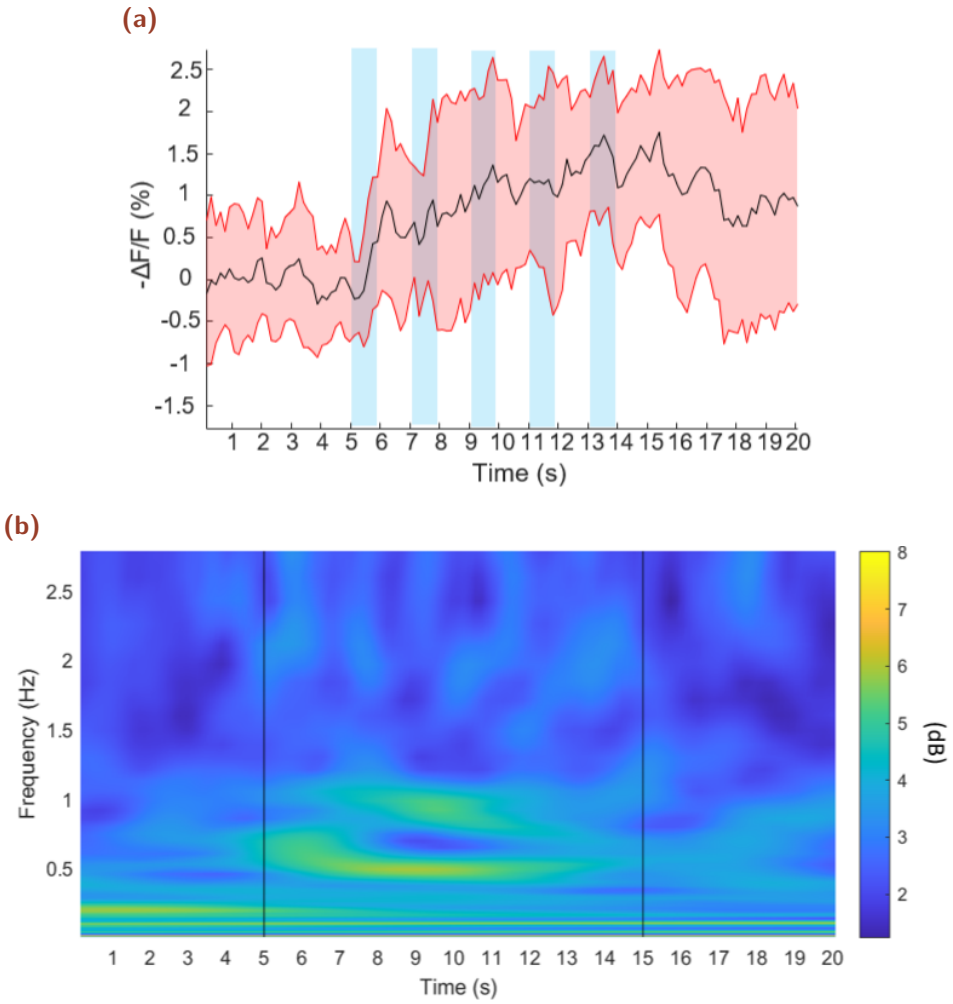


**Figure 4.13.:** (a) Time-series recordings of fluorescence activity in the AOTu during pulsed visual stimulation, showing the percentage change in fluorescence averaged over 15 trials. Red curves indicate responses that are significantly active, exceeding the 95% confidence threshold from the pre-stimulus standard deviation. (b) Corresponding wavelet transform of AOTu fluorescence activity during the same pulsed stimulus.

### 4.2.2 Magnetic Stimuli Results

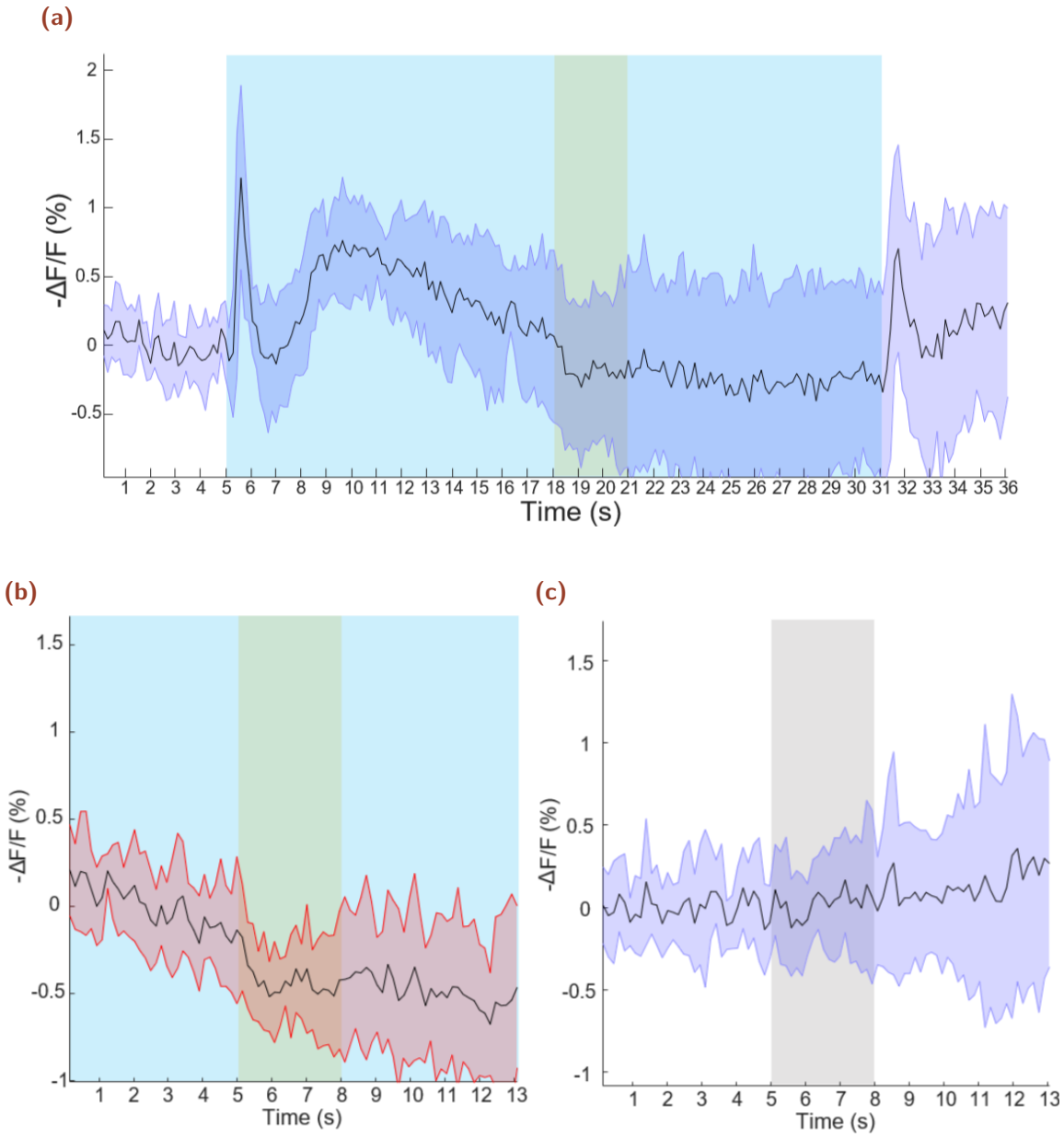


**Figure 4.14.:** Unprocessed time-series recordings of Fura-2 calcium fluorescence in the AOTu during magnetic stimulation, showing the percentage change in fluorescence averaged over 10 trials. (a) Fluorescence response of the AOTu over the full stimulus sequence. (b) Response of the AOTu to the magnetic stimulus, in this recording the fluorescence is normalized to the mean fluorescence during the pre-magnetic stimulus interval. (c) The unstimulated brain activity recording of the AOTu during the control interval. Red curves indicate responses that are significantly active, exceeding the 95% confidence threshold from the pre-stimulus standard deviation.

Unprocessed fluorescence recordings from a single bee exposed to the stimulus sequence illustrated in Figure 3.19a are presented in Figure 4.14a. In this experiment, the magnetic field along the $X$-axis was rapidly changed from 0 to 0.5 Gauss. Distinct "on" and "off" responses to the visual stimulus are clearly visible in the data. Immediately following the "on" response, the tonic response is temporarily absent but reappears after approximately 2–3 seconds, followed by a slow, linear decay in signal intensity. At the onset of the magnetic field stimulus, a fluorescence offset of -0.3% is observed and no change is observed at the offset of the magnetic field (Figure 4.14b). The corresponding fluorescence trace recorded under control conditions, shown in Figure 4.14c, remains stable and flat.

The gradual baseline drift caused by the decay of the tonic response was corrected using piecewise linear detrending. This procedure produced a noticeably flatter response during the period of visual stimulation (Figure 4.15b). Following detrending, the temporal profile of the fluorescence signal to the magnetic stimulus changed substantially, revealing distinct responses at both the onset and offset of the magnetic field. At the onset, the fluorescence exhibited an initial decrease of -0.2% within the first second, followed by a gradual increase throughout the remainder of the stimulus period. After the magnetic field was turned off, the signal returned to its pre-stimulus level. A paired t-test comparing across the different trials, the fluorescence during the pre-stimulus and stimulus periods yielded a p-value of 0.13, indicating that the observed change was not statistically significant.

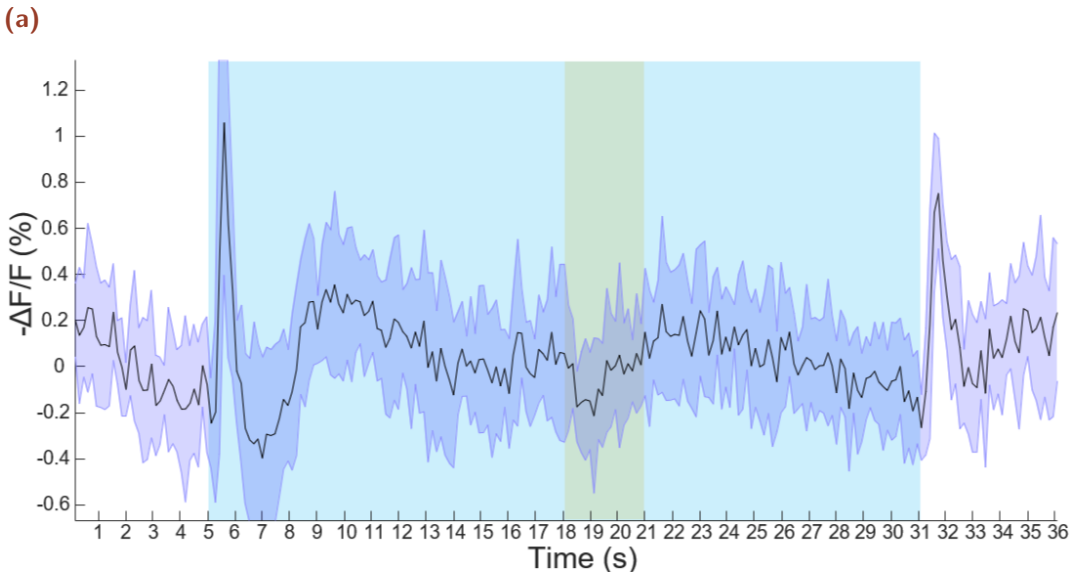

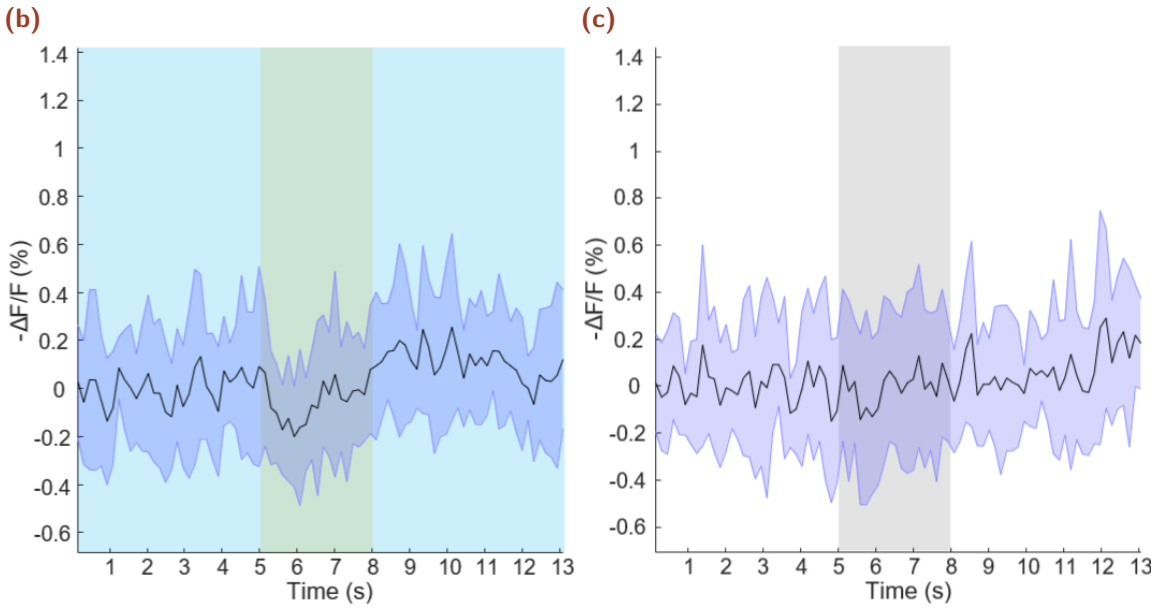


**Figure 4.15.:** Detrended time-series recordings of Fura-2 calcium fluorescence in the AOTu during magnetic stimulation, showing the percentage change in fluorescence averaged over 10 trials. (a) Fluorescence response of the AOTu over the full stimulus sequence. (b) Response of the AOTu to the magnetic stimulus, in this recording the fluorescence is normalized to the mean fluorescence during the pre magnetic stimulus interval. (c) The unstimulated brain activity recording of the AOTu during the control interval. Curves in red indicate responses that are significantly active, exceeding the 95% confidence threshold from the pre-stimulus standard deviation.

Over the course of three months, approximately 200 bees were prepared, of which about 150 showed successful AOTu staining. However, only around 80 exhibited sufficiently low noise levels and a measurable response to the visual stimulus. Among those responsive individuals, most displayed only basic “on” and “off” activity, while just four bees consistently produced strong, reliable tonic responses of approximately 0.5% with a standard deviation of about 0.2% during the visual stimulation. As the tonic response to the visual stimulus is necessary to show inhibition to the magnetic stimulus, only these four bees exhibited a measurable response to the rapid magnetic field stimulus. The mean fluorescence amplitudes for the pre-stimulus, stimulus, and post-stimulus periods, after baseline correction using the pre-stimulus mean for each bee, are shown in Figure 4.16. The average fluorescence changes relative to the pre-stimulus baseline were -0.051%, -0.12%, -0.029%, and -0.063% for the four responsive bees (Figure 4.16a, 4.16b, 4.16c, and 4.16d, respectively). A preliminary one-sample t-test performed on this limited dataset yielded a p-value of 0.047, indicating a statistically significant difference between the stimulus and baseline periods. However, given the

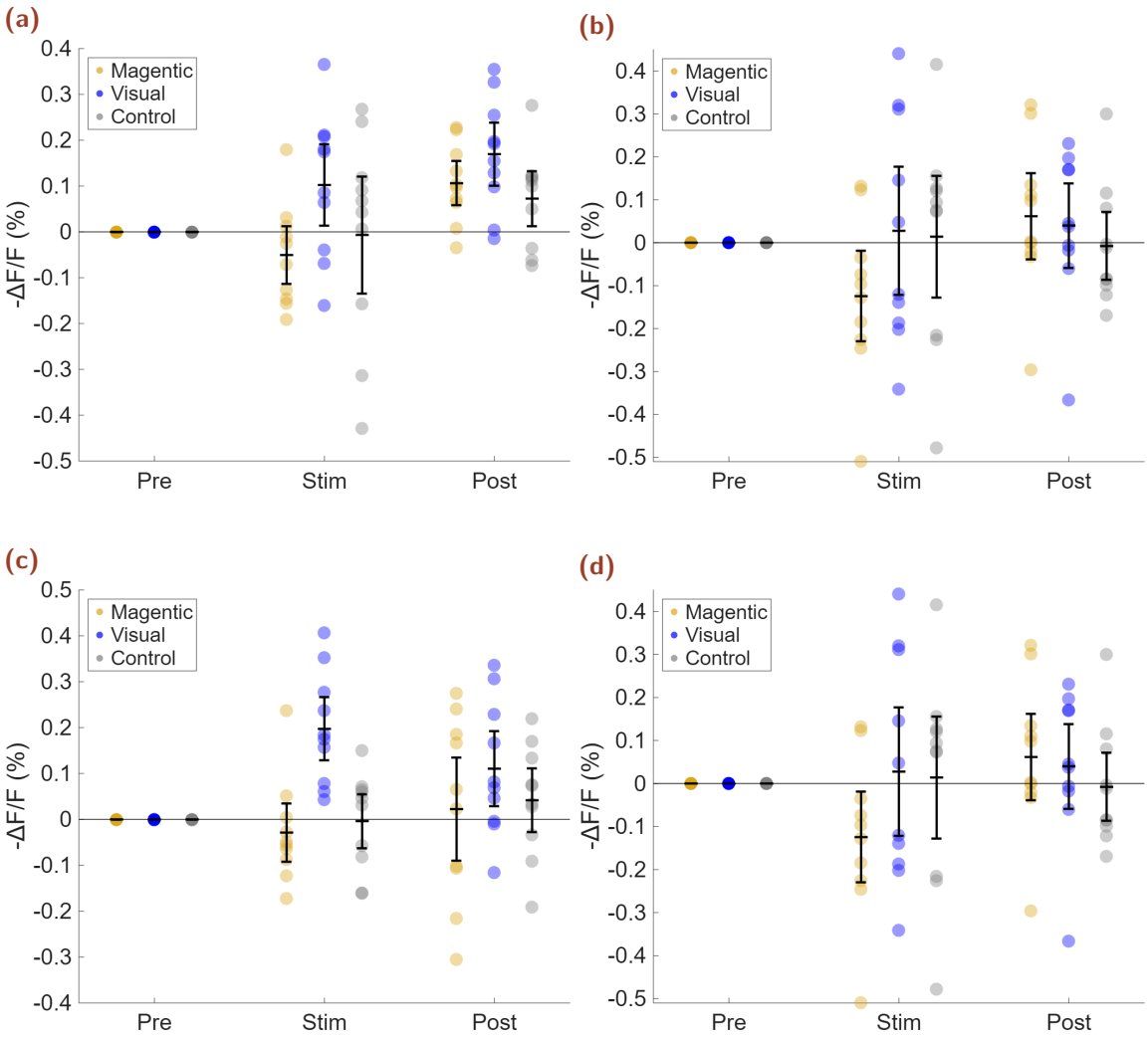


**Figure 4.16.:** Average fluorescence change across the 10 trials of each of the four bees. For each trial, fluorescence was averaged over the pre-stimulus, stimulus, and post-stimulus intervals and normalized to the pre-stimulus baseline. The magnetic stimulus is shown in yellow, the visual stimulus in blue, and the control interval representing unstimulated brain activity in gray. All pre-stimulus and post-stimulus intervals are 5 s in duration; the visual stimulus lasts 5 s, whereas the magnetic and control stimuli last 3 s.

small sample size, this result should be interpreted with caution and considered indicative rather than conclusive. Further experiments with a larger sample are required to confirm the consistency and robustness of this response across individuals.

The unprocessed fluorescence response from a single bee exposed to a gradually increasing magnetic field, reaching 0.5 Gauss along the X-axis as illustrated in Figure 3.19b, is presented in Figure 4.17. The temporal profile of the response exhibited similar characteristics to that observed under the rapidly changing magnetic field

stimulus. At the onset of the slowly increasing magnetic field, a fluorescence offset of approximately -0.3% was observed (Figure 4.17b). No further changes in fluorescence were detected neither during the gradual increase nor at the offset of the magnetic field.

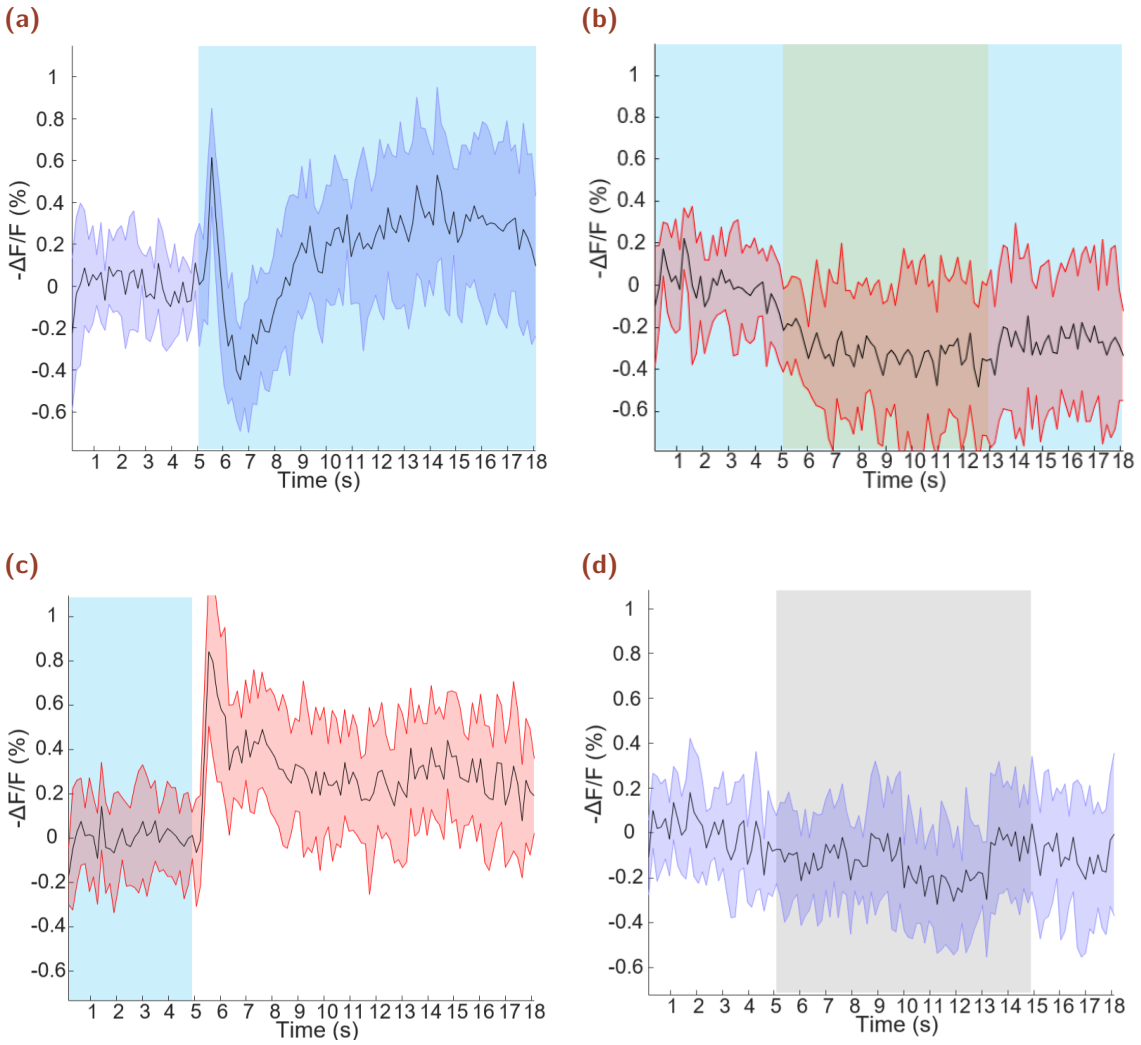


**Figure 4.17.:** Unprocessed time-series recordings of Fura-2 calcium fluorescence in the AOTu exposed to a gradually increasing magnetic field, showing the percentage change in fluorescence averaged over 10 trials. (a) Fluorescence response of the AOTu to the onset of the visual stimulus. (b) Response of the AOTu to the gradually increasing magnetic stimulus. (c) Fluorescence response of the AOTu to the offset of the visual stimulus. (d) The unstimulated brain activity recording of the AOTu during the control interval. Red curves indicate responses that are significantly active, exceeding the 95% confidence threshold from the pre-stimulus standard deviation.

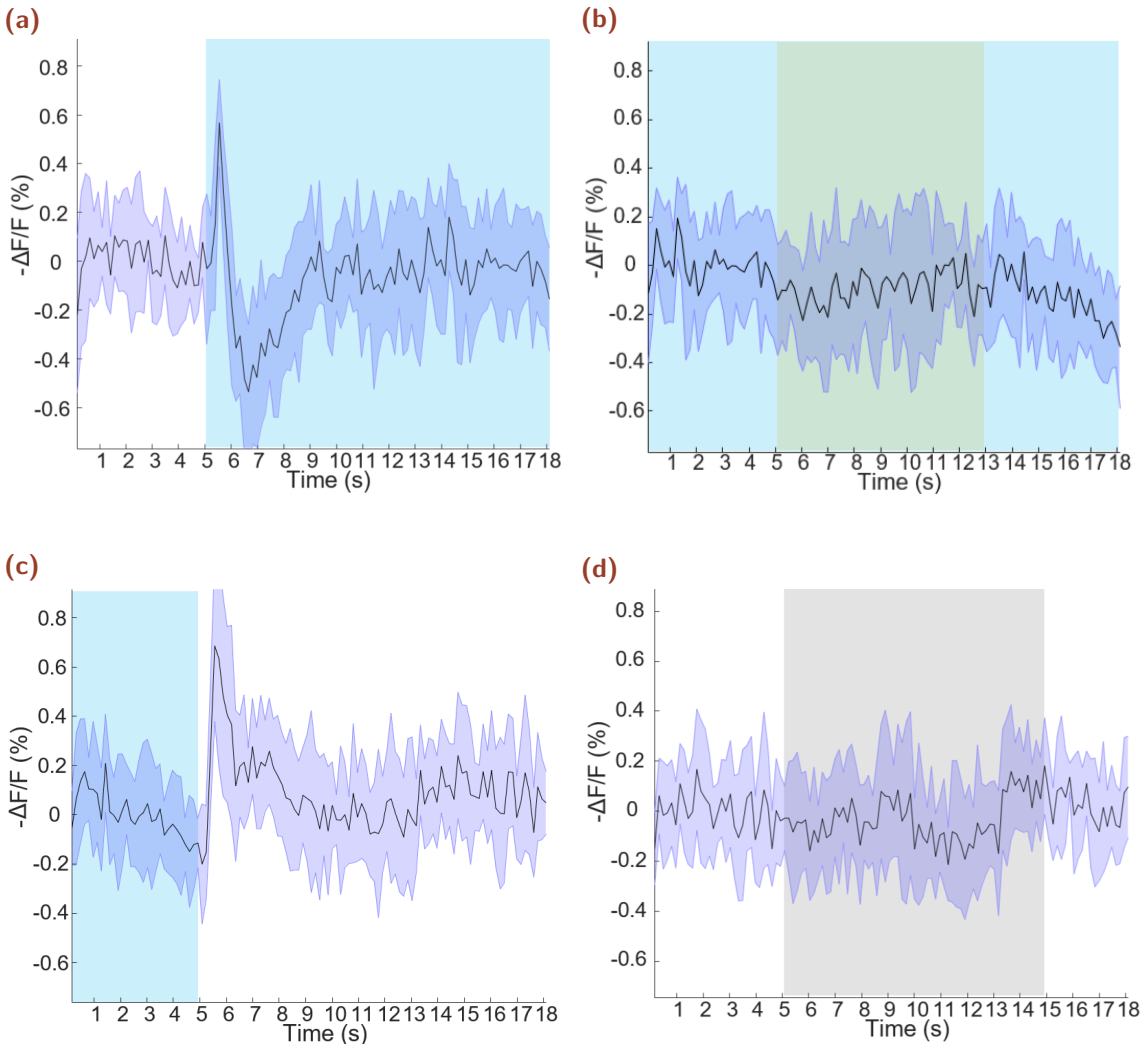


**Figure 4.18.:** Detrended time-series recordings of Fura-2 calcium fluorescence in the AOTu exposed to a gradually increasing magnetic field, showing the percentage change in fluorescence averaged over 10 trials. (a) Fluorescence response of the AOTu to the onset of the visual stimulus. (b) Response of the AOTu to the gradually increasing magnetic stimulus. (c) Fluorescence response of the AOTu to the offset of the visual stimulus. (d) The unstimulated brain activity recording of the AOTu during the control interval. Curves in red indicate responses that are significantly active, exceeding the 95% confidence threshold from the pre-stimulus standard deviation.

In the detrended response shown in Figure 4.18, the temporal profile differs from that observed under the rapidly changing magnetic field stimulus. At the onset of the slowly increasing magnetic field, a small fluorescence decrease of approximately -0.1% was observed. Throughout the gradual increase of the magnetic field, the signal remained stable, showing a flat response for the duration of the stimulus. Following the offset of the magnetic field, the fluorescence signal began to decline. A paired

t-test comparing across the different trials, the fluorescence during the pre-stimulus and stimulus periods yielded a p-value of 0.044.

The response of a bee to a rapid magnetic stimulus under horizontally and vertically polarized light is shown in Figure 4.19. The detailed responses to each segment of the full stimulus sequence for both polarization conditions are presented in Figures A.5 and A.4. Under vertically polarized light, the response to the magnetic stimulus closely resembled that observed with unpolarized light, showing a decrease in fluorescence intensity of approximately -0.2% during the presence of the stimulus. In contrast, no distinct response to the magnetic stimulus was observed under horizontally polarized light, although the same individual bee was used for the horizontally polarized condition and the response shown in Figure 4.14. A direct comparison of the magnetic response across horizontal, vertical, and unpolarized light conditions within the same bee has not yet been performed.

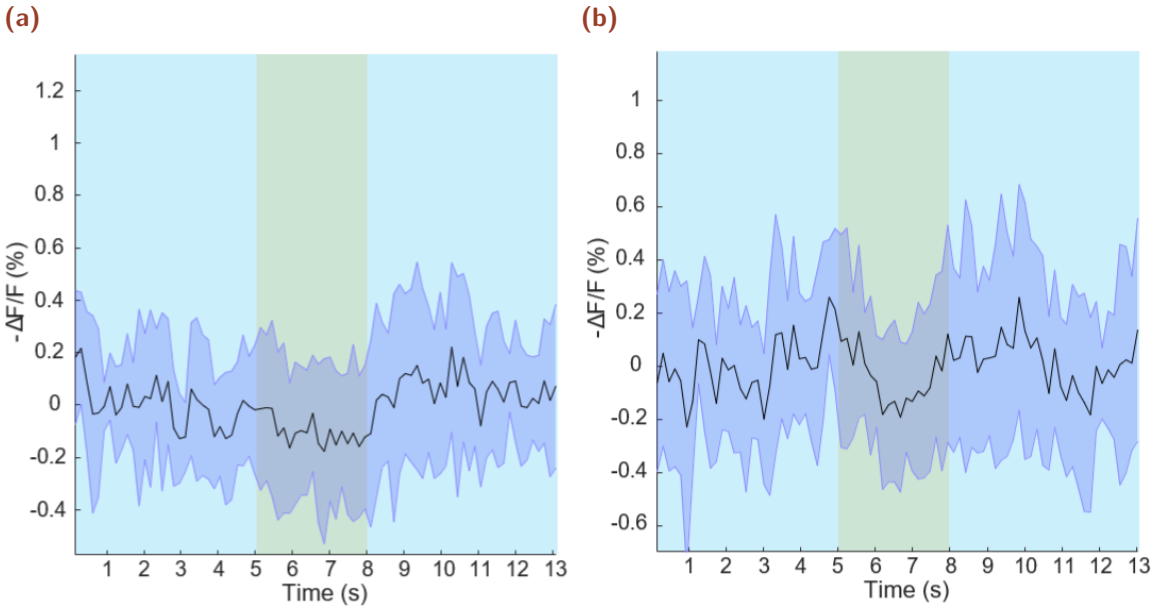


**Figure 4.19.:** Detrended time-series recordings of Fura-2 calcium fluorescence in the AOTu during magnetic stimulation, showing the percentage change in fluorescence averaged over 10 trials, with horizontal (a) and vertical (b) light polarization. Curves in red indicate responses that are significantly active, exceeding the 95% confidence threshold from the pre-stimulus standard deviation.

### 4.2.3 Magnetic Stimuli Discussion

The results obtained with the visual stimulus reveal a much clearer temporal resolution of neuronal response dynamics than those reported by Mota et al. [7].

This discrepancy may stem from their use of higher stimulus intensities, which could have saturated photoreceptor activity, or from limitations in the temporal resolution of their imaging system. Our findings provide evidence, for the first time using calcium imaging, that AOTu neurons respond almost exclusively to changes in light intensity, closely aligning with the electrophysiological data reported by Mota et al. [79]. The fluorescence recordings with the magnetic pulse stimuli sequence, indicate that neural activity within the visually stimulated AOTu decreases in response to magnetic stimulation (Figure 4.14). Following linear detrending, distinct fluorescence changes were observed at both the onset and offset of a rapidly changing magnetic field, suggesting a magnetically induced modulation of activity. As no previous studies reporting magnetic field responses in higher-order brain structures of the visual pathway of any animal have been found, direct comparison with existing literature is not possible. Given the current SNR of the temporal recordings, the observed -0.2% change in fluorescence is insufficient to be considered statistically significant at the single-trial level. Nevertheless, a preliminary group analysis using a one-sample t-test indicated a statistically significant effect. However, due to the limited sample size, this finding should be interpreted cautiously and regarded as indicative rather than conclusive evidence of magnetically responsive neural activity.

To reliably detect a response to magnetic stimulation, the bee must exhibit a strong and stable response to the visual stimulus, characterized by a high tonic response with low noise. Among all bees examined, those lacking sustained visual responses showed no detectable change during magnetic stimulation. In most of the bees that exhibited sustained visual activity, the fluorescence of the continuous response decreased back down to pre-visual stimulus levels following the initial “on” response and recovered after approximately 2–3 seconds. This reduction was never seen in the recordings with the visual stimulus sequence and the reason for this temporary reduction in activity remains uncertain. It was at first believed that this effect stemmed from repeated prolonged exposure to the visual stimulus which induces fatigue within the AOTu. The duration of the visual stimulus sequence was extended from 3 s to 5 s, but the loss of activity after the “on” response was not observed. However further analysis revealed that the reduction in activity could occur even during the first trial of the magnetic stimulus sequence. The only difference in the onset of the visual stimulus between the visual and magnetic stimulus sequences is that the latter one is done in a zero magnetic field environment. This observation raises the possibility that the AOTu may respond differently to different magnetic field environments, although further experiments are required to confirm this.

All recordings that displayed sustained visual activity also exhibited a slow, linear decline in fluorescence during visual stimulation. This gradual decay made it challenging to discern whether the small observed changes were elicited by the onset of the magnetic field or merely reflected baseline fluctuations. This can be seen clearly in Figure A.6, where a rapid decrease in fluorescence occurs just before the magnetic field was applied. In contrast, recordings obtained with the visual stimulus sequence did not exhibit such a drift, suggesting that reducing the delay between the onset of the light and the stimulation of the magnetic field in the magnetic stimulation sequence may yield a clearer response to magnetic stimulus. It may also be important to consider whether the visual stimulation laser needs to be turned on and off between trials, rather than left on for the entire duration of the experiment. The visual stimulus laser was turned on and off in the magnetic stimulus sequence initially to verify that the AOTu remained responsive and undamaged throughout the recording session. However, since the onset of the magnetic field appeared to shift the fluorescence signal back toward pre-visual stimulus onset levels in the unprocessed signal, turning on and off the visual stimulation laser in each trail might play a significant role in obtaining a stable response from the magnetic stimuli. Obtaining bees with a strong tonic response in response to the visual stimulus proved challenging, limiting the number of successful recordings. As a result, measurable responses to the magnetic field were obtained from only five bees. However, every bee that displayed a robust visual response yielded at least one recording showing a detectable magnetic field response.

In cases where a fluorescence change was observed, it consistently manifested as a decrease, indicating that the magnetic stimulus suppressed neural activity. In the unprocessed signal, the onset of the magnetic field appeared to shift the fluorescence signal back down to pre-visual stimulus onset levels, with no observable change when the magnetic field was subsequently set back to zero. This raised the possibility that the magnetic stimulus might contain additional artifacts beyond the intended field generated by the coils, potentially arising from transient magnetic fields induced by eddy currents either in the microscope objective, the aluminum shielding, or elsewhere. To investigate this, the magnetic field stimulus was modified to increase from 0 G to 0.5 G over 5 s instead of 0.5 s. This adjustment would not only substantially reduce the strength of the eddy currents generated but also allow recording of the AOTu response to a magnetic field with a different temporal profile.

However, this adjustment did not alter the overall shape of the response in the unprocessed signal. In both types of magnetic stimuli, the fluorescence decreased linearly during the first second and then remained stable for the duration of the

stimulus, with no observable response upon the offset of magnetic field. Consequently, there is a possibility that the responses attributed to the magnetic stimuli are not caused by the change in the magnetic field, but instead are triggered by the activation of the current ramp in the power supply. The current ramp is not triggered by changing the current or voltage settings on the power supply, it is only activated when the output channel is turned on. This necessitates briefly turning off the output channel used to compensate for the residual magnetic field, resulting in a sharp drop of approximately 0.05 G before the magnetic field begins to increase (Figure 3.5). While this artifact triggered at the onset of the magnetic field may be small, it remains possible that it could account for the observed change in fluorescence. However, the detrended signal indicates that a decrease in neural activity occurs only during the presence of the magnetic stimulus (Figure 4.15), providing evidence that the observed effect may represent a genuine neural response to magnetic stimulation. The temporal profile of the detrended signal obtained under the gradually increasing magnetic field stimulus also differs, showing small changes at the onset and offset of the stimulus. However, no noticeable change in fluorescence is observed while the magnetic field is increasing. It is possible that the change in neural activity may be too small to be detected given the current SNR and and that a different type of dynamic magnetic stimulus may be required to produce a detectable response.

While polarized light is not considered to be necessary for magnetoreception, it is thought that polarized light in any orientation may enhance the neural response to magnetic fields. Neither horizontally nor vertically polarized light altered the bee's response to the visual stimulus, provided that the reduction in light intensity was appropriately compensated. However, although vertically polarized light produced responses to the magnetic field similar to those observed under unpolarized light, none of the recordings obtained under horizontally polarized light showed a clear response to the magnetic stimulus. As the recording conducted immediately after the horizontally polarized light condition (Figure 4.19a) using the same bee showed a clear response to the magnetic stimulus (Figure 4.14a), it is likely that the absence of a response under horizontally polarized light was due to the light's polarization rather than the condition of the AOTu. These results suggest that the polarization state of the visual stimulus may influence the bee's sensitivity to magnetic stimuli or that there is a potential polarization-dependent component in the visual response and when this visual response is absent, magnetic field modulation appears to be absent as well. However, since responses from the same individual bee under vertical, horizontal, and non-polarized conditions were not obtained, it remains difficult to

draw firm conclusions at this stage and further experiments are needed to confirm and characterize this effect.

Simply switching the visual stimulus from horizontally polarized to unpolarized light produced a neural response to the magnetic stimulus. This observation confirms that the change in fluorescence arises from a genuine neural response to altered visual information rather than from an external artifact, such as movement of the bee in response to the magnetic field. The reason for the decrease in brain activity in response to the magnetic stimulus remains to be determined. Examining the neural pathway of the blue-light photoreceptors, as described in Section 2.2.1, their axons first terminate in the medulla and then project through the lobula before reaching the AOTu. Both the medulla and lobula contain color-opponent neurons that can exhibit excited or inhibited in response to brightness contrasts, while the lobula also has spatial-opponent neurons that may be either excited or inhibited depending on the spatial distribution of light. If magnetoreception is perceived as a pattern of alternating brightness and darkness within the visual pathway, the activity of color- and spatial-opponent neurons may lead to inhibition of neural activity in the AOTu in the presence of a magnetic stimulus. Whether the AOTu may exhibit excitation in response to magnetic stimuli presented in different orientations remains to be determined through further experimentation.

The experimental setup additionally enables the application of diverse magnetic stimulus conditions. Besides testing magnetic stimuli in different orientations, experiments could also be performed in which the magnetic field transitions from one direction to another or varies sinusoidally over time. Incorporating differently polarized light alongside these magnetic stimuli may provide insight into the potential interactions between the magnetic and sun compass systems. Several key predictions of the RPM can also be tested with this setup, including the polarity independence of the magnetic field and the disruptive effects of radio-frequency fields. Although the design was intended to probe the RPM's predicted light dependence, this aspect will be difficult to evaluate given that the visually stimulated AOTu exhibited inhibitory responses to magnetic stimulation. Identifying a magnetic stimulus capable of producing AOTu excitation would therefore be necessary before light-dependent effects can be meaningfully examined. Nonetheless, the observation that magnetic stimulation alters neural activity within a visually associated brain region not only provides additional support for the RPM as a potential mechanism of insect magnetoreception but also suggests that this imaging approach may be valuable for investigating its underlying neural processes. However, the current dataset remains insufficient to determine

whether the AOTu itself constitutes a functional component of the neural circuitry underlying magnetoreception.

# 5 Conclusion and Outlook

The aim of this project was to investigate the biophysical and neurological mechanisms underlying magnetoreception using honeybees as a model organism. To investigate how bees respond to different magnetic stimuli, a dedicated behavioral setup was designed and built. In parallel, an *in vivo* two-photon imaging system was developed to investigate the neural responses of their higher-order brain structures. The behavioral setup utilized classical conditioning with the PER to train bees to associate a visual stimulus with a reward, serving as a preliminary step to optimize the protocol before training with magnetic stimuli. Both the setup and preparation protocol were continuously improved until a learning rate of about 50% was achieved. However no bees exhibited learning when trained with magnetic stimuli in isolation and pairing magnetic cues with visual stimuli was presumed to accelerated learning, though the findings were inconclusive. Similarly, the two-photon imaging system and preparation methods for *in vivo* imaging of the AOTu underwent continuous refinement to limit visual-stimulus interference and to achieve stronger, more reliable AOTu responses. In the detrended recording of a visually stimulated AOTu, a 0.2% decrease in fluorescence was observed in response to the magnetic stimulus. Although the change in fluorescence was not large enough relative to the pre-stimulus standard deviation to be considered significant, a one-sample t-test on the mean fluorescence change in response to the magnetic stimulus, computed from the four bees that had a reliable tonic responses of about $0.5\% \pm 0.2\%$ to the visual stimulus, yielded a p-value of 0.046.

Although the original aim of this project was to use behavioral experiments to identify the optimal magnetic stimulus parameters for fluorescence imaging and to determine which magnetic cues bees can reliably discriminate, training bees to associate even a visual stimulus proved more challenging than anticipated. Because no conclusive learning responses to magnetic stimuli have been obtained so far, the behavioral setup requires further refinement, or alternative experimental parameters should be explored. These could include using differential learning paradigms that pair visual and magnetic cues in one direction versus visual cues alone or paired with magnetic cues in a different direction, or assessing learning through changes in

proboscis extension latency rather than relying solely on conventional conditioning success rates. Additionally, other types of behavioral experiments could be explored, such as using tethered bees [93]. On the imaging side, fluorescence measurements of the AOTu revealed that neural activity decreased in the presence of a magnetic stimulus, providing a proof of concept that the imaging setup is capable of detecting magnetically induced responses. However, the observed responses were very weak, and a larger sample size is required before any conclusions can be drawn. The primary obstacle to increasing sample size is the difficulty of preparing bees that consistently exhibit sustained activity to a visual stimulus rather than only an "on" and "off" responses, because detectable magnetic stimulus evoked activity was observed only in bees that showed tonic responses to visual stimulation and every bee that produced stable visual activity yielded at least one recording with a measurable response to the magnetic stimulus. Achieving the desirable response to the visual stimulus is hindered by factors such as the bee's movement, damage to the AOTu during preparation, and variability in the amount of dye that ultimately reaches the AOTu. While the bee's movement can be restricted more reliably and tissue damage minimized with increasing experience, obtaining the correct amount of dye remains a significant challenge, and this is influenced not only by the amount injected but also by the precise injection site, the size of the opening, and the overall health of the bee. All of these factors affect how effectively the dye diffuses into the AOTu. As both excessive and insufficient dye lead to the loss of the desired tonic response, further improvements in the preparation to achieve consistent dye levels are critical in order to get a sufficient sample size. Similarly, modifying the setup to handle higher visual stimulus intensities could help address challenges related to dye concentration, as stronger stimuli would elicit larger AOTu responses, making them detectable even at higher dye concentrations or reducing the impact of background fluorescence changes at lower dye concentrations.

Now that the two-photon imaging setup has been demonstrated to detect AOTu responses to magnetic stimulation, it can be used to investigate how this brain region responds to a broader range of magnetic cues, such as changes in magnetic-field orientation, transitions between field directions, variations in field strength, or sinusoidally oscillating magnetic fields. Using differently polarized light alongside magnetic stimuli may reveal if and how the magnetic and sun compass systems interact with one another. The observation of magnetic responses within a higher-order visual processing region provides preliminary evidence that can be used to investigate the RPM. Several key predictions of the RPM can now be tested with this setup, for example the polarity-independence of the magnetic field or the disruptive influence of radio-frequency fields. Moreover, using honeybees may offer new insight into how radical pairs are formed

in cryptochrome, as they possess only Cry2, a light-insensitive cryptochrome. Overall, this imaging setup provides a new approach to investigate magnetoreception, along the natural neural pathway, taking advantage of natural neural amplification to detect retinal signals that are potentially mediated by cryptochrome. Importantly, this findings reveals a new experimental correlation between magnetic field and light stimulation in honey bees, leading to new possible insights in quantum neuroscience. Thus, this work provides a methodological framework for future studies that systematically vary magnetic parameters and light conditions to disentangle the respective contributions of different sensory systems to the honeybee's compass sense and navigation.

# Appendix

# A

## A.1 Bee Imaging Preparation Pictures

Supplementary images illustrating additional steps involved in preparing the bee for *in vivo* two-photon calcium imaging (see Section 3.3.3) are presented in Figure A.1.The fixation of the antenna with a wire, followed by immobilization with a droplet of n-eicosane, is shown in Figures A.1a and A.1b. The incision and removal of the rectangular window in the cuticle are depicted in Figures A.1c and A.1d. Figures A.1e and A.1f illustrate how the air sacs and salivary glands are displaced or removed, and how the tracheae near the AOTu are cleared. Finally, the replacement of the rectangular cuticle piece to seal the brain is shown in Figure A.1g.

(a)

(b)

(c)

(d)

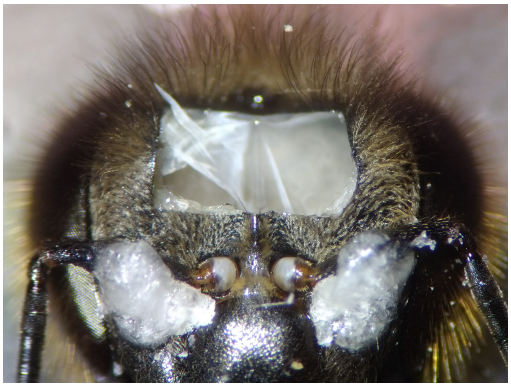

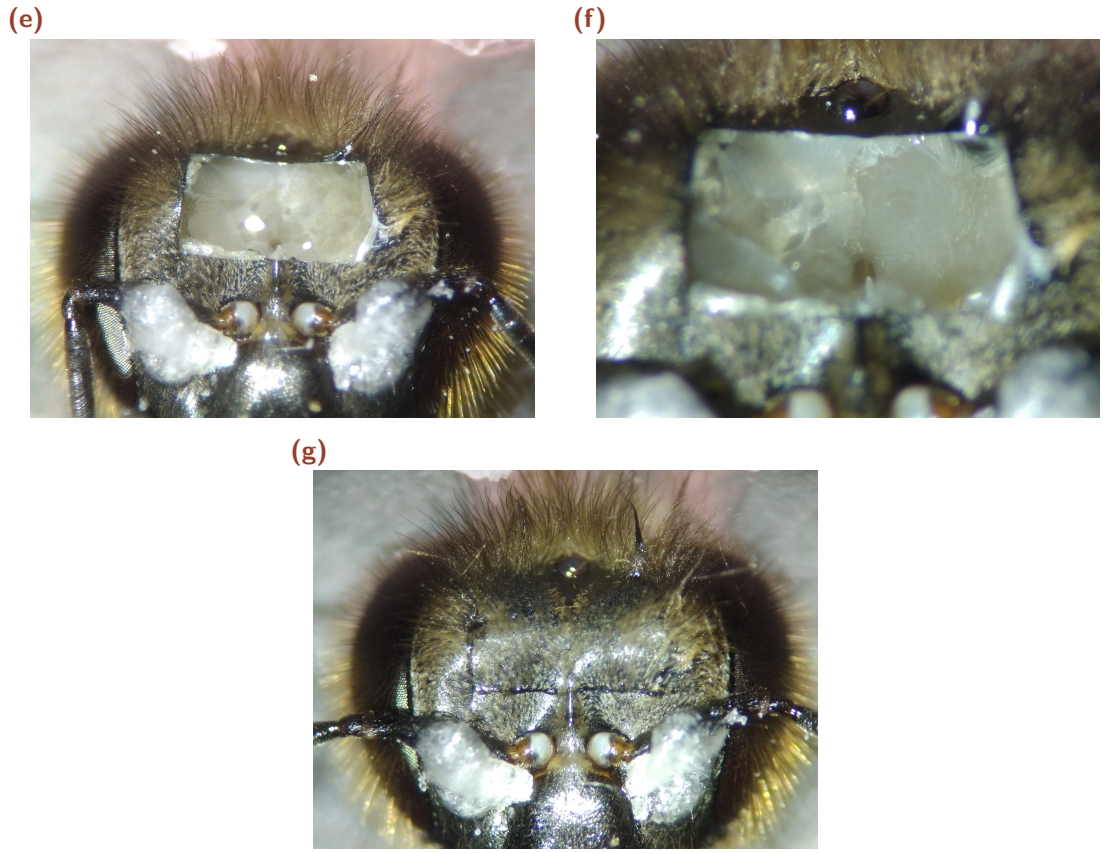


**Figure A.1.:** Preparation steps for *in vivo* two-photon calcium imaging (2/2). (a) Fixation of the antenna using a wire. (b) subsequent immobilization with a droplet of n-eicosane. (c) Incision of the rectangular cuticle window. (d) Removal of the rectangular cuticle window. (e) Displacement or removal of the air sacs and salivary glands. (f) Removal of the tracheae near the AOTu. (g) Replacement of the rectangular cuticle piece to reseal the brain.

## A.2 Magnetic Stimulus Additional bees

Fluorescence recordings from additional bees that exhibited responses to the magnetic stimulus are presented in Figures A.2, A.3, and A.4. The responses of bees to the complete magnetic pulse sequence (Figure 3.19a) under horizontally and vertically polarized light are shown in Figures A.5 and A.4, respectively.

Figure A.6 displays an unprocessed recording from a bee that previously demonstrated a clear magnetic response. In this trial, a sharp decline in fluorescence occurs immediately before the magnetic stimulus is applied. The detrended version of this recording is shown in Figure A.7.

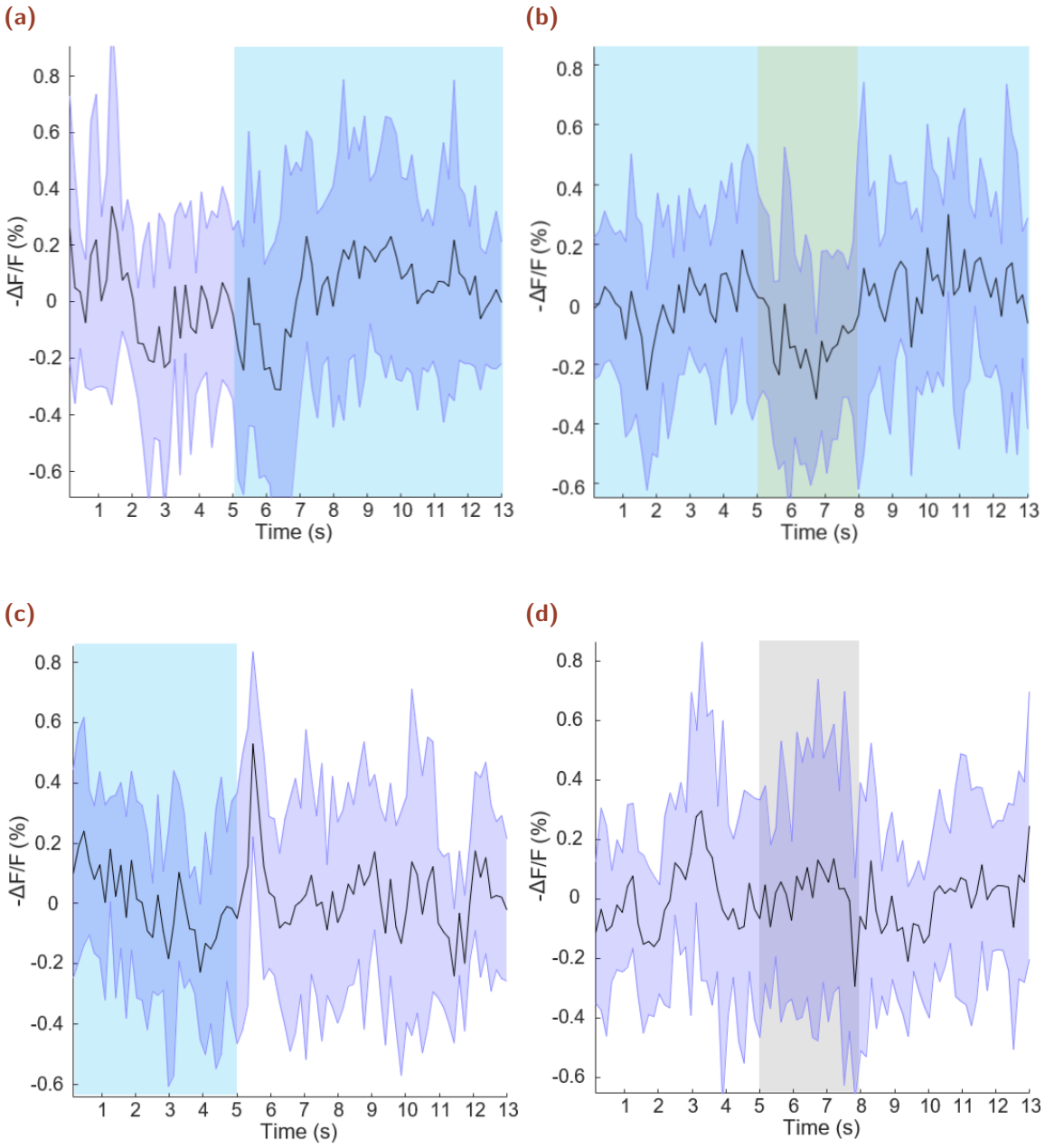


**Figure A.2.:** Detrended time-series recordings of Fura-2 calcium fluorescence in the AOTu exposed to magnetic stimulus sequence of bee 2. (a) Fluorescence response of the AOTu to the onset of the visual stimulus. (b) Response of the AOTu to the magnetic stimulus. (c) Fluorescence response of the AOTu to the offset of the visual stimulus. (d) Activity recorded of the AOTu during the control interval. Curves in red indicate responses that are significantly active based on a 95% confidence threshold.

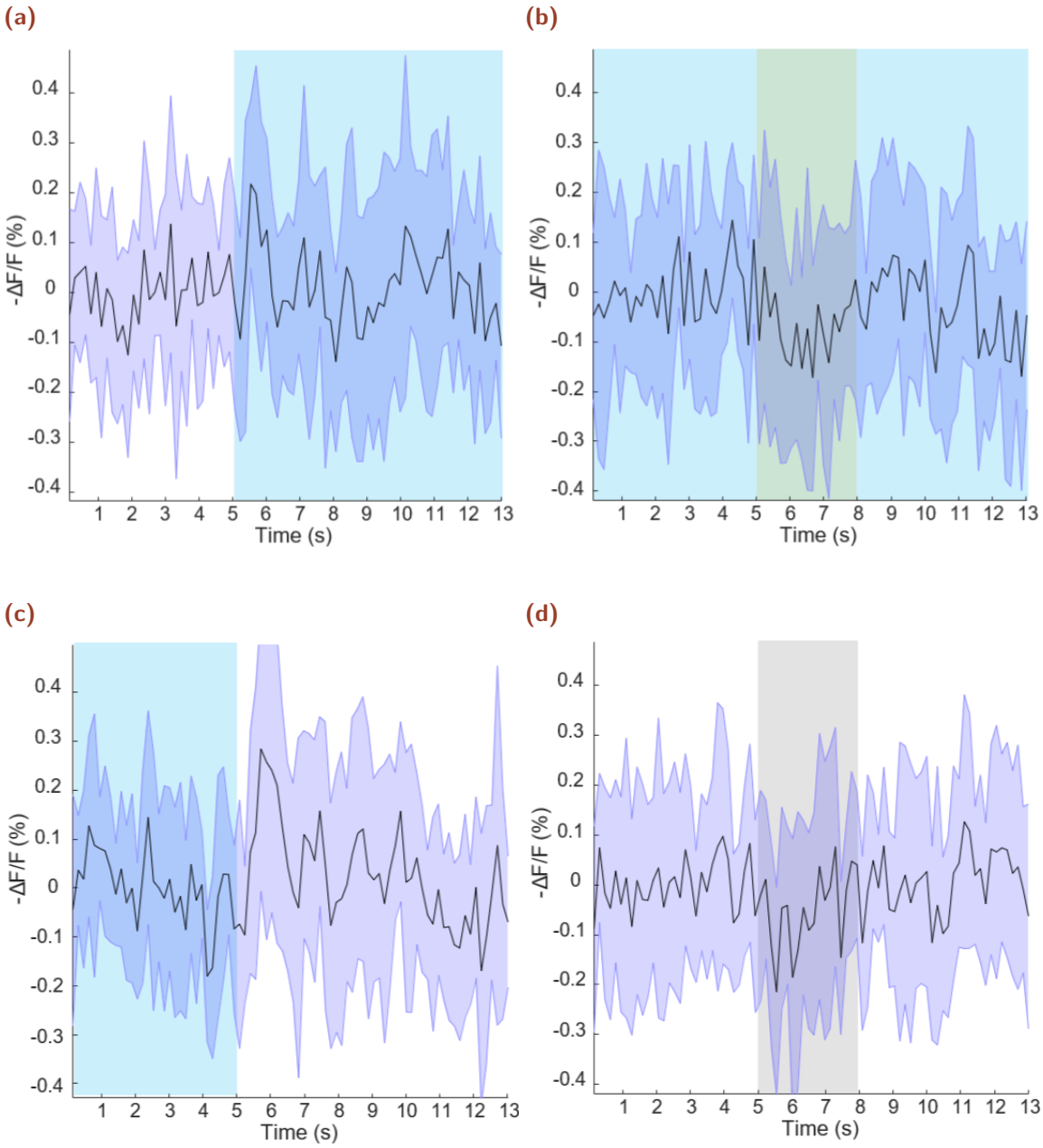


**Figure A.3.:** Detrended time-series recordings of Fura-2 calcium fluorescence in the AOTu exposed to magnetic stimulus sequence of bee 3. (a) Fluorescence response of the AOTu to the onset of the visual stimulus. (b) Response of the AOTu to the magnetic stimulus. (c) Fluorescence response of the AOTu to the offset of the visual stimulus. (d) Activity recorded of the AOTu during the control interval. Curves in red indicate responses that are significantly active based on a 95% confidence threshold.

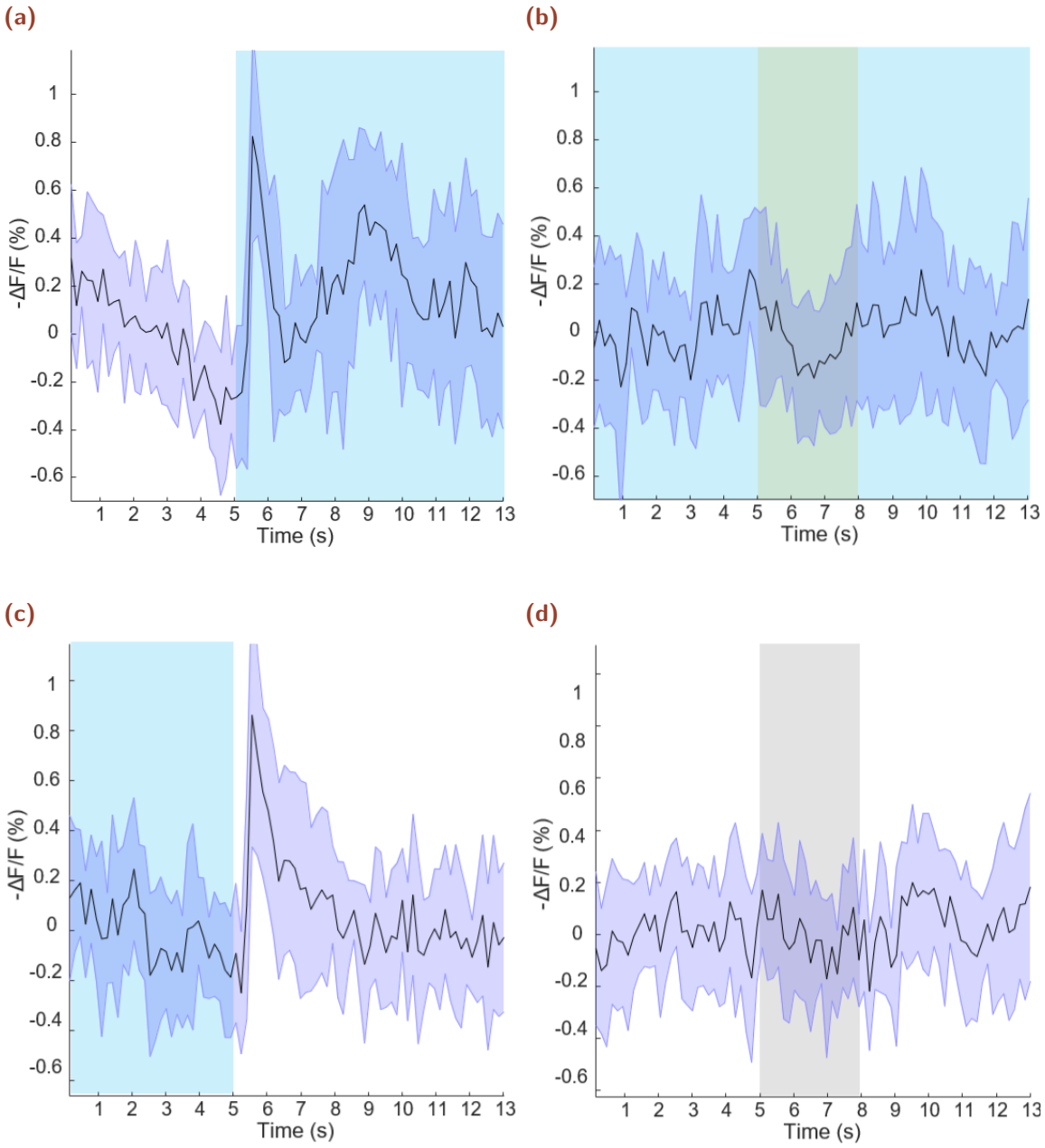


**Figure A.4.:** Detrended time-series recordings of Fura-2 calcium fluorescence in the AOTu exposed to magnetic stimulus sequence of bee 4 under vertically polarized light. (a) Fluorescence response of the AOTu to the onset of the visual stimulus. (b) Response of the AOTu to the magnetic stimulus. (c) Fluorescence response of the AOTu to the offset of the visual stimulus. (d) Activity recorded of the AOTu during the control interval. Curves in red indicate responses that are significantly active based on a 95% confidence threshold.

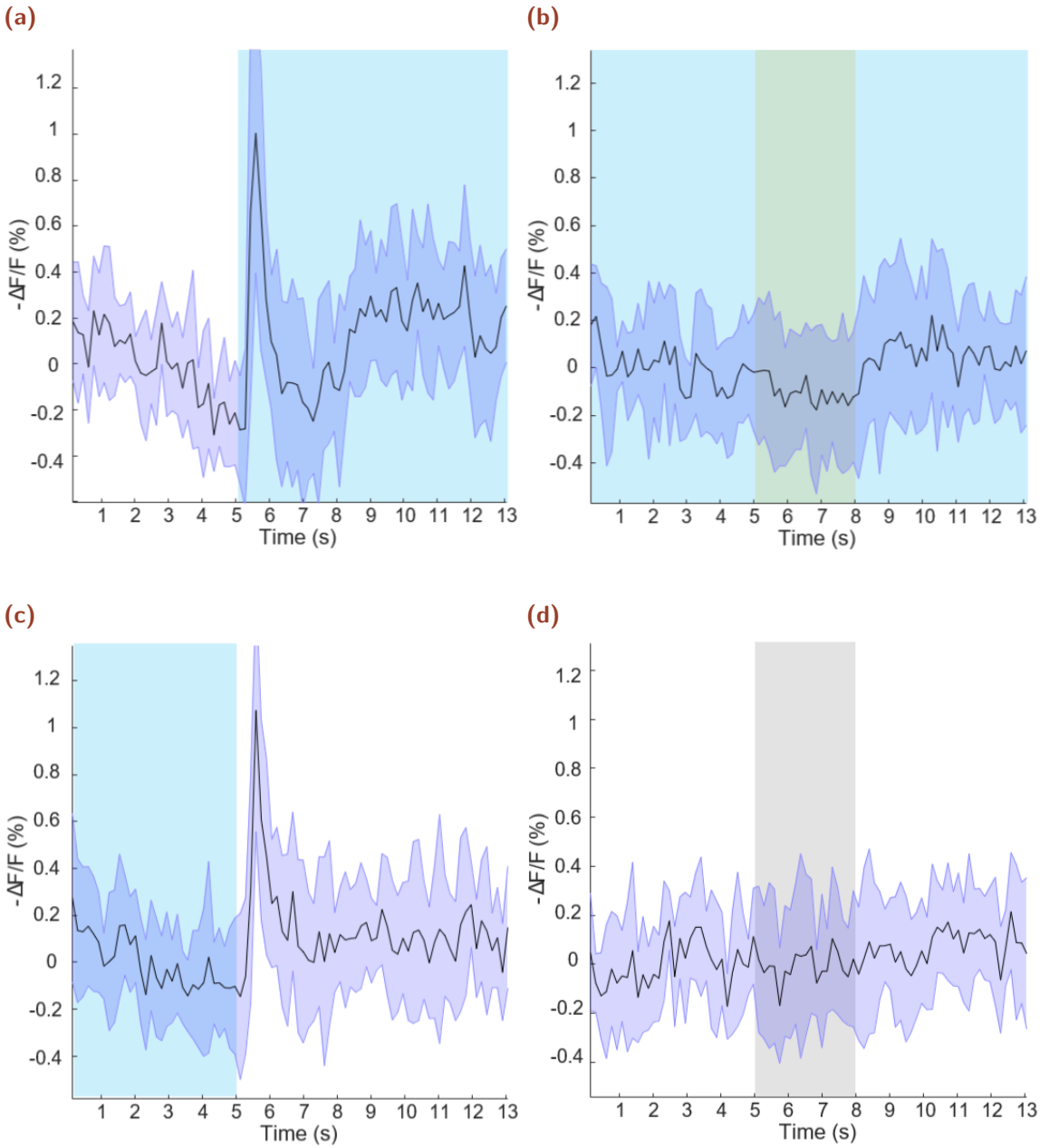


**Figure A.5.:** Detrended time-series recordings of Fura-2 calcium fluorescence in the AOTu exposed to magnetic stimulus sequence of bee 1 under horizontally polarized light. (a) Fluorescence response of the AOTu to the onset of the visual stimulus. (b) Response of the AOTu to the magnetic stimulus. (c) Fluorescence response of the AOTu to the offset of the visual stimulus. (d) Activity recorded of the AOTu during the control interval. Curves in red indicate responses that are significantly active based on a 95% confidence threshold.

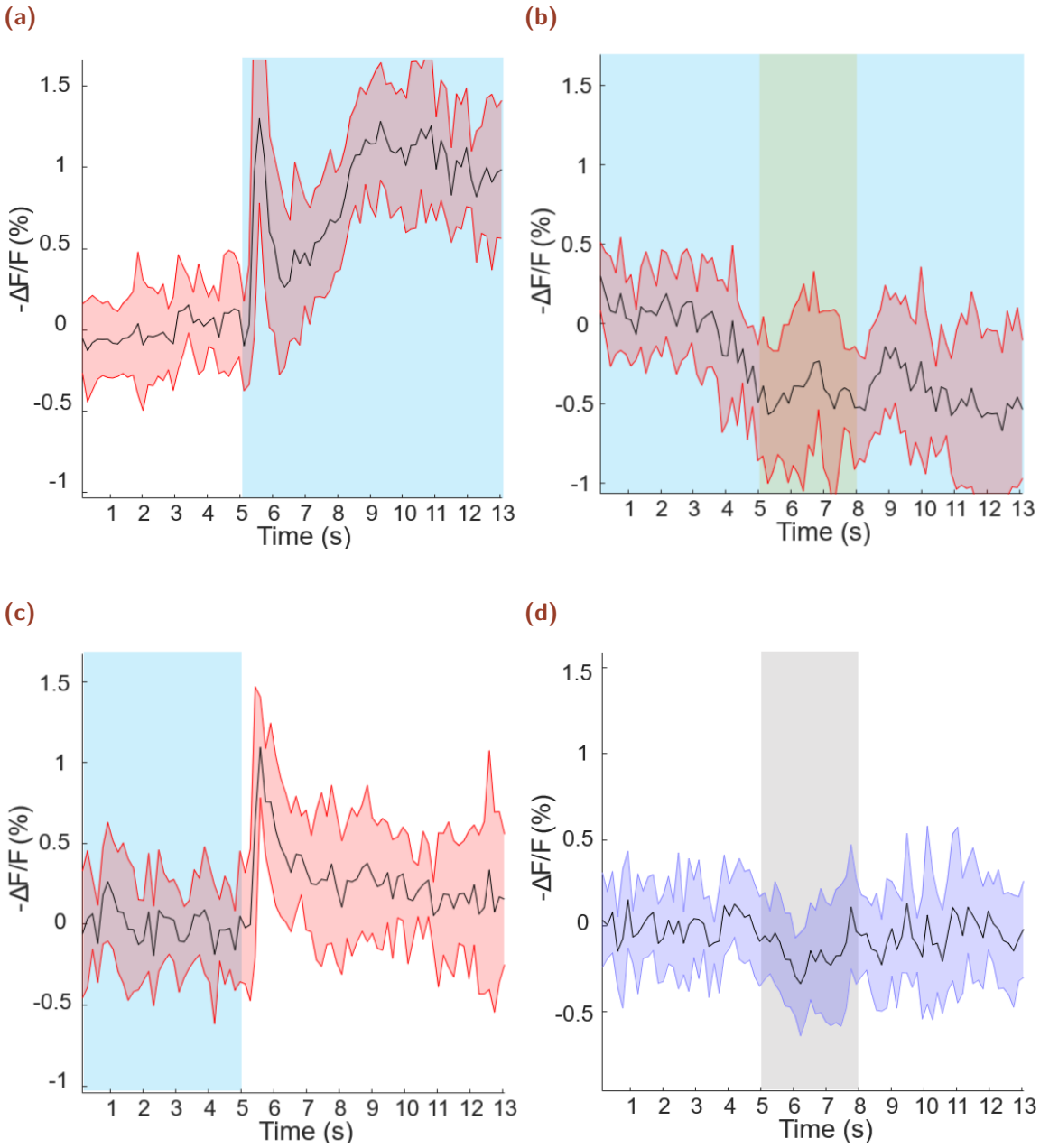


**Figure A.6.:** An unprocessed time-series recordings of Fura-2 calcium fluorescence in the AOTu exposed to magnetic stimulus sequence of bee 1. (a) Fluorescence response of the AOTu to the onset of the visual stimulus. (b) Response of the AOTu to the magnetic stimulus. (c) Fluorescence response of the AOTu to the offset of the visual stimulus. (d) Activity recorded of the AOTu during the control interval. Curves in red indicate responses that are significantly active based on a 95% confidence threshold.

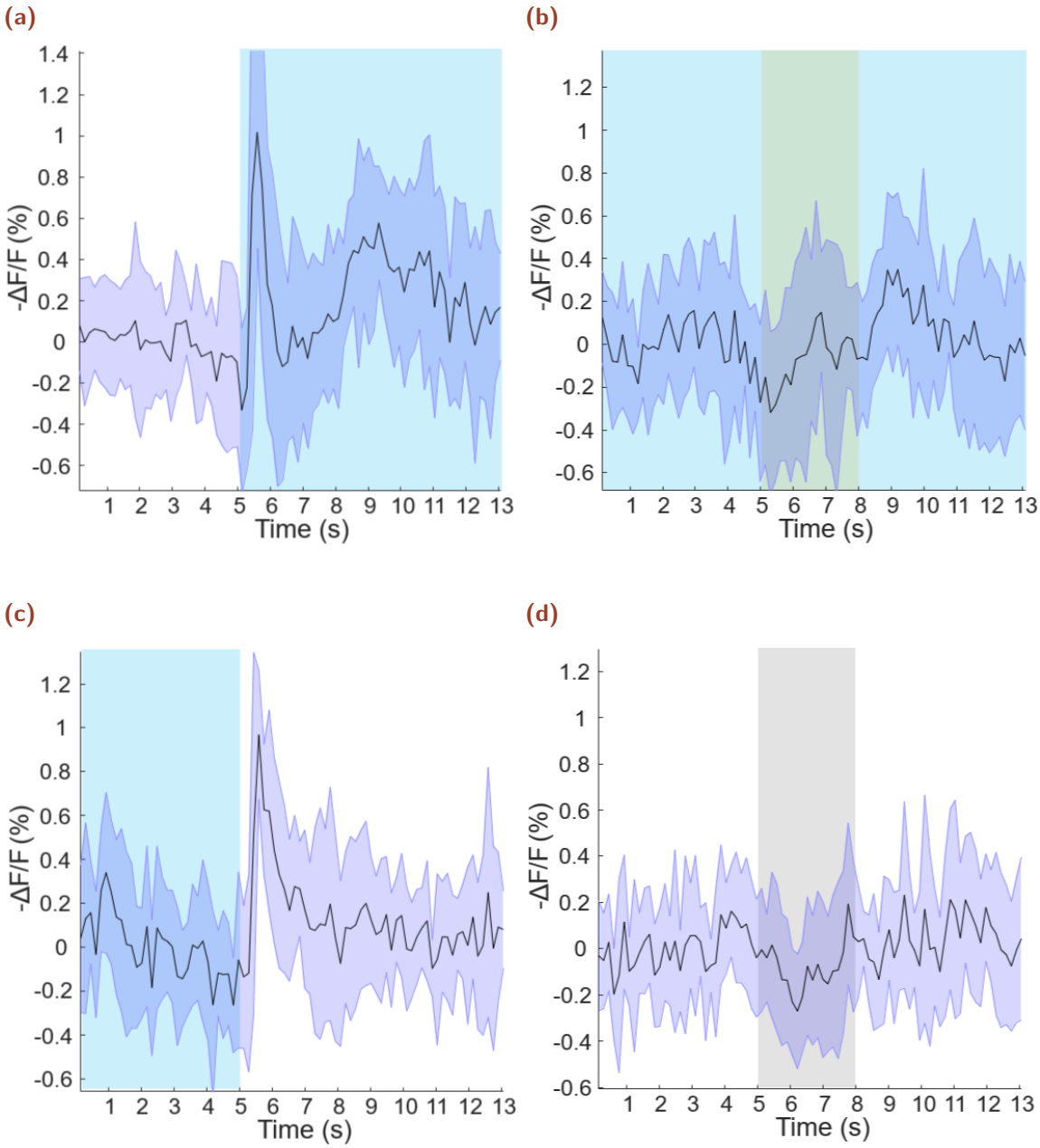


**Figure A.7.:** A detrended time-series recordings of Fura-2 calcium fluorescence in the AOTu exposed to magnetic stimulus sequence of bee 1. (a) Fluorescence response of the AOTu to the onset of the visual stimulus. (b) Response of the AOTu to the magnetic stimulus. (c) Fluorescence response of the AOTu to the offset of the visual stimulus. (d) Activity recorded of the AOTu during the control interval. Curves in red indicate responses that are significantly active based on a 95% confidence threshold.

## A.3 Experimental Code and Analysis Scripts

The MATLAB code used to run the experiment and to perform the data analysis for both the behavioral and calcium-imaging experiments is available in the following repository: `https://github.com/NeurophysicsTrento/BeeMagnetoreception`. The scripts `LED_protocal.m` and `mag_protocal.m` control the PER setup with visual and magnetic stimuli, respectively. Behavioral data analysis is carried out using `analyse_PER.m`. The imaging setup is operated using `magnetic_MAG.m`, while `Preprocess_Data.m` and `MultiROI_analysis2025.m` are used for data preprocessing and imaging-data analysis, respectively.

# Bibliography

# B


[1] M Beekman and F L W Ratnieks. *Long-range foraging by the honey-bee, Apis mellifera L.* Tech. rep. 2000, pp. 490–496. DOI: 10.1046/j.1365-2435.2000.00443.x.

[2] Samuel Rossel and Rudiger Wehner. *How Bees Analyse the Polarization Patterns in the Sky: Experiments and Model*. Tech. rep. 1984, pp. 607–615. DOI: 10.1007/BF00324508.

[3] Avarguès Weber Aurore, Theo Mota, and Martin Giurfa. *New vistas on honey bee vision*. May 2012. DOI: 10.1007/s13592-012-0124-2.

[4] Martin Vacha. *Magnetoreception of Invertebrates*. September 2018. 2017, pp. 367–388. DOI: 10.1093/oxfordhb/9780190456757.013.16.

[5] P. J. Hore and Henrik Mouritsen. „The Radical-Pair Mechanism of Magnetoreception“. In: *Annual Review of Biophysics* 45 (July 2016), pp. 299–344. DOI: 10.1146/annurev-biophys-032116-094545.

[6] John Phillips, Rachel Muheim, Michael Painter, *et al. Why is it so difficult to study magnetic compass orientation in murine rodents?* Jan. 2022. DOI: 10.1007/s00359-021-01532-z.

[7] Theo Mota, Wulfila Gronenberg, Martin Giurfa, and Jean Christophe Sandoz. „Chromatic processing in the anterior optic tubercle of the honey bee brain“. In: *Journal of Neuroscience* 33.1 (Jan. 2013), pp. 4–16. DOI: 10.1523/JNEUROSCI.1412-12.2013.

[8] W. Wiltschko and R. Wiltschko. „Light-dependent magnetoreception in birds: the behaviour of European robins, Erithacus rubecula, under monochromatic light of various wavelengths and intensities“. In: *The Journal of experimental biology* 204 (2001), pp. 3295–3302. DOI: 10.1242/jeb.204.19.3295.

[9] Dmitry Kobylkov, Joe Wynn, Michael Winklhofer, Raisa Chetverikova, Jingjing Xu, Hamish Hiscock, P. J. Hore, and Henrik Mouritsen. „Electromagnetic 0.1-100 kHz noise does not disrupt orientation in a night-migrating songbird implying a spin coherence lifetime of less than 10 $\mu$s“. In: *Journal of the Royal Society Interface* 16.161 (Dec. 2019). DOI: 10.1098/rsif.2019.0716.

[10] Johnjoe McFadden and Jim Al-Khalili. *Life on the edge : the coming of age of quantum biology*. Crown Publishers, 2015, p. 353.

[11] Nathan F. Putman, P. Verley, C. S. Endres, and K. J. Lohmann. „Magnetic navigation behavior and the oceanic ecology of young loggerhead sea turtles“. In: *Journal of Experimental Biology* 218.Pt 7 (Apr. 2015), pp. 1044–1050. DOI: 10.1242/jeb.109975.

[12] Guijun Wan, Ashley N. Hayden, Samantha E. Iiams, and Christine Merlin. „Cryptochrome 1 mediates light-dependent inclination magnetosensing in monarch butterflies“. In: *Nature Communications* 12.1 (Dec. 2021). DOI: 10.1038/s41467-021-21002-z.

[13] Olga Bazalova, Marketa Kvicalova, Tereza Valkova, *et al.* „Cryptochrome 2 mediates directional magnetoreception in cockroaches“. In: *Proceedings of the National Academy of Sciences of the United States of America* 113.6 (Feb. 2016), pp. 1660–1665. DOI: 10.1073/pnas.1518622113.

[14] David A. Ernst and Kenneth J. Lohmann. „Effect of magnetic pulses on Caribbean spiny lobsters: implications for magnetoreception“. In: *Journal of Experimental Biology* 219.Pt 15 (2016), pp. 2247–2251. DOI: 10.1242/jeb.136036.

[15] Sönke Johnsen and Kenneth J. Lohmann. *The physics and neurobiology of magnetoreception*. Sept. 2005. DOI: 10.1038/nrn1745.

[16] John B. Phillips, Paulo E. Jorge, and Rachel Muheim. *Light-dependent magnetic compass orientation in amphibians and insects: Candidate receptors and candidate molecular mechanisms*. Apr. 2010. DOI: 10.1098/rsif.2009.0459.focus.

[17] Michael Winklhofer and Joseph L. Kirschvink. „A quantitative assessment of torque-transducer models for magnetoreception“. In: *Journal of the Royal Society Interface* 7.SUPPL. 2 (Apr. 2010). DOI: 10.1098/rsif.2009.0435.focus.

[18] Joseph L. Kirschvink, Michael M. Walker, and Carol E. Diebel. „Magnetite-based magnetoreception“. In: *Current Opinion in Neurobiology* 11.4 (2001), pp. 462–467. DOI: 10.1016/S0959-4388(00)00235-X.

[19] John B. Phillips, Rachel Muheim, and Paulo E. Jorge. *A behavioral perspective on the biophysics of the light-dependent magnetic compass: A link between directional and spatial perception?* Oct. 2010. DOI: 10.1242/jeb.020792.

[20] Ulrich E Steiner and Thomas Ulrich. „Magnetic Field Effects in Chemical Kinetics and Related Phenomena“. In: *Chemical reviews* 89 (1989), pp. 51–147. DOI: 10.1021/cr00091a003.

[21] John B. Phillips and O. Sayeed. „Wavelength-dependent effects of light on magnetic compass orientation in Drosophila melanogaster“. In: *Journal of Comparative Physiology A* 172.3 (Apr. 1993), pp. 303–308. DOI: 10.1007/BF00216612.

[22] Li Zhang and E. Pascal Malkemper. *Cryptochromes in mammals: a magnetoreception misconception?* 2023. DOI: 10.3389/fphys.2023.1250798.

[23] Roswitha Wiltschko, Margaret Ahmad, Christine Nießner, Dennis Gehring, and Wolfgang Wiltschko. „Light-dependent magnetoreception in birds: The crucial step occurs in the dark“. In: *Journal of the Royal Society Interface* 13.118 (May 2016). DOI: 10.1098/rsif.2015.1010.

[24] Adam A. Bradlaugh, Giorgio Fedele, Anna L. Munro, Celia Napier Hansen, John M. Hares, Sanjai Patel, Charalambos P. Kyriacou, Alex R. Jones, Ezio Rosato, and Richard A. Baines. „Essential elements of radical pair magnetosensitivity in Drosophila“. In: *Nature* 615.7950 (Mar. 2023), pp. 111–116. DOI: 10.1038/s41586-023-05735-z.

[25] Marco Bassetto, Thomas Reichl, Dmitry Kobylkov, Daniel R. Kattnig, Michael Winklhofer, P. J. Hore, and Henrik Mouritsen. „No evidence for magnetic field effects on the behaviour of Drosophila“. In: *Nature* 620.7974 (Aug. 2023), pp. 595–599. DOI: 10.1038/s41586-023-06397-7.

[26] T. Válková and M. Vácha. „How do honeybees use their magnetic compass? Can they see the North?“ In: *Bulletin of Entomological Research* 102.4 (Aug. 2012), pp. 461–467. DOI: 10.1017/S0007485311000824.

[27] Kayla M. Goforth and Christine Merlin. *From skylight cues to magnetic fields: the toolkit of insect long-distance navigation*. 2025. DOI: 10.1007/s00359-025-01770-5.

[28] Elad B. Rubin, Yair Shemesh, Mira Cohen, Sharona Elgavish, Hugh M. Robertson, and Guy Bloch. „Molecular and phylogenetic analyses reveal mammalian-like clockwork in the honey bee (Apis mellifera) and shed new light on the molecular evolution of the circadian clock“. In: *Genome Research* 16.11 (2006), pp. 1352–1365. DOI: 10.1101/gr.5094806.

[29] Alexander Yu. Rotov, Arsenii A. Goriachenkov, Roman V. Cherbunin, Michael L. Firsov, Nikita Chernetsov, and Luba A. Astakhova. „Magnetoreceptory Function of European Robin Retina: Electrophysiological and Morphological Non-Homogeneity“. In: *Cells* 11.19 (2022), p. 3056. DOI: 10.3390/cells11193056.

[30] E. Pascal Malkemper, Simon Nimpf, Gregory C. Nordmann, and David A. Keays. *Neuronal circuits and the magnetic sense: Central questions*. Nov. 2020. DOI: 10.1242/jeb.232371.

[31] Fritjof Helmchen and Winfried Denk. *Deep tissue two-photon microscopy*. 2005. DOI: 10.1038/nmeth818.

[32] Martin Oheim, Emmanuel Beaurepaire, Emmanuelle Chaigneau, Jerome Mertz, and Serge Charpak. „Two-photon microscopy in brain tissue: Parameters influencing the imaging depth“. In: *Journal of Neuroscience Methods* 111.1 (2001), pp. 29–37. DOI: 10.1016/S0165-0270(01)00438-1.

[33] Theo Mota, Nobuhiro Yamagata, Martin Giurfa, Wulfila Gronenberg, and Jean Christophe Sandoz. „Neural organization and visual processing in the anterior optic tubercle of the honeybee brain“. In: *Journal of Neuroscience* 31.32 (Aug. 2011), pp. 11443–11456. DOI: 10.1523/JNEUROSCI.0995-11.2011.

[34] L. J. Kinsey, W. S. Beane, and K. A. Tseng. „Accelerating an integrative view of quantum biology“. In: *Frontiers in Physiology* 14 (2024). Published 2024 Jan 11, p. 1349013. DOI: 10.3389/fphys.2023.1349013.

[35] M. E. Bitterman, Randolf Menzel, A. Fietz, and S. Schäfer. „Classical conditioning of proboscis extension in honeybees (Apis mellifera).“ In: *Journal of comparative psychology (Washington, D.C. : 1983)* 97.2 (1983), pp. 107–119. DOI: 10.1037/0735-7036.97.2.107.

[36] Martin Giurfa and Jean-Christophe Sandoz. „Invertebrate learning and memory: Fifty years of olfactory conditioning of the proboscis extension response in honeybees.“ In: *Learning & memory (Cold Spring Harbor, N.Y.)* 19.2 (Feb. 2012), pp. 54–66. DOI: 10.1101/lm.024711.111.

[37] Chao Hung Liang, Cheng Long Chuang, Joe Air Jiang, and En Cheng Yang. „Magnetic Sensing through the Abdomen of the Honey bee“. In: *Scientific Reports* 6 (Mar. 2016). DOI: 10.1038/srep23657.

[38] Aurore Avarguès-Weber and Theo Mota. *Advances and limitations of visual conditioning protocols in harnessed bees*. Oct. 2016. DOI: 10.1016/j.jphysparis.2016.12.006.

[39] Sayaka Hori, A E Hideaki, Takeuchi Ae, Kentaro Arikawa, Michiyo Kinoshita, A E Naoko, Ichikawa Masami, Sasaki Ae, and Takeo Kubo. „Associative visual learning, color discrimination, and chromatic adaptation in the harnessed honeybee Apis mellifera L“. In: (2006). DOI: 10.1007/s00359-005.

[40] G. S. Balamurali, Hema Somanathan, and N. Hempel de Ibarra. „Motion cues improve the performance of harnessed bees in a colour learning task“. In: *Journal of Comparative Physiology A: Neuroethology, Sensory, Neural, and Behavioral Physiology* 201.5 (May 2015), pp. 505–511. DOI: 10.1007/s00359-015-0994-7.

[41] Heather Strelevitz, Ettore Tiraboschi, and Albrecht Haase. „Associative Learning of Quantitative Mechanosensory Stimuli in Honeybees“. In: *Insects* 15.2 (Feb. 2024). DOI: 10.3390/insects15020094.

[42] Christopher T. Rodgers. *Magnetic field effects in chemical systems*. 2009. DOI: 10.1351/PAC-CON-08-10-18.

[43] Jilder Dandy Peña Serna, Odivaldo Cambraia Alves, Fernanda Abreu, and Daniel Acosta-Avalos. „Magnetite in the abdomen and antennae of Apis mellifera honeybees“. In: *Journal of Biological Physics* 50.2 (June 2024), pp. 215–228. DOI: 10.1007/s10867-024-09656-4.

[44] Jandira Ferreira, Geraldo Cernicchiaro, Michael Winklhofer, Humberto Dutra, Paulo S. De Oliveira, Darci M.S. Esquivel, and Eliane Wajnberg. „Comparative magnetic measurements on social insects“. In: *Journal of Magnetism and Magnetic Materials*. Vol. 289. Mar. 2005, pp. 442–444. DOI: 10.1016/j.jmmm.2004.11.124.

[45] Peter Hore. *The Quantum Robin | NAVIGATION NEWS*. Tech. rep. 2011, pp. 15–17.

[46] Henrik Mouritsen and P. J. Hore. *The magnetic retina: Light-dependent and trigeminal magnetoreception in migratory birds*. Apr. 2012. DOI: 10.1016/j.conb.2012.01.005.

[47] Jason C.S. Lau, Christopher T. Rodgers, and P. J. Hore. „Compass magnetoreception in birds arising from photo-induced radical pairs in rotationally disordered cryptochromes“. In: *Journal of the Royal Society Interface* 9.77 (Dec. 2012), pp. 3329–3337. DOI: 10.1098/rsif.2012.0374.

[48] Markus Tiersch and Hans J. Briegel. „Decoherence in the chemical compass: The role of decoherence for avian magnetoreception“. In: (Aug. 2012). DOI: 10.1098/rsta.2011.0488.

[49] J. R. Woodward. „Radical pairs in solution“. In: *Progress in Reaction Kinetics and Mechanism* 27.3 (2002), pp. 165–207. DOI: 10.3184/007967402103165388.

[50] Jiate Luo. „Sensitivity enhancement of radical-pair magnetoreceptors as a result of spin decoherence“. In: *Journal of Chemical Physics* 160.7 (Feb. 2024). DOI: 10.1063/5.0182172.

[51] Thomas P. Fay, Lachlan P. Lindoy, David E. Manolopoulos, and P. J. Hore. „How quantum is radical pair magnetoreception?“ In: *Faraday Discussions* 221 (2019), pp. 77–91. DOI: 10.1039/c9fd00049f.

[52] Thomas P. Fay, Lachlan P. Lindoy, and David E. Manolopoulos. „Spin-selective electron transfer reactions of radical pairs: Beyond the Haberkorn master equation“. In: *Journal of Chemical Physics* 149.6 (Aug. 2018). DOI: 10.1063/1.5041520.

[53] Saja Isabella Ilott, Cass D. Pearse, Benjamin Tigg, and Daniel R. Kattnig. „Electron hopping in cryptochrome: Implications for radical pair magnetoreception and the role of the fourth tryptophan“. In: *Journal of Chemical Physics* 163.2 (July 2025). DOI: 10.1063/5.0278806.

[54] Margaret Ahmad and Anthony R Cashmore. *Mini-review Seeing blue: the discovery of cryptochrome*. Tech. rep. 1996, pp. 851–861. DOI: 10.1007/BF00020798.

[55] Anthony R. Cashmore, Jose A. Jarillo, Ying-Jie Wu, and Dongmei Liu. *Cryptochrome: Blue-Light Receptors for Plants and Animals?* 1998. DOI: 10.1046/j.1365-313x.1998.00282.x.

[56] Roger J. Kutta, Nataliya Archipowa, Linus O. Johannissen, Alex R. Jones, and Nigel S. Scrutton. „Vertebrate Cryptochromes are Vestigial Flavoproteins“. In: *Scientific Reports* 7 (Mar. 2017). DOI: 10.1038/srep44906.

[57] Dominik Immeln, Alexander Weigel, Tilman Kottke, and J. Luis Pérez Lustres. „Primary events in the blue light sensor plant cryptochrome: Intraprotein electron and proton transfer revealed by femtosecond spectroscopy“. In: *Journal of the American Chemical Society* 134.30 (Aug. 2012), pp. 12536–12546. DOI: 10.1021/ja302121z.

[58] M. Hammad, M. Albaqami, M. Pooam, E. Kernevez, J. Witczak, T. Ritz, C. Martino, and M. Ahmad. „Cryptochrome mediated magnetic sensitivity in: Arabidopsis occurs independently of light-induced electron transfer to the flavin“. In: *Photochemical and Photobiological Sciences* 19.3 (Mar. 2020), pp. 341–352. DOI: 10.1039/c9pp00469f.

[59] Robert J. Gegear, Lauren E. Foley, Amy Casselman, and Steven M. Reppert. „Animal cryptochromes mediate magnetoreception by an unconventional photochemical mechanism“. In: *Nature* 463.7282 (Feb. 2010), pp. 804–807. DOI: 10.1038/nature08719.

[60] Lauren E. Foley, Robert J. Gegear, and Steven M. Reppert. „Human cryptochrome exhibits light-dependent magnetosensitivity“. In: *Nature Communications* 2.1 (2011). DOI: 10.1038/ncomms1364.

[61] Lauren E Foley and Patrick Emery. „Drosophila Cryptochrome: Variations in Blue“. In: *Journal of Biological Rhythms* (Oct. 2019), p. 074873041987829. DOI: 10.1177/0748730419878290.

[62] Taishi Yoshii, Takeshi Todo, Corinna Wülbeck, Ralf Stanewsky, and Charlotte Helfrich-Förster. „Cryptochrome is present in the compound eyes and a subset of Drosophila's clock neurons“. In: *Journal of Comparative Neurology* 508.6 (2008), pp. 952–966. DOI: 10.1002/cne.21702.

[63] Ilia A. Solov'Yov, Henrik Mouritsen, and Klaus Schulten. „Acuity of a cryptochrome and vision-based magnetoreception system in birds“. In: *Biophysical Journal* 99.1 (July 2010), pp. 40–49. DOI: 10.1016/j.bpj.2010.03.053.

[64] Thorsten Ritz, Salih Adem, and Klaus Schulten. „A model for photoreceptor-based magnetoreception in birds“. In: *Biophysical Journal* 78.2 (2000), pp. 707–718. DOI: 10.1016/S0006-3495(00)76629-X.

[65] Matthew J. Golesworthy, Tilo Zollitsch, Jiate Luo, *et al.* „Singlet-triplet dephasing in radical pairs in avian cryptochromes leads to time-dependent magnetic field effects“. In: *Journal of Chemical Physics* 159.10 (2023). DOI: 10.1063/5.0166675.

[66] Daniel R. Kattnig, Jakub K. Sowa, Ilia A. Solov'Yov, and P. J. Hore. „Electron spin relaxation can enhance the performance of a cryptochrome-based magnetic compass sensor“. In: *New Journal of Physics* 18.6 (2016). DOI: 10.1088/1367-2630/18/6/063007.

[67] Thorsten Ritz, Peter Thalau, John B. Phillips, Roswitha Wiltschko, and Wolfgang Wiltschko. „Resonance effects indicate a radical-pair mechanism for avian magnetic compass“. In: *Nature* 429.6988 (2004), pp. 177–180. DOI: 10.1038/nature02534.

[68] Svenja Engels, Nils Lasse Schneider, Nele Lefeldt, Christine Maira Hein, Manuela Zapka, Andreas Michalik, Dana Elbers, Achim Kittel, P. J. Hore, and Henrik Mouritsen. „Anthropogenic electromagnetic noise disrupts magnetic compass orientation in a migratory bird“. In: *Nature* 509.7500 (2014), pp. 353–356. DOI: 10.1038/nature13290.

[69] Giorgio Fedele, Edward W. Green, Ezio Rosato, and Charalambos P. Kyriacou. „An electromagnetic field disrupts negative geotaxis in Drosophila via a CRY-dependent pathway“. In: *Nature Communications* 5 (July 2014). DOI: 10.1038/ncomms5391.

[70] Hamish G. Hiscock, Henrik Mouritsen, David E. Manolopoulos, and P. J. Hore. „Disruption of Magnetic Compass Orientation in Migratory Birds by Radiofrequency Electromagnetic Fields“. In: *Biophysical Journal* 113.7 (2017), pp. 1475–1484. DOI: 10.1016/j.bpj.2017.07.031.

[71] Motohiro Wakakuwa, Masumi Kurasawa, Martin Giurfa, and Kentaro Arikawa. „Spectral heterogeneity of honeybee ommatidia“. In: *Naturwissenschaften* 92.10 (Oct. 2005), pp. 464–467. DOI: 10.1007/s00114-005-0018-5.

[72] Thomas Labhart and Eric P Meyer. *Detectors for Polarized Skylight in Insects: A Survey of Ommatidial Specializations in the Dorsal Rim Area of the Compound Eye*. Tech. rep. 1999, pp. 368–379. DOI: 10.1002/(SICI)1097-0029(19991215)47:6<368::AID-JEMT2>3.0.CO;2-Q.

[73] Randolf Menzel. *Spectral Sensitivity of Monopolar Cells in the Bee Lamina*. Tech. rep. 1974, pp. 337–346. DOI: 10.1007/BF00606801.

[74] En Cheng Yang, Hsiao Chun Lin, and Yu Shan Hung. „Patterns of chromatic information processing in the lobula of the honeybee, Apis mellifera L.“ In: *Journal of Insect Physiology* 50.10 (Oct. 2004), pp. 913–925. DOI: 10.1016/j.jinsphys.2004.06.010.

[75] Jutta Kien and Randolf Menzel. *Chromatic Properties of Interneurons in the Optic Lobes of the Bee II. Narrow Band and Colour Opponent Neurons*. Tech. rep. 1977, pp. 35–53. DOI: 10.1007/BF00657349.

[76] Horst Hertel. „Chromatic Properties of Identified Interneurons in the Optic Lobes of the Bee“. In: *Journal of Comparative Physiology A* 137 (1980), pp. 215–238. DOI: 10.1007/BF00605104.

[77] A. C. Paulk, A. M. Dacks, J. Phillips-Portillo, J.-M. Fellous, and W. Gronenberg. „Visual Processing in the Central Bee Brain“. In: *Journal of Neuroscience* 29.32 (2009), pp. 9987–9999. DOI: 10.1523/JNEUROSCI.1325-09.2009.

[78] P. G. Mobbs. „The brain of the honeybee Apis mellifera . I. The connections and spatial organization of the mushroom bodies“. In: *Philosophical Transactions of the Royal Society of London. B, Biological Sciences* 298.1091 (July 1982), pp. 309–354. DOI: 10.1098/rstb.1982.0086.

[79] Theo Mota, Benjamin Paffhausen, and Randolf Menzel. „Chromatic processing and receptive-field structure in neurons of the anterior optic tract of the honeybee brain“. In: *PLoS ONE* 19.9 September (Sept. 2024). DOI: 10.1371/journal.pone.0310282.

[80] Jürgen Rybak and R. Menzel. „Anatomy of the mushroom bodies in the honey bee brain: The neuronal connections of the alpha-lobe“. In: *Journal of Comparative Neurology* 334.3 (Aug. 1993), pp. 444–465. DOI: 10.1002/cne.903340309.

[81] Maximilian Zeller, Martina Held, Julia Bender, Annuska Berz, Tanja Heinloth, Timm Hellfritz, and Keram Pfeiffer. „Transmedulla Neurons in the Sky Compass Network of the Honeybee (Apis mellifera) Are a Possible Site of Circadian Input“. In: *PLoS ONE* 10.12 (Dec. 2015). DOI: 10.1371/journal.pone.0143244.

[82] Martina Held, Annuska Berz, Ronja Hensgen, Thomas S. Muenz, Christina Scholl, Wolfgang Rössler, Uwe Homberg, and Keram Pfeiffer. „Microglomerular synaptic complexes in the sky-compass network of the honeybee connect parallel pathways from the anterior optic tubercle to the central complex“. In: *Frontiers in Behavioral Neuroscience* 10.OCT (Oct. 2016). DOI: 10.3389/fnbeh.2016.00186.

[83] Malte T. Ahlers, Christoph T. Block, Michael Winklhofer, and Martin Greschner. „Integration and evaluation of magnetic stimulation in physiology setups“. In: *PLoS ONE* 17.7 July (July 2022). DOI: 10.1371/journal.pone.0271765.

[84] Pasquale Arpaia, Philip Nicholas Burrows, Marco Buzio, Chetan Gohil, Mariano Pentella, and Daniel Schulte. „Magnetic characterization of Mumetal® for passive shielding of stray fields down to the nano-Tesla level“. In: *Nuclear Instruments and Methods in Physics Research, Section A: Accelerators, Spectrometers, Detectors and Associated Equipment* 988 (Feb. 2021). DOI: 10.1016/j.nima.2020.164904.

[85] Christine Grienberger, Andrea Giovannucci, William Zeiger, and Carlos Portera-Cailliau. „Two-photon calcium imaging of neuronal activity“. In: *Nature Reviews Methods Primers* 2.1 (Dec. 2022). DOI: 10.1038/s43586-022-00147-1.

[86] R. Madelaine Paredes, Julie C. Etzler, Lora Talley Watts, Wei Zheng, and James D. Lechleiter. „Chemical calcium indicators“. In: *Methods* 46.3 (Nov. 2008), pp. 143–151. DOI: 10.1016/j.ymeth.2008.09.025.

[87] Karel Svoboda and Ryohei Yasuda. *Principles of Two-Photon Excitation Microscopy and Its Applications to Neuroscience*. June 2006. DOI: 10.1016/j.neuron.2006.05.019.

[88] Warren R. Zipfel, Rebecca M. Williams, and Watt W. Webb. *Nonlinear magic: Multiphoton microscopy in the biosciences*. Nov. 2003. DOI: 10.1038/nbt899.

[89] Luca Dalbosco, Giulia Zanini, Elvira D'Amato, Francesco Tessarolo, Sebastiana Boi, Paolo Bauer, Albrecht Haase, and Renzo Antolini. „Photodamage in deep tissue two-photon optical biopsy of human skin". In: *Journal of Biophotonics* 8.10 (Oct. 2015), pp. 816–825. DOI: 10.1002/jbio.201400083.

[90] Marco Paoli, Mara Andrione, and Albrecht Haase. „Imaging techniques in insects". In: *Neuromethods*. Ed. by Lesley J. Rogers and Giorgio Vallortigara. 1st ed. Vol. 122. Neuromethods. New York, NY: Springer New York, 2017. Chap. 16, pp. 471–519. DOI: 10.1007/978-1-4939-6725-4{_}15.

[91] Martin Strube-Bloss, Patrick Günzel, Carmen A. Nebauer, and Johannes Spaethe. „Visual accelerated and olfactory decelerated responses during multimodal learning in honeybees". In: *Frontiers in Physiology* 14 (2023). DOI: 10.3389/fphys.2023.1257465.

[92] Scott E. Dobrin and Susan E. Fahrbach. „Visual Associative Learning in Restrained Honey Bees with Intact Antennae". In: *PLoS ONE* 7.6 (June 2012). Ed. by Adrian G. Dyer, e37666. DOI: 10.1371/journal.pone.0037666.

[93] Baptiste Buatois, Aurore Avargués-Weber, Ana Clara David Fernandes de Mello Goulart, and Martin Giurfa. „Associative visual learning by tethered bees in a controlled visual environment". In: *Scientific Reports* 7.1 (2017), p. 12711. DOI: 10.1038/s41598-017-12631-w.